2018

USE OF RADIATION TO KILL CANCER BY NANOPARTICLES AND IN A BIODOSIMETER USING GENE EXPRESSION ANALYSIS

Samana Shrestha
University of Rhode Island, samana_shrestha@uri.edu

USE OF RADIATION TO KILL CANCER BY NANOPARTICLES AND IN A BIODOSIMETER USING GENE EXPRESSION ANALYSIS

BY

SAMANA SHRESTHA

A DISSERTATION SUBMITTED IN PARTIAL FULFILLMENT OF THE REQUIREMENTS FOR THE DEGREE OF

DOCTOR OF PHILOSOPHY

IN

PHYSICS

UNIVERSITY OF RHODE ISLAND

2018

DOCTOR OF PHILOSOPHY DISSERTATION

OF

SAMANA SHRESTHA

APPROVED:

Dissertation Committee:

Major Professor:

Michael Antosh

Feruz Ganikhanov

Stephen M Kennedy

Nasser H Zawia

DEAN OF THE GRADUATE SCHOOL

UNIVERSITY OF RHODE ISLAND

2018

ABSTRACT

The use of radiation is broad in biological systems, in different areas of research mostly in health.

Radiation is used to kill cancer. In radiation therapy proper calculation is done so that a maximum dose is delivered to the cancer . Inspite of this precaution, radiation effects healthy tissue. This effect is especially dangerous when the tumor is located near important organs. Thus in radiation therapy, it is important to reduce the dose and the damage to the healthy tissues and organs. The damage on the healthy tissues due to radiation therapy in cancer could be reduced by reducing the radiation dose to get the same treatment effect or by enhancing the radiation. The enhancement of radiation effect *in vitro* and *in vivo* can be obtained by targeted drug delivery on the cancer. Also photo dynamic therapy can be supplemented by the use of radiation therapy on the cancer by targeted drug delivery.

Another use is the development of a bio dosimeter. In a large scale nuclear event it is important to measure the radiation dose exposed to humans. Also it is likely that the people who are exposed to radiation are not wearing the dosimeter. So a method of estimating radiation dose to a person exposed to radiation without a physical dosimeter would be a very useful procedure. One possible method is the use of gene expression analysis, which is based on the fact that the expression of the genes will change due to the absorbed radiation. So developing a biological dosimeter based on the gene expression analysis could quantify the radiation dose given to the patients during radiation therapy or to assess the risk of cancer developing in the general population. This biological dosimeter could even be used when the physical

dosimeters are insufficient to estimate the risk caused by the radiation exposure or even years after being exposed to nuclear accidents.

The main goal of the work presented here is to investigate the following topics

- Use of gold pHLIP to enhance the radiation effect in cancer cells
- Review on the *in vivo* research done to enhance radiation using gold nanoparticles
- Analyze the gene expression results from irradiated drosophila melanogaster to develop a biological dosimeter.
- Use of X-ray to activate targeted Copper Cysteamine nanoparticles photosensitizer to reduce tumor size in mice.

A review work I have done on the researches related to enhancement of radiation using gold nanoparticles in tumor bearing mice showed that the targeted nanoparticles are a promising method for achieving radiation enhancement due to their shape, size , surface chemistry and the properties of the nanoparticles..

Gold nanoparticles are susceptible to X-rays compared to tissues and release extra electrons by Auger effect when the tumor treated with gold is irradiated. These auger electrons have low energy and are localized within the tumor site killing the cancer cells. However tumor targeting peptide pHLIP (pH Low Insertion Peptide) conjugated to gold nanoparticle specifically targets low pH medium (tumor) which when irradiated reduces the risk of killing healthy tissues near by and increases the uptake of the particles in the cancer mostly in the cellular membranes compared to only gold. The experimental results on cellular uptake of gold showed that there was an enhancement of gold uptake by 52% at low pH compared to normal pH (P value =

.008)and also in targeted gold by 34% compared to non targeted gold at low pH (P value= .023). The images obtained by distribution of gold experiment showed that the cellular uptake of gold-pHLIP is higher compared to gold alone . The targeting of plasma membrane by gold-pHLIP is seen clearly on all the images and some staining of internal organelles and nuclei membranes as well. The clonogenic assay experiment at 1.5Gray radiation showed a statistically significant 24% decrease in survival for cells treated with gold-pHLIP at low pH compared with cells treated with no gold. Also a statistically significant 21% decrease in survival for cells treated with gold-pHLIP at low pH compared with cells treated with gold alone. Thus Gold nanoparticles conjugated with pHLIP significantly increases the amount of gold particles in cancer cells thus enhancing the radiation effect and increasing the amount of cancer cell death from radiation.

Copper cysteamine nanoparticles placed in the tumor site release cytotoxic singlet oxygen molecules on irradiation. The Cu-Cy nanoparticles being photosensitizers kill tumor when activated by radiation. Photosensitizers are limited to shallow tumors. Here we use X-radiation to photosensitize the pHLIP targeted Cu-Cy nanoparticles to kill even the deeply seated tumors *in vivo*. The results from the *in vivo* experiment we have done shows significant tumor destruction under X-ray activation. ANOVA analysis showed that the mice treated with targeted particles had a significantly different tumor sizes than mice treated with no particles, as well as mice treated with non-targeted particles. Also the use of targeted copper cysteamine nanoparticles affected the survival time after irradiation, compared to irradiation using no particles on mice. This work confirms the effectiveness of Copper Cysteamine nanoparticles,

targeted to tumors, as a photosensitizer when activated by radiation therapy. Thus the aid of radiation therapy to photodynamic therapy by the use of tumor targeted CuCy nanoparticles efficiently does tumor destruction shrinkage with the increase in mice survival.

Gene expression analysis on a published data showed that the expression of genes are radiation dose dependent and some genes behaving predictably as a function of radiation dose at different time points after radiation can be used as a bio dosimeter.

The data analysis showed that 6 genes from drosophila melanogaster show linear response ($R^2 > 0.9$) with radiation dose at all time points after irradiation. Four of these genes have human homologues. Dropping off the lowest radiation dose (10 roentgen being very low for the fruit flies), 13 genes show a linear response with dose at all time points including 5 of 6 genes in whole data set. Of these 13 genes, 4 have human homologues and 8 have known functions. The Irbp (inverted repeat – binding protein) gene among the above is very important as it is a DNA repair gene. It is reasonable to predict that DNA damage is linear with radiation dose; thus, it is logical that some DNA repair genes may respond linearly in expression. Irbp has homologues in organisms that are as complex as humans and chimpanzees and in organisms as Japanese rice . The expression of this panel of gene, particularly those with human homologues, could potentially be used as the biological indicator of radiation exposure in dosimeter applications.

Thus we could use radiation to kill tumors more effectively or the development of a biological dosimeter could help people to estimate the risk of cancer caused due to their exposure to radiation.

ACKNOWLEDGMENTS

I would like to express my deepest gratitude to my major adviser Dr Michael Antosh for providing me an opportunity to work in his laboratory as a first graduate student. This dissertation would not have been possible without his continuous support, encouragement and valuable advice. I appreciate him for being patient and keep motivating me during my research work. His faith on me helped me to work as a self motivated independent researcher, exploit the potential on me and be mature as a scientist, which helped me to grow professionally and intellectually. As a mentor he provided me a platform that a good researcher needs.

I would also like to thank Dr Stephen M Kennedy, Elec, Computer and Bio Engineering, Dr Feruz Ganikhanov, Physics, Dr Niall G HOwlett, Cell and Molecular Biology as my committee members for giving their valuable time and input into my research during my comprehensive exams, dissertation proposal and dissertation defense as well.

I would like to thank Dr Leon N Cooper, Brown University for his constant motivation, encouragement and support during my work in Brown University. I would like to thank Dr Yana Reshetnyak and Dr Oleg Andreev, Physics for letting me work in their lab during my initial phase as a researcher.

Dr Leonard M Kahn's support as a graduate program director is an immense help for me and his suggestions are always valuable.

I would also like to thank my lab members for their help with experiments.

I would like to express my eternal gratitude and dedicate this work towards my family for their constant emotional support during this long journey.

I owe my thanks to my mom and dad for believing on me, my work and making me even stronger im my hard times to achieve my goal.

I greatly appreciate my son Soyuz's contribution towards this work by letting me work instead of spending time with me as a child.

Finally I am indebted to my husband Sandeep Shrestha for sacrificing his own comfort and wishes to make my dream come true. You have always been there to support me morally, emotionally and not letting me down. No words are enough to thank you.

I wold like to thank everybody who has helped me thoughout my PhD and made my journey easier.

PREFACE

This dissertation is written in the 'Manuscript Format' using the Thesis/ Dissertation template of University of Rhode Island. There are four manuscripts, each organized into a chapter. Tables and figures of each manuscript are listed under the corresponding chapter in the list of tables and figures.

The results of our studies presented here were published in four papers:

1. Antosh, M.P., Wijesinghe, D.D., **Shrestha, S.,** Lanou, R., Huang, Y.H., Hasselbacher, T., Fox, D., Neretti, N., Sun, S., Katenka, N. and Cooper, L.N., 2015. Enhancement of radiation effect on cancer cells by gold-pHLIP. *Proceedings of the National Academy of Sciences*, *112*(17), pp.5372-5376.
2. **Shrestha, S.,** Cooper, L.N., Andreev, O.A., Reshetnyak, Y.K. and Antosh, M.P., 2016. Gold nanoparticles for radiation enhancement in vivo. *Jacobs journal of radiation oncology*, *3*(1).
3. **Shrestha, S.,** Vanasse, A., Cooper, L.N. and Antosh, M.P., 2017. Gene Expression as a Dosimeter in Irradiated Drosophila melanogaster. *Journal of Computational Biology*, *24*(12), pp.1265-1274.
4. **Shrestha, S.,** Sah, Bindeshwar.,Vanasse, A., Cooper, L.N., Ma L., Chen, W., and Antosh, M.P. X-ray Induced Photodynamic Therapy with Targeted Copper-Cysteamine Nanoparticles in Mice. *In preparation of submission*

TABLE OF CONTENTS

LIST OF TABLES

CHAPTER 4

LIST OF FIGURES

CHAPTER 1 PAGE

CHAPTER 3

CHAPTER 4

CHAPTER 1

Published in Proceedings of National Academy of Sciences (PNAS) on

13th of April, 2015

Enhancement of Radiation Effect on Cancer Cells by Gold-pHLIP

Michael Antosh[a,b], Diluka Wijesinghe[c], Samana Shrestha[c], Robert Lanou[b], Yun Hu Huang[b,] Thomas Hasselbacher[a], David Fox[a], Nicola Neretti[a,d], Shouheng Sun[e], Natallia Katenka[f], Leon N Cooper[a,b], Oleg A. Andreev[c] and Yana K. Reshetnyak[c]

[a]Institute for Brain and Neural Systems, Brown University, 184 Hope St, Providence, RI, 02906

[b]Department of Physics, Brown University, 184 Hope St, Providence, RI, 02906

[c]Physics Department, University of Rhode Island, 2 Lippitt Rd, Kingston, RI, 02881

[d]Department of Molecular Biology, Cell Biology and Biochemistry, Brown University, 7 Ship St, Providence, RI, 02906

[e]Department of Chemistry, Brown University, 184 Hope St, Providence, RI, 02906

[f]Department of Computer Science and Statistics, University of Rhode Island, 9 Greenhouse Rd, Kingston, RI, 02881

Corresponding authors:

E-mail: reshetnyak@mail.uri.edu or Leon_Cooper@brown.edu

Authors Contribution

M.P.A., D.D.W., R.L., Y.H.H., T.H., D.F., S.Sun, L.N.C., O.A.A., and Y.K.R. designed research; M.P.A., D.D.W., and S. Shrestha performed research; M.P.A., N.N., N.K., L.N.C., O.A.A., and Y.K.R. analyzed data; and M.P.A., D.D.W., S.Shrestha, L.N.C., and Y.K.R. wrote paper.

Abstract

Previous research has shown that gold nanoparticles can increase the effectiveness of radiation on cancer cells. Improved radiation effectiveness would allow lower radiation doses given to patients, reducing side effects; alternatively, it would provide more cancer killing at current radiation doses. Damage from radiation and gold nanoparticles depends in part on the Auger Effect, which is very localized; thus, it is important to place the gold nanoparticles on or in the cancer cells. In this work, we use the pH-sensitive, tumor-targeting agent, pH Low Insertion Peptide (pHLIP), to tether 1.4 nm gold nanoparticles to cancer cells. We find that the conjugation of pHLIP to gold nanoparticles increases gold uptake in cells compared to gold nanoparticles without pHLIP, with the nanoparticles distributed mostly on the cellular membranes. We further find that gold nanoparticles conjugated to pHLIP produce a statistically significant decrease in cell survival with radiation, compared to cells without gold nanoparticles as well as to cells with gold alone. In the context of our previous findings demonstrating efficient pHLIP-mediated delivery of gold-nanoparticles to tumors, the obtained results serve as a foundation for further pre-clinical evaluation of dose enhancement.

Keywords: Tumor, acidity, targeting, gold nanoparticles, radiation

Statement of Significance

Nanometer-sized gold particles are shown to increase the effectiveness of radiation in killing cancer cells. Improved radiation effectiveness allows less radiation to be used,

reducing side effects to patients. Alternatively, more cancer killing could be had for current radiation doses. Here we used pH Low Insertion Peptide (pHLIP) to tether gold nanoparticles to membranes of cancer cells. This increases their effectiveness because the radiation/particle effect is very localized. We find that pHLIP significantly increases the amount of gold particles in cancer cells, as well as the amount of cancer cell death from radiation. This methodology is promising for clinical research, as previous results show efficient targeting of gold nanoparticles to tumors by pHLIP.

Introduction

Gold is an inert and generally non-toxic material with unique properties suitable for many applications such as cancer diagnosis and treatment (1-7). Nanometer-size gold particles have recently been shown to increase radiation damage to tumors (2,8-11). With enhanced radiation, the same level of tumor killing can be had with less radiation to a patient, reducing side effects of radiation treatments. Similarly, more tumor killing can be had for the levels of radiation that are currently given.

The increase in radiation effectiveness with gold nanoparticles is due largely to two causes. First, gold is capable of absorbing radiation at a significantly higher rate than tissue, up to about 100 times more for keV energies (2). Second, gold nanoparticles that interact with radiation can release extra electrons via the Auger Effect. The Auger Effect occurs when an atom releases electrons post-ionization. Multiple electrons, called Auger electrons, can be released per ionization. The Auger electrons usually have low enough energy so that their effect is localized to the area surrounding the gold nanoparticles; see for example figure 1 in ref.11. Thus, it is very important to

effectively deliver gold nanoparticles to cancer cells in tumors and locate them near DNA or other vital cellular structures and components.

Specific delivery can be accomplished by conjugating gold (or other nanoparticles) to antibodies or ligands that target overexpressed proteins on cancer cell surfaces; this approach has been actively explored for many years for delivery of small molecules. However, several recent studies have raised serious questions about the efficacy of targeting ligands on the nanoparticle accumulation in tumor tissues. Multiple reports have shown that targeted nanoparticles did not lead to increased tumor accumulation over non-targeted controls, although increased cellular uptake was observed in each case (12-14). In addition, histological studies showed that antibodies conjugated with gold nanoparticles do not penetrate deeply into tumors, but mostly stain peripheral tumor regions (15). The direct injection of micron-sized gold particles does not lead to tumor targeting, as particles stayed only at the injection site and were not able to diffuse even within a tumor, hindering tumor coverage (16).

Our approach is based on targeting of tumor acidity, which correlates with tumor malignancy (17-19). The pH-sensitive targeting agents we are developing are based on the action of a family of pHLIPs (pH Low Insertion Peptides), which can "sense" acidity at the surface of cancer cells and deliver diagnostic and therapeutic molecules to tumors of different origins (20-25). It was shown that pHLIP can promote fusion of liposomes with cancer cells and cellular delivery of various payloads (26, 27) including small gold nanoparticles (26). Recently, pHLIP was successfully employed

for the targeting of various nanoparticles to tumors and other acidic diseased tissue (28-31).

pHLIP has also been used to mediate pH-controlled delivery of both 13 nm water soluble gold nanoparticles coated with luminescent europium into human platelets in vitro (32), and 1.4 nm gold nanoparticles to tumors (33). Intratumoral and i.v administrations of both demonstrated a significant enhancement of tumor uptake of 1.4 nm gold nanoparticles conjugated with pHLIP. Statistically significant reduction of gold accumulation was observed in acidic tumors and kidney when pH-nonsensitive K-pHLIP was used as a vehicle, suggesting an important role of pH in the pHLIP-mediated targeting of gold nanoparticles.

In this work, we made another important step toward clinical application of 1.4 nm gold nanoparticles conjugated with pHLIP. We show that pHLIP can deliver gold to cellular components in a pH-dependent manner and enhance the radiation damage in cells.

Results

In this work we used 1.4 nm diameter gold clusters functionalized with maleimide. Maleimide-gold clusters were conjugated with WT-pHLIP containing a single Cys residue at the N-terminus:

ACEQNPIYWARYADWLFTTPLLLLDLALLVDADET

After conjugation, the construct was purified, lyophilized, redissolved in DMSO, quantified and used in experiments with cells. As a control (gold alone) we used non-functionalized 1.4 nm gold clusters.

Cellular Uptake and Distribution of Gold

We investigated uptake of gold nanoparticles at normal and low pHs (pH 7.4 and 6.0, respectively), with and without pHLIP on human lung carcinoma (A549 cells). At pH 6.0 pHLIP was found to increase cellular uptake of gold nanoparticles by 34% compared to gold nanoparticles alone (p value 0.023) (Fig.1 and *SI Appendix*, Table S1). The uptake of pHLIP-gold at pH 6.0 increased by 53% compared to the uptake at pH 7.4 (p value 0.008). The uptake of gold alone was also enhanced at pH 6.0 compared with pH 7.4 (P value = 0.014). The uptake of gold-pHLIP was ~60% of the treated dose (1.8µg), which was about 1.1µg gold. Because each treatment had ~1 million cells, the amount of gold per cell was ~ $1.1X10^{-6}$ µg. We expect that uptake of pHLIP-gold at normal pH by noncancerous cells will be much lower, since pH at the surface of glycolytic cancer cells is about 6.6-6.8 even when bulk pH of media is 7.4 (unpublished data). The uptake of gold alone was also enhanced at pH 6.0 compared to pH 7.4 (p value 0.014).

Light microscopy was used to establish the distribution of gold nanoparticles in cells. Bright field images of cells treated with gold-pHLIP or gold alone and enhanced with silver are shown in Figure 2. The cellular uptake of gold-pHLIP is higher compared to the uptake of gold alone (Figure 2A and -B; the images are taken using 20x objective). The representative bright field image of cell treated with gold-pHLIP and enhanced

with silver obtained at high magnification is shown in figure 2C (the image is taken using 100x objective). The overlay of fluorescent images of nuclear stained with DAPI (blue) and cellular membrane stained with HQ silver deposited on the gold-nanoparticles (red) are shown in figure 2D. The targeting of the plasma membrane by gold-pHLIP is clearly seen on all images. We also observed some staining of internal organels and nuclei membranes. Targeting of mitochondria and nuclear membranes was observed in experiments with pHLIP-coated liposomes containing lipids conjugated with fluorescent dyes and gold nanoparticles (27).

Clonogenic Assay

Clonogenic assay experiments were performed to assess cell survival after treatment of cells with gold or gold-pHLIP and radiation of treated and non-treated cells. The results of the experiments are summarized in figure 3 and *SI Appendix*, Tables S2-S5.

We tested 0, 1.5 and 3 Gray of radiation. Gold nanopoarticles alone or conjugated with pHLIP were not toxic for cells in the absence of radiation. For 1.5 Gray of radiation, we observed a statistically significant 24% decrease in survival for cells treated with gold-pHLIP at low pH, as compared to cells treated with no gold. We also observed a statistically significant 21% decrease in survival for cells treated with gold-pHLIP at low pH as compared to cells treated with gold alone. The effect of gold was not significant at 3 Gray of radiation, likely because the survival of cells at 3 Gray was low.

Two different methodologies were used: excess of gold or gold-pHLIP was removed after treatment with cells before radiation, or excess of gold and gold-pHLIP was not

removed (non-removal corresponds with the values shown in red in *SI Appendix*, Tables S2-S5). The clonogenic assay results in Fig. 3A include data obtained at both different methodologies. Fig. 3B shows the data obtained in the experiments when gold constructs were not removed before radiation. Surprisingly, overall the non-removal data have better survival than the removal data; perhaps this is a result of the removal process stressing the cells.

We assessed statistical significance for data obtained at 1.5 Gray of radiation by performing an analysis of variance (ANOVA), summarized in Table 1 and *SI Appendix*, Table S6. When determining the p values between different gold treatments, we accounted for the difference in methodology as an additional variable in the analysis of variance (see *Methods* section for more details). Our data clearly indicate that cell treatment with gold-pHLIP results in a statistically significant decrease in cell survival as compared to a treatment with no gold (p value $3.6 \cdot 10^{-5}$) or gold alone (p value = 0.015).

In a separate experiment, cells were treated with gold constructs at pH 7.4, where pHLIP is less effective at inserting into the cellular membranes. Only small and statistically insignificant differences in survival between non-treated and treated cells were seen; the data is given in *SI Appendix*, Tables S2, S3, and S5.

Discussion

The treatment of cancer involves a trade-off between killing all cancer cells and impacting healthy tissue and organs as little as possible. To reduce side effects and enhance lethal effects of radiation for cancer cells the approaches of binary therapy

were introduced. Binary radiation therapy targets cells at the biological level with a noncytotoxic agent that is "activated" by low energy radiation, thereby destroying cancer cells wherever they may reside, while sparing normal cells in proximity to the diseased cells. A number of binary radiation therapies have been and are being explored (9, 34-36) one of the more promising approaches is based on dose enhancement through Auger electron emission secondary to the photoelectric effect dominant at low photon energies. Auger electron emission generates a cascade of low-energy electrons that travel very short distances and deposit their energy locally. The number of Auger electrons generated in targeted cells can be increased significantly by introducing material of a high atomic number (high-Z) into the target as long as the radiation energy is at or near the K, L, or M electron shell binding energies for the material. High-Z nanoparticles made of iodine, gadolinium, or gold are predicted to produce a clinically achievable dose enhancement of as much as 10 fold. Because low energy electrons travel very short distances, it is crucial to deliver and accumulate high-Z material on or in cancer cells in tumors.

Our strategy is to deliver gold, which is an inert, high-Z material widely used in medicine, to cancer cells for enhancement of radiation effects. The delivery approach we propose is based on the energy of membrane-associated folding of peptides from the pHLIP family to target cellular membranes in a pH-dependent manner (22, 24, 37). At pH <7.0 pHLIPs insert into the lipid bilayer of the membrane, which is accompanied by a coil-helix transition and formation of a transmembrane helix. It has been shown that pHLIP delivery agents can target acidic tumors with high accuracy

and deliver nanoparticles, including gold, to cancer cells in tumors (33). In this work, we show the effect of gold-pHLIP on radiation-induced cell death.

The dose enhancement depends strongly on the photon energies used for irradiation, as well as on the location and the size of gold nanoparticles. Regarding the photon energy, the ratio of gold absorption to human absorption is highest between ~10 and 100keV, with the ratio reaching approximately as high as 100 (2). We used 250 kVp X-rays with Sn-Thoraeus filtering to use the high relative absorption by gold while also accounting for the fact that lower-energy photons will be absorbed at too small of a depth to be useful. Regarding the location, it is very important to deliver gold nanoparticles as close as possible to cancer cells, as the dose deposited by Auger electrons increases as distance from the gold nanoparticles decreases(11). We used pHLIP to locate the gold nanoparticles to cancer cells. Regarding the nanoparticle size, it is best to use as small a gold nanoparticle size as possible to minimize the energy deposited inside the gold by Auger electrons. Simulations by McMahon et al. (11) predict an increase in relative biological effectiveness for decreasing sizes of gold nanoparticles. We used 1.4-nm –diameter gold nanoparticles.

The results of our present study indicate that pHLIP causes cells to take up more 1.4-nm gold nanoparticles than cells without pHLIP. The gold nanoparticles deposited by pHLIP mostly accumulate on the plasma membrane. As a result, gold nanoparticles delivered to cells by pHLIP can enhance radiation-induced decreases in cell survival. Gold nanoparticles tethered to the lipid bilayer of the plasma membrane by pHLIP may trigger cell death by inducing oxidation of lipids, cholesterol and membrane proteins. The oxidized lipids are known to modify membrane physical properties, such

as thickness, permeability, level of hydration and polarity, lipid transbilayer diffusion, loss of lipid asymmetry and phase segregation, which results in apoptosis (38, 39). The exposure of phosphatidylserine lipids to the outer leaflet of the lipid bilayer, promoted by lipid oxidation, serves as a recognition signal for macrophages to phagocytose the apoptotic cell (40).

The combination of the clonogenic and uptake results suggests that pHLIP is able to enhance radiation-induced death by targeting cancer cells and increasing gold uptake. This is particularly important for future pre-clinical testing. Experiments on cultured cells reflect steady-state conditions, when constructs are exposed to cancer cells during the time of incubation. However, *in vivo* studies reflect kinetic conditions, when blood flow is high and constructs have limited time to reach cancer cells and accumulate there. Our previous *in vivo* studies indicate that pHLIP targeting of 1.4 nm gold nanoparticles to tumors was 11 and 6 times higher compared to tumor targeting by gold alone (when administrated intratumorally and intravenously, respectively) (33). Thus, in an upcoming experiment on mice, we expect to observe more significant enhancement of radiation-induced cancer killing in mice compared to data obtained on cells. This might open a new avenue for the treatment of acidic, highly metastatic tumors in humans.

Methods

Materials: Materials include nonfuctionalized (from Nanoprobes), monomaleimido nanogold (from Nanoprobes), Cys-pHLIP (synthesized and purified by CS Bio), Tris-(2-carboxyethyl) phosphine, hydrochloride (from Life Technologies), Dulbecco's

Modified Eagle's Medium (from Sigma Aldrich), gluteraldehyde [25%(wt/wt) in water; from Sigma Aldrich], crystal violet (from Sigma Aldrich), Synaptophysin (from Molecular Probes by Life Technologies), DAPI (from Sigma Aldrich) and silver enhancement reagent (from Nanoprobes). Cell type was human lung carcinoma A549 cells (from American Type Culture Collection).

Preparation of Gold (Gold Alone), Gold conjugated to pHLIP (Gold-pHLIP): Gold nanoparticles were cluster gold, 1.4 nm diameter, from Nanoprobes, Inc. Monomaleimido nanogold was conjugated to Cys-pHLIP in 40 mM phosphate buffer containing 300 mM NaCl at pH 6.5. A reducing agent, Tris-(2-carboxyethyl) phosphine, was added into the reaction mixture (10x excess compared to pHLIP) to reduce pHLIP-S-S-pHLIP dimers and promote reaction with gold-malemide . The reaction vial was incubated overnight at room temperature on shaker. The next day, the gold-pHLIP conjugates were purified using Amicon Ultra (10K) centrifugal filters according to company recommended protocol. The product was then lyophilized, redissolved in DMSO. The concentration of peptide and nanogold was determined by absorbance at 280 nm (ε =13,940 M^{-1} cm^{-1}) and 420 nm (ε =155,000 M^{-1} cm^{-1}), respectively Nonfunctionalized gold (gold alone) was dissolved in DMSO and quantified using absorbance of gold at 420 nm.

Cellular Uptake of Gold: Approximately 1 million cells A549 were treated with 0.3 μM of either gold Alone or gold-pHLIP in cell suspension in serum free DMEM at pH 6.0 and 7.4 for 1 hour. One nanogold particle(1.4nm in diameter) contains, on average,

60 gold atoms, and 0.3uM particles in 0.5mL solution correspond to 1.8µg of gold. After 1 hour of treatment, the cells were pelleted using centrifugation (2,000 rpm x g for 5 min) followed by removal of treatment and washing cells with PBS three times. The cells were then dissolved in concentrated nitric acid followed by sonication for about 2 hours. Concentrated solution samples were diluted to give 2%(wt/vol) nitric acid and analyzed via inductively coupled plasma mass spectroscopy (Thermo-Scientific x7 series) against calibration standards (IMS 103; UltraScientific).

Cellular Distribution of Gold: About 20,000 A549 cells were seeded on collagen coated glass bottom dishes (MatTek) in 200 µl volume. The next day, cells were treated for 1 hour with gold and gold-pHLIP at 0.5 µM concentration at pH 6.0 in DMEM with no FBS. After treatment, the cells were washed 3 times with PBS followed by fixation in 4% formaldehyde for 20 min. The cells were permeabalized with 0.3% Triton X100 for 5 min, followed by washing with PBS and deionized water. Next, the cells were developed with freshly prepared HQ Silver reagent (Nanoprobes) for about 20 min, followed by washing with deionized water. Finally the cells were stained with 5 µM DAPI in PBS for 5 min, followed by washing with deionized water. The cells were imaged using light microscope in bright field regime to visualize gold enhanced by silver, and in the fluorescent regime to monitor DAPI and silver fluorescence using cut off filters (ex:em 360 nm/460 nm andex:em 542 nm/620 nm, respectively).

Irradiation of Cells: Irradiation was done using a Philips RT 250 X-ray machine, at settings of 250 kVp and 15 mA. A 0.4 mm Sn-Thoraeus Filter was used. The half-value thickness for this setup is listed as 2.8mm Cu. The dose rate was ~ 1.5 Gray/minute for each irradiation. Calibration readings were performed before each measurement using a Radcal 2026C dosimeter, and the reading was corrected for differences in temperature and pressure from standard temperature and pressure. The irradiation dose varied by ~ 7% between the center of the cell dish and the rightmost well in the irradiation plate that we used (there was ~ 1-2% variation in the leftmost well); the rightmost well was only used in experiments 7-11 and there were always at least 3 wells used per treatment.

Clonogenic Assay: The day before irradiation, 25,000 A549 cells per well were seeded in 48-well plates the day before irradiation. One plate with different treatment conditions was used for each radiation dose. The next day, the cells were treated with no gold, gold alone or gold-pHLIP at 8 µM concentration in 300 µl DMEM with no FBS at pH 6.0 for 3h. In experiment 11, the medium pH during treatment was 7.4 instead of 6.0. In one set of experiments, the excess of gold was removed and 500 µl of fresh DMEM medium of pH 7.4 with 10% FBS was added. In the other set of experiments the excess of gold was not removed, then 200 µl of fresh DMEM medium of pH 7.4 with 25% serum was added into wells to have 10% of FBS in final volume in the well. The treatment period was ~ 3 h.

Cells were irradiated as described in the irradiation methods; control cells accompanied the irradiated cells to and from the x-ray machine. Irradiated cells were

dissociated and combined for each treatment type, counted (using a Coulter Counter Z1 instrument from Beckman Coulter for experiments 1-11 and an Auto T4 instrument from Nexcelom Bioscience for experiments 12-17) and then reseeded in a 6-well plate. Two hundred cells per well were seeded for 0- and 1.5- Gray radiation doses and 500 cells per well were seeded for 3- Gray radiation dose. In generally, six wells were seeded per treatment type; the number of entries in SI Appendix, Table S2 is the number of wells. A table entry with 12 values represents a treatment that was done twice in the same experiment, with the results combined. After ~ 10 days, each well was fixed and stained using a 2- mL mixture of 4% glutaraldehyde and 0.5% crystal violet in distilled water. Stained cell colonies were hand-counted under a microscope. A colony was defined as a distinct group of cells that contained 50 or more cells.

Analysis of Cellular Uptake Data: The values in SI Appendix, Table S1 are six readings from a mass spectrometer. P values for statistical significance were computed using the t test, because the between-reading variance was much greater than the error in each reading.

Analysis of Clonogenic Assay Data: To calculate statistical significance, the data summarized in SI Appendix, Tables S2-S5 were analyzed using an ANOVA, followed by a post hoc test using Tukey's Honest Significant Difference. Each individual measurement from the clonogenic assay dish was treated as a biological replicate, and normalized to the average of the "0 Radiation, No Gold" measurements from the same experiment.

The linear model fitted for the ANOVA had three variables: normalized survival (dependent variable), gold treatment (independent variable) and removal/non-removal of excess gold (independent variable). We left the data for 0 Radiation out of the analysis because normalizing by the "0 Radiation, No Gold" data points introduces a correlation if we use the data by which we are normalizing. We analyzed the data for 1.5 Gray and 3 Gray separately because we were only really interested in the effect at 1.5 Gray.

In the 1.5 Gray data, the interaction term between gold treatment and removal/non-removal was significant. This is consistent with the gold treatments having different effectiveness depending on whether or not the excess gold was removed.

We also did one experiment at high pH, as mentioned in the results section. This was analyzed with a separate analysis of variance. The data are included as experiment 11 in *SI Appendix*, Tables S2. S3, and S5.

In Fig. 3, error shown is the SEM (41). SE was calculated using R, as SD divided by square root of the number of samples. In checking the procedure for this calculation, we used StatPlus, version v5 (AnalystSoft Inc.).

Acknowledgements

We'd like to thank Susan Hall and her laboratory for help with irradiation, and Anna Moshnikova for help in the experiments with cells. We also thank Professor Jean Wu at Brown University for a helpful conversation regarding statistics. The inductively coupled plasma mass spectroscopy measurements presented in this publication were

performed and supported by an Institutional Development Award from the National Institute of General Medical Sciences of the NIH under grant 2 P20 GM103430.

This work was supported by NIH grants CA133890 and GM073857 (to O.A.A and Y.K.R)

Author Contributions

Designed Experiment: Andreev, Reshetnyak, Cooper, Antosh, Wijesinghe, Lanou, Sun, Hasselbacher, Fox, Huang; **Performed Experiment**: Antosh, Wijesinghe, Shrestha; **Analyzed Data**: Antosh, Katenka, Neretti, Andreev, Reshetnyak, Cooper; **Wrote Paper**: Antosh, Reshetnyak, Cooper, Wijesinghe, Shrestha.

References

1. Black KC, et al. (2008) Gold nanorods targeted to delta opioid receptor: Plasmonresonant contrast and photothermal agents. Mol Imaging 7(1):50–57. 2
2. Hainfeld JF, Dilmanian FA, Slatkin DN, Smilowitz HM (2008) Radiotherapy enhancement with gold nanoparticles. J Pharm Pharmacol 60(8):977–985.
3. Hainfeld JF, Slatkin DN, Focella TM, Smilowitz HM (2006) Gold nanoparticles: A new X-ray contrast agent. Br J Radiol 79(939):248–253.
4. Huang X, Jain PK, El-Sayed IH, El-Sayed MA (2007) Gold nanoparticles: Interesting optical properties and recent applications in cancer diagnostics and therapy. Nanomedicine (Lond) 2(5):681–693.
5. Jain PK, El-Sayed MA (2007) Universal scaling of plasmon coupling in metal nanostructures: Extension from particle pairs to nanoshells. Nano Lett 7(9):2854–2858
6. Mahmoud MA & El-Sayed MA (2010) Gold nanoframes: very high surface plasmon fields and excellent near-infrared sensors. *J Am Chem Soc* 132(36):12704-12710.
7. von Maltzahn G, et al. (2009) Computationally guided photothermal tumor therapy using long-circulating gold nanorod antennas. Cancer Res 69(9):3892–3900.
8. Babaei M, Ganjalikhani M (2014) The potential effectiveness of nanoparticles as radio sensitizers for radiotherapy. Bioimpacts 4(1):15–20.
9. Hainfeld JF, Slatkin DN, Smilowitz HM (2004) The use of gold nanoparticles to enhance radiotherapy in mice. Phys Med Biol 49(18):N309–N315.

10. Jain S, et al. (2011) Cell-specific radiosensitization by gold nanoparticles at megavoltage radiation energies. Int J Radiat Oncol Biol Phys 79(2):531–539.

11. McMahon SJ, et al. (2011) Biological consequences of nanoscale energy deposition near irradiated heavy atom nanoparticles. Sci Rep 2011;1:18.

12. Sonvico F, et al. (2005) Folate-conjugated iron oxide nanoparticles for solid tumor targeting as potential specific magnetic hyperthermia mediators: Synthesis, physicochemical characterization, and in vitro experiments. Bioconjug Chem 16(5):1181–1188.

13. Kirpotin DB, et al. (2006) Antibody targeting of long-circulating lipidic nanoparticles does not increase tumor localization but does increase internalization in animal models. Cancer Res 66(13):6732–6740.

14. Huang X, et al. (2010) A reexamination of active and passive tumor targeting by using rod-shaped gold nanocrystals and covalently conjugated peptide ligands. ACS Nano 4(10):5887–5896.

15. Hainfeld JF, et al. (2011) Micro-CT enables microlocalisation and quantification of Her2-targeted gold nanoparticles within tumour regions. Br J Radiol 84(1002): 526–533.

16. Herold DM, Das IJ, Stobbe CC, Iyer RV, Chapman JD (2000) Gold microspheres: A selective technique for producing biologically effective dose enhancement. Int J Radiat Biol 76(10):1357–1364

17. Damaghi M, Wojtkowiak JW, Gillies RJ (2013) pH sensing and regulation in cancer. Front Physiol 4:370.

18. Gillies RJ, Verduzco D, Gatenby RA (2012) Evolutionary dynamics of carcinogenesis and why targeted therapy does not work. Nat Rev Cancer 12(7):487–493.

19. Robey IF, et al. (2009) Bicarbonate increases tumor pH and inhibits spontaneous metastases. Cancer Res 69(6):2260–2268.

20. Adochite RC, et al. (2014) Targeting breast tumors with pH (low) insertion peptides. Mol Pharm 11(8):2896–2905

21. Cruz-Monserrate Z, et al. (2014) Targeting pancreatic ductal adenocarcinoma acidic microenvironment. Sci Rep 4:4410.

22. Andreev OA, Engelman DM, Reshetnyak YK (2014) Targeting diseased tissues by pHLIP insertion at low cell surface pH. Front Physiol 5:97.

23. Viola-Villegas NT, *et al.* (2014) Understanding the pharmacological properties of a metabolic PET tracer in prostate cancer. *Proc Natl Acad Sci U S A* 111(20):7254-7259.

24. Weerakkody D, *et al.* (2013) Family of pH (low) insertion peptides for tumor targeting. *Proc Natl Acad Sci U S A* 110(15):5834-5839.

25. An M, Wijesinghe D, Andreev OA, Reshetnyak YK, & Engelman DM (2010) pH-(low)-insertion-peptide (pHLIP) translocation of membrane impermeable phalloidin toxin inhibits cancer cell proliferation. *Proc Natl Acad Sci U S A* 107(47):20246-20250.

26. Yao L, Daniels J, Wijesinghe D, Andreev OA, & Reshetnyak YK (2013) pHLIP(R)-mediated delivery of PEGylated liposomes to cancer cells. *J Control Release* 167(3):228-237.

27. Wijesinghe D, Arachchige MC, Lu A, Reshetnyak YK, & Andreev OA (2013) pH dependent transfer of nano-pores into membrane of cancer cells to induce apoptosis. *Sci Rep* 3:3560.

28. Emmetiere F, *et al.* (2013) (18)F-labeled-bioorthogonal liposomes for in vivo targeting. *Bioconjug Chem* 24(11):1784-1789.

29. Sosunov EA, *et al.* (2013) pH (low) insertion peptide (pHLIP) targets ischemic myocardium. *Proc Natl Acad Sci U S A* 110(1):82-86.

30. Han L, *et al.* (2013) pH-Controlled Delivery of Nanoparticles into Tumor Cells. *Adv Healthc Mater*.

31. Zhao Z, *et al.* (2013) A Controlled-Release Nanocarrier with Extracellular pH Value Driven Tumor Targeting and Translocation for Drug Delivery. *Angew Chem Int Ed Engl* 52(29):7487-7491.

32. Davies A, Lewis DJ, Watson SP, Thomas SG, & Pikramenou Z (2012) pH-controlled delivery of luminescent europium coated nanoparticles into platelets. *Proc Natl Acad Sci U S A* 109(6):1862-1867.

33. Yao L, *et al.* (2013) pHLIP peptide targets nanogold particles to tumors. *Proceedings of the National Academy of Sciences of the United States of America* 110(2):465-470.

34. Morris KN, Weil MD, & Malzbender R (2006) Radiochromic film dosimetry of contrast-enhanced radiotherapy (CERT). *Physics in medicine and biology* 51(22):5915-5925.

35. Norman A, et al. (1997) X-ray phototherapy for canine brain masses. Radiat Oncol Investig 5(1):8–14.

36. Tisljar-Lentulis G, Feinendegen LE, Bond VP (1973) [Biological radiation effects of inclusion of moderately heavy nuclei into the tissue and use of soft roentgen rays]. Strahlentherapie 145(6):656–662.

37. Karabadzhak AG, *et al.* (2012) Modulation of the pHLIP transmembrane helix insertion pathway. *Biophys J* 102(8):1846-1855.

38. Kinnunen PK, Kaarniranta K, & Mahalka AK (2012) Protein-oxidized phospholipid interactions in cellular signaling for cell death: from biophysics to clinical correlations. *Biochimica et biophysica acta* 1818(10):2446-2455.

39. Volinsky R & Kinnunen PK (2013) Oxidized phosphatidylcholines in membrane-level cellular signaling: from biophysics to physiology and molecular pathology. *The FEBS journal* 280(12):2806-2816.

40. Leventis PA & Grinstein S (2010) The distribution and function of phosphatidylserine in cellular membranes. *Annual review of biophysics* 39:407-427.

41. Altman DG, Bland JM (2005) Standard deviations and standard errors. BMJ 331(7521):903.

Tables

Table 1. Summary of ANOVA results for 1.5 Gray radiation. Detailed results are in *SI Appendix*, Table S6.

Model Normalized Survival=Treatment+Removal+(Treatment·Removal)	
	P Values
No Gold vs. Gold pHLIP	$3.64 \cdot 10^{-5}$
Gold pHLIP vs. Gold Alone	0.015
No Gold vs. Gold Alone	0.832
Removal vs. Non-Removal	$5.95 \cdot 10^{-6}$

Figures

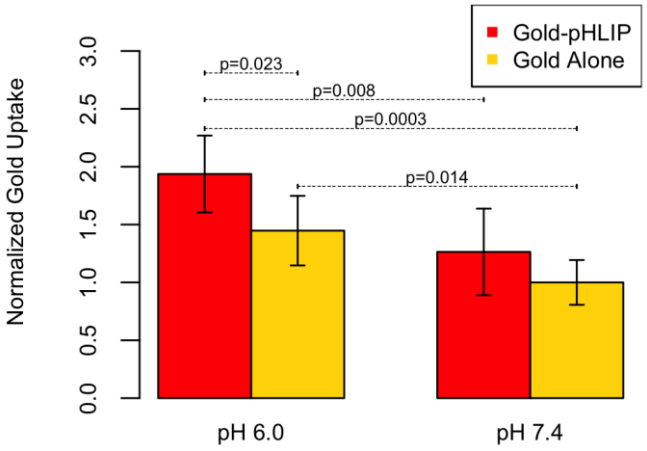

Figure 1. Cellular uptake of gold. Values are averaged from normalized readings on a mass spectrometer, as detailed in *Methods*. All measurements are given in *SI Appendix*, Table S1. Data are normalized to gold Alone at pH 7.4.

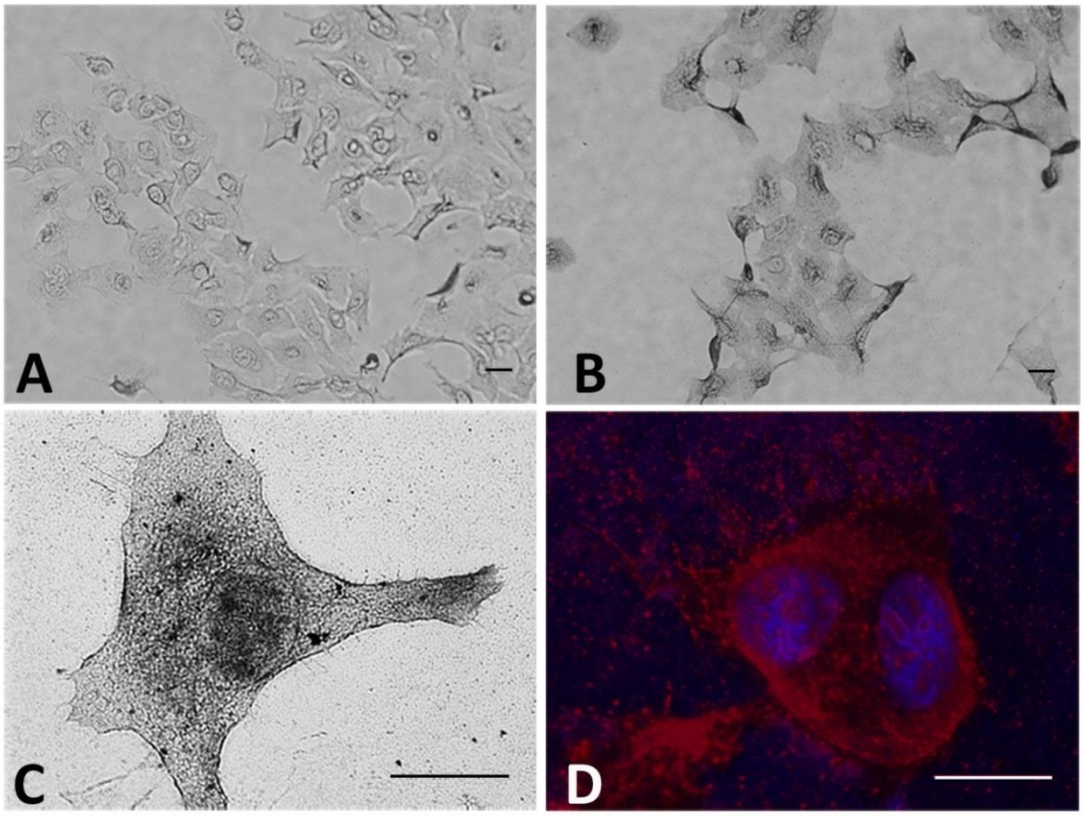

Figure 2. Gold distribution in cells. The bright field (A-**C**) and fluorescence (D) images of cells treated with gold (A) and gold-pHLIP (B-D), followed by washing, fixation and enhancement with HQ silver, are shown at different magnifications (the bar on each image shows 10 μm- scale). The overlay of fluorescent images of nuclear stained with DAPI (blue) and cellular membrane stained with HQ silver (red) are shown on D.

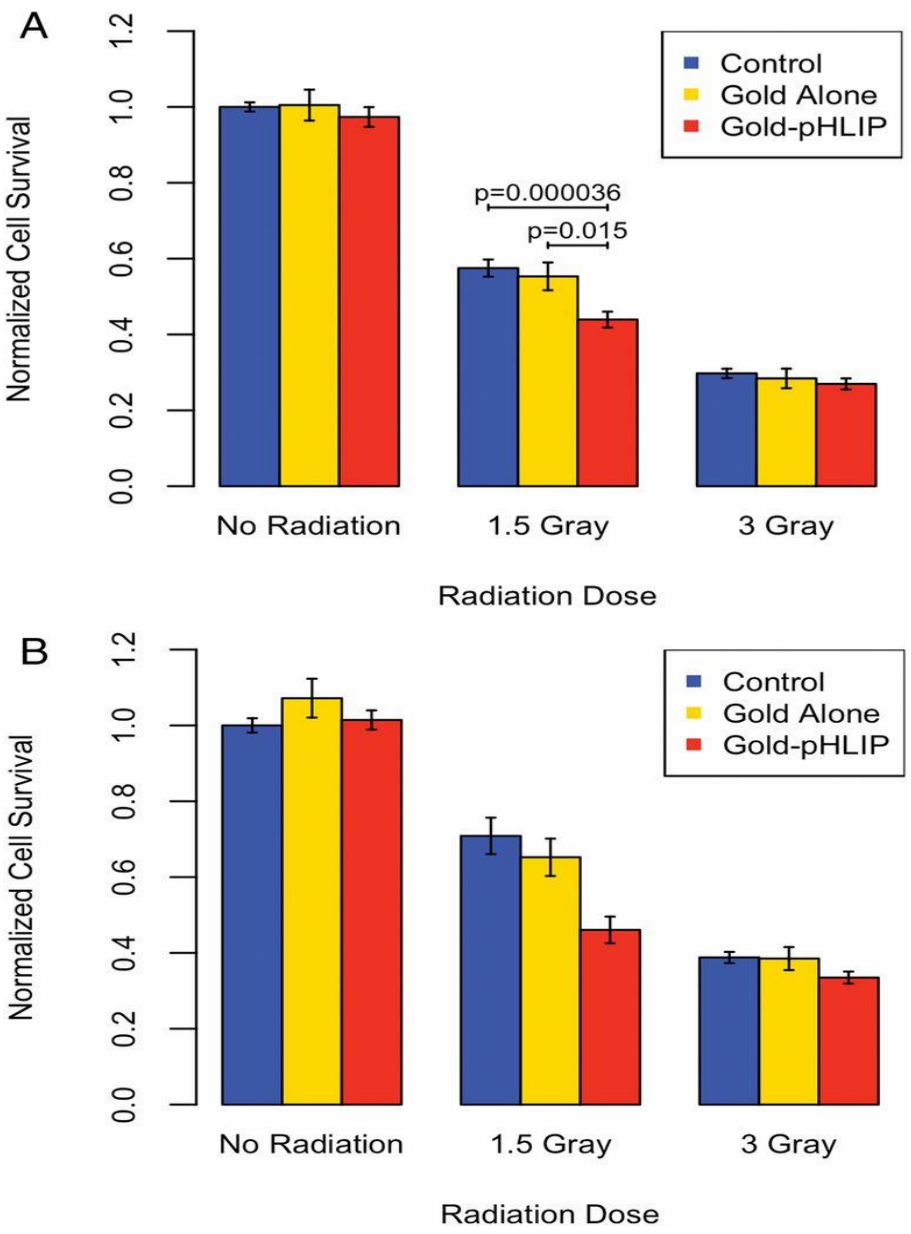

Figure 3: Average cell survival after radiation and treatment (or no treatment, control) with gold or gold-pHLIP at pH 6.0. The data shown in A are from the experiments with either removal or non-removal of excess gold before radiation. The data shown in B are only from the experiments with non-removal of excess gold before radiation. Error shown is SEM.

Supplementary Information (SI) Appendix

Table S1. Cellular uptake of gold-pHLIP and gold. The mean and standard deviation of these data points are presented in figure 1, and the calculation of statistical significance is described in the methods section. Data are normalized so that Gold Alone, pH 7.4 has a mean of 1.

Gold-pHLIP, pH 6.0	1.602±0.038, 1.538±0.013, 2.441±0.012, 2.006±0.006, 2.012±0.006, 2.023±0.000
Gold-pHLIP, pH7.4	0.838±0.006, 0.901±0.010, 1.525±0.006, 1.246±0.003, 1.826±0.004, 1.246±0.006
Gold Alone, pH 6.0	1.023±0.005, 1.122±0.006, 1.733±0.004, 1.687±0.005, 1.542±0.004, 1.577±0.006
Gold Alone, pH 7.4	1.004±0.008, 0.996±0.005, 1.339±0.004, 1.032±0.006, 0.835±0.012, 0.794±0.002

Table S2. Clonogenic Assay Colony Counts. For 0 and 1.5 Gray radiation, 200 cells were seeded; 500 cells were seeded for 3 Gray radiation. Treatment for experiments 1-10 and 12-17 were done at pH 6.0; experiment 11 was done at pH 7.4. The values shown in red were obtained in the experiments where excess of gold constructs was not removed before radiation; the other data were obtained in the experiments where the excess gold was removed before radiation. The input for the analysis of variance (detailed in the methods section) was the values from this table, divided by the mean of the "0 Radiation, No Gold" values for its corresponding experiment.

	Exp.1	Exp.2	Exp.3	Exp.4	Exp.5	Exp.6	Exp.7	Exp.8	Exp.9	Exp.10	Exp.11	Exp.12	Exp.13	Exp.14	Exp.15	Exp.16	Exp.17
0 Radiation, No Gold	102,98, 99	32,24,2 5,32,32 ,31,35, 28,32,3 6,35,33	69,76,8 9,83,73 ,90,82, 72,77,8 5,64,86	54,35, 44,49, 42,47, 55,59, 40,58, 54,48	59,54, 51,73, 65,65	60,49, 43,62, 55,70	55,54,4 8,43,48 ,57	54,47,5 5,59,57 ,52	39,39,4 6,47,33, 45,	48,47,6 3,64,58 ,73,57, 33,63,7 1,62,57	74,50, 67,57, 70,72, 72,69, 77,69, 63,82	49, 38, 53, 33, 50, 44,41, 50, 64, 67, 69, 50	62, 61, 54, 64, 57, 61,59, 56, 60, 50, 43, 53	42, 40, 52, 59, 40, 49,33, 47, 37, 43, 38, 47	39, 45, 49, 41, 37, 48,48, 52, 50, 57, 49, 49	65, 49, 44, 55, 46, 42,37, 43, 39, 34, 33, 34	57, 54, 50, 54, 64, 49,37, 32, 42, 37, 47, 42
0 Radiation, Gold Alone			81,66,9 6,70,47 ,88						47,37,4 8,30,42, 44	59,53,6 9,71,56 ,65	67,49, 53,68, 56,65						
0 Radiation, Gold pHLIP									24,26,4 5,34,23, 36	71,53,5 6,66,54 ,55	63,51, 66,48, 49,56	45, 57, 43, 40, 41, 38	53, 62, 58, 65, 53, 55	44, 44, 38, 32, 42, 46	42, 50, 41, 42, 51, 44	56, 63, 41, 50, 48, 48	49, 65, 44, 41, 50, 51
1.5 Gray Radiation, No Gold	80,58, 59	12,16,1 1,18,15 ,13,14, 14,16,1 9,15,22	33,45,4 5,28,34 ,40	27,21, 26,20, 16,27	46,37, 43,31, 28,46		46,25,3 0,32,32 ,18	26,23,2 1,31,19 ,31	23,32,2 5,24,21, 27	59,46,5 6,62,36 ,53	50,37, 38,61, 44,51						
1.5 Gray Radiation, Gold Alone			56,31,3 6,56,33 ,29						30,16,2 4,18,12, 24	37,39,4 1,31,30 ,49	57,37, 41,49, 34,49						
1.5 Gray Radiation, Gold-pHLIP					34,20, 28,43, 28,26	27,27, 36,25, 23,29	16,17,1 7,21,12 ,18	23,22,2 0,30,15 ,22	16,15,1 6,18,10, 13	36,28,3 9,29,20 ,44	41,34, 39,45, 44,48						
3 Gray Radiation, No Gold	104,99, 85	27,17,3 1,25,22 ,34,21, 7, 21,39,2 2,14	44,26,3 7,54,35 ,52	43,27, 36,39, 24,26	59,57, 54,62, 43,53	29,25, 27,28, 31,35	52,45,5 5,44,42 ,56	27,21,2 4,35,31 ,27	33,25,2 9,34,21, 33	61,44,7 2,50,66 ,73	60,53, 60,67, 53,55						
3 Gray Radiation, Gold Alone			44,24,4 2,39,41 ,26						36,33,4 1,20,16, 31	66,56,6 5,49,38 ,61	63,48, 49,50, 39,63						
3 Gray Radiation, Gold-pHLIP					58,46, 43,52, 46,39	32,29, 30,25, 17,24	39,33,4 7,52,57 ,50	35,33,2 9,18,23 ,23	21,18,2 7,28,20, 28	51,28,6 1,49,42 ,57	65,49, 60,62, 51,62						

Table S3. Summary of Clonogenic Assay Colony Counts: Means and St.D. Data are calculated using SI Appendix, table 2. The values shown in red were obtained in the experiments where excess of gold constructs was not removed before radiation; the other data were obtained in the experiments where the excess gold was removed before radiation

	Exp.1	Exp.2	Exp.3	Exp.4	Exp.5	Exp.6	Exp.7	Exp.8	Exp.9	Exp.10	Exp.11	Exp.12	Exp.13	Exp.14	Exp.15	Exp.16	Exp.17
0 Radiation, No Gold	100±2	31±4	79±8	49±8	61±8	57±10	51±5	54±4	42±5	58±11	69±9	51±11	57±6	44±7	47±6	43±9	47±9
0 Radiation, Gold Alone			75±18						41±7	62±7	60±8						
0 Radiation, Gold-pHLIP									31±9	59±7	56±8	44±7	58±5	41±5	45±4	51±8	50±8
1.5 Gray Radiation, No Gold	66±12	15±3	38±7	23±5	39±8		31±9	25±5	25±4	52±10	47±9						
1.5 Gray Radiation, Gold Alone			40±12						21±7	38±7	45±9						
1.5 Gray Radiation, Gold-pHLIP					30±8	28±4	17±3	22±5	15±3	33±9	42±5						
3 Gray Radiation, No Gold	96±10	23±9	41±11	33±8	55±7	29±3	49±6	28±5	29±5	61±12	58±5						
3 Gray Radiation, Gold Alone			36±9						30±10	56±11	52±9						
3 Gray Radiation, Gold-pHLIP					47±7	26±5	46±9	27±7	24±5	48±12	58±7						

Table S4. **Summary of Normalized Clonogenic Data for Low pH**. Cells were treated with the constructs at low pH before radiation. The average values from SI Appendix, table S3 were divided by the average for "0 Radiation, No Gold" for each experiment. The values shown in red were obtained in the experiments where excess of gold constructs was not removed before radiation; the other data were obtained in the experiments where the excess gold was removed before radiation.

	Exp.1	Exp.2	Exp.3	Exp.4	Exp.5	Exp.6	Exp.7	Exp.8	Exp.9	Exp.10	Exp.12	Exp.13	Exp.14	Exp.15	Exp.16	Exp.17
0 Radiation, No Gold	1	1	1	1	1	1	1	1	1	1	1	1	1	1	1	1
0 Radiation, Gold Alone			0.947						0.996	1.072						
0 Radiation, Gold-pHLIP									0.755	1.02	0.868	1.018	0.934	0.957	1.175	1.062
1.5 Gray Radiation, No Gold	0.659	0.493	0.476	0.468	0.629		0.6	0.466	0.61	0.897						
1.5 Gray Radiation, Gold Alone			0.51						0.498	0.652						
1.5 Gray Radiation, Gold-pHLIP					0.488	0.493	0.331	0.407	0.353	0.563						
3 Gray Radiation, No Gold	0.385	0.299	0.21	0.267	0.357	0.206	0.386	0.204	0.281	0.421						
3 Gray Radiation, Gold Alone			0.183						0.284	0.385						
3 Gray Radiation, Gold-pHLIP					0.31	0.185	0.365	0.199	0.228	0.331						

Table S5. Summary of Normalized Clonogenic Assay Data for High pH. Cells were treated with the constructs at normal pH before radiation. This table is analogous to SI Appendix, table S 4, which is for the low pH experiments.

	Exp.11
0 Radiation, No Gold	1.000
0 Radiation, Gold Alone	0.871
0 Radiation, Gold-pHLIP	0.810
1.5 Gray Radiation, No Gold	0.684
1.5 Gray Radiation, Gold Alone	0.650
1.5 Gray Radiation, Gold-pHLIP	0.611
3 Gray Radiation, No Gold	0.339
3 Gray Radiation, Gold Alone	0.304
3 Gray Radiation, Gold-pHLIP	0.340

Table S6. Detailed Results of ANOVA for 1.5 Gray Radiation.

Model **Normalized Survival = Treatment + Removal + (Treatment·Removal)**					
ANOVA Results					
	Degrees of Freedom	Sum of Squares	Mean Squares	F Value	P Value
Treatment	2	0.421	0.21	10.9	$4.96 \cdot 10^{-5}$
Removal	1	0.453	0.453	23.5	$4.39 \cdot 10^{-6}$
Treatment*Removal	2	0.122	0.061	3.2	0.0465
Residuals	105	2.026	0.019		
Posthoc Test Results					
	Difference in Means	Lower Bound of 95% Confidence Interval	Upper Bound of 95% Confidence Interval	Adjusted P Value	
No Gold vs. Gold-pHLIP	0.136	0.065	0.206	$3.64 \cdot 10^{-5}$	
Gold-pHLIP vs. Gold Alone	-0.114	-0.209	-0.019	0.015	
No Gold vs. Gold Alone	0.022	-0.068	0.111	0.832	
Removal vs. Non-Removal	-0.13	-0.184	-0.076	$5.95 \cdot 10^{-6}$	

CHAPTER 2

Published in Jacobs Journal of Radiation Oncology

27th of April, 2016

Gold Nanoparticles for Radiation Enhancement *in Vivo*

Samana Shrestha[a], Leon N Cooper[b,c] , Oleg A. Andreev[a], Yana K. Reshetnyak[a] and Michael P. Antosh[a,b]

[a]Physics Department , University of Rhode Island, 2 Lippitt Rd,Kingston, RI, 02881

[b]Institute for Brain and Neural Systems, Brown University, 184 Hope St, Providence, RI, 02906

[c]Department of Physics, Brown University, 184 Hope St, Providence, RI, 02906

Corresponding author : Dr. Michael Antosh, 2 Lippitt Rd, Kingston, RI, Tel: 401-874-2048

Abstract

Enhancing the effect of radiation on tumors would be a significant improvement in radiation therapy. With radiation enhancement, less radiation could be used to achieve the same goals, lessening damage to healthy tissue and lessening side effects. Gold nanoparticles are a promising method for achieving this enhancement, particularly when the gold nanoparticles are targeted to cancer. This literature review discusses the properties of gold nanoparticles as well as existing *in vivo* radiation enhancement results using both targeted and non-targeted gold nanoparticles.

Keywords

tumors; radiation; gold nanoparticles; enhancement; targeted; dose; mice

Abbreviations

GNP : Gold nanoparticles

PEG : Polyethylene Glycol

kVp : Kilovolt Peak

Gy : Gray

pHLIP : pH-Low Insertion Peptide

IV : Intravenous

CTR : Complete Tumor Regression

DTPA : Diethylenetriamine pentaacetic acid

BSA : Bovine Serum Albumin

Introduction

In radiation therapy for cancer, radiation is delivered after precise calculations so that a maximum dose is given to the tumor and a minimum dose is given to healthy tissue. Despite these efforts, radiation still affects healthy tissue. This effect is especially dangerous when the tumor is located near important organs. Thus, it is important in radiation therapy to reduce the dose and the damage to healthy tissues and organs(1).

One of the current strategies to reduce radiation is the use of radiation enhancers, which can absorb and make tumor cells more susceptible to it. They are designed to improve tumor cell killing, since making a tumor more susceptible to radiation means

that less radiation can be used. And if less radiation is used, there will be less adverse effects on normal tissues(2).

Radiation enhancers can include materials like nanoparticles, e.g. carbon nanotubes, gold nanoparticles and quantum dots. In this paper, we will focus on the use of gold nanoparticles (GNPs). Gold is a good radiation enhancer. The radiosensitization of biomolecules by GNPs can be caused by locally increased radiation absorbed energy. Gold, a high Z material, is capable of absorbing radiation at significantly higher rates than tissue. The advantage in absorption can grow to about a factor of 100 for certain keV photon energies (20 keV shown in (3), can be checked in a database (4)). Additionally, gold nanoparticles that interact with radiation can release a number of Auger electrons via the Auger effect. The Auger effect occurs when an excited atom (for example, an ionized gold atom) releases its extra energy in a form of an electron instead of a photon.

Radiosensitization can also be caused by modified sensitivity of targeted biomolecules to radiation (5). The efficiency of chemical radiosensitization mechanism is significantly influenced by the strong binding of GNPs to the biological target as DNA(5). Jain et al. (6) suggests a possible biological mechanism of radiosensitization by GNPs even in the absence of radiation, with GNPs potentiating the effect of bleomycin. The results showed that the GNPs caused chemosensitization to the radiomimetic agent bleomycin at a range of concentrations with a sensitizer enhancement ratio similar to that observed for the kilovoltage photons.

Auger electrons have comparatively low energies (approximately 80 keV or less in gold), and because of this they have a short range of action in tissues. It can result in

the delivery of a precise and lethal dose in their immediate vicinity. However, this short range also indicates that gold nanoparticles need to be located within tumors, near the vital cellular structures, in order to maximize the radiation enhancement effect(7, 8). This suggests the need for the gold nanoparticles to be targeted to cancer cells.

In this paper, we will review the use of gold nanoparticles as a radiation enhancer *in vivo*. Specific topics include:

- Properties of gold nanoparticles
- Important Experimental Variables
- *In vivo* radiation enhancement results for non-targeted gold nanoparticles
- Nanoparticle Targeting
- *In vivo* radiation enhancement results for targeted gold nanoparticles

Properties of Gold Nanoparticles

Gold nanoparticles properties include the following:

i) Gold is an inert material and can be made to be biocompatible using surface modification, like surface coating of the GNPs (2, 3, 6-17).

ii) Gold nanoparticles can be linked to biomolecules, either via stabilizers (polyethylene glycol, maleimide) or directly to sulfhydryl (-SH) groups of moieties such as peptides, antibodies, small molecules or proteins.

Tumor targeting can be achieved by conjugating the GNP surface to peptides, ligands, antibodies or drugs (2, 3, 6-9, 11-14, 16, 18, 19).

iii) Gold nanoparticles, as any nanoparticle, have a large surface to volume ratio. The relatively large surface area provides opportunity for interactions with molecules. Having large number of surface ligands, gold nanoparticles allow flexible design and multi-functionality by incorporating mixed ligands (3, 12, 18) .

iv) The nanoparticles including GNPs exhibit preferential deposition at tumor sites due to the enhanced permeation and retention (EPR) effect. This makes them to be effective as drug carriers and radiation enhancers (1, 8, 16). This is related to the small size of GNPs, and the leaky vasculature of tumors.

v) The size of GNPs can be tuned to a wide range (1-1000 nm) and various shapes (2, 3, 6, 9, 12, 18, 19).

Important Experimental Variables

The following variables are known to affect the amount of radiation enhancement that the gold nanoparticles are capable of delivering:

Concentration of gold: The concentration of gold nanoparticles in the tumor sites (and thus the number of gold atoms) affects the radiation enhancement capability. Hainfeld et al. (20)doubled the concentration of non-targeted gold nanoparticles (from 1.35 to 2.7 grams of Au per kilogram mouse weight), and increased survival by 72% (from 50% to 86%).

Size, Shape and Surface Chemistry of GNPs: There are various sizes and shapes of gold nanoparticles available, and this affects their uptake by the cells. Also, surface chemistry is an important parameter, which affects biodistribution and cellular uptake of nanoparticles. Chithrani et al. (21) found that the cellular uptake of spherical GNPs of 14, 30, 50, 74, 100 nm in diameter is size dependent. Cells *in vitro* had a maximum uptake for 50 nm sized spherical GNPs. The rod shaped nanoparticles exhibited less uptake by cells compared to spherical particles. For example, cells took up 500 and 375% more 74 and 14 nm spherical gold nanoparticles than 74 × 14 nm rod-shaped gold nanoparticles, respectively. The authors noted that in addition to size and shape of GNPs the surface chemistry might also affect cellular uptake of nanoparticles. Non-homogeneous coating of nanoparticles with citric acid ligands and presence of cetyl trimethylammonium bromide (CTAB) molecules at the surface of rod GNPs could result in lower cellular uptake. In an *in vitro* study of GNPs as radiation enhancers in cancer therapy, 50 nm spherical GNPs showed the highest radiosensitization enhancement factor (REF) (1.42 at 220kVp) compared to gold nanoparticles of 14 and 74 nm (1.20 and 1.26 respectively) (10). 12.1 and 27.3 nm size spherical GNPs coated with polyethylene glycol (PEG) showed high radiation enhancement compared to 4.8 and 46.6 nm size, both *in vitro* and *in vivo*, with accumulation of GNPs in the tumor with high concentration (22). This is in contrast to the computation study performed by McMahon et al.(17) , which predicts an increase in radiation enhancement with decreasing size of spherical GNPs. Puvanakrishnan et al.(23) compared cellular uptake for gold nanoshells and gold nanorods. The results indicated a higher accumulation of smaller rod GNPs in tumor compared to the larger nanoshell

GNPs . However, the accumulation of nanorods and nanoshells in the liver increased significantly for higher doses. This suggests that the particle shape and size significantly affects tumor targeting and confirms that the smaller particles have enhanced accumulation in tumors compared to larger nanoparticles. Huang et al. (24)found that GNPs smaller than 10 nm have unique advantages over GNPs greater than 10 nm in localization and penetration of breast cancer cells, multicellular tumor spheroids and tumors in mice. The *in vivo* results showed that 2 and 6 nm tiopronin-coated GNPs were distributed throughout the cytoplasm and nucleus whereas 15 nm samples became aggregated in the cytoplasm. Tumor bearing mice were intravenously injected with a dose of 5 mg of Au per kg of mice. After 24 hours the amount of gold in tumor was 2.93 micrograms per gram of tumor for 2 nm, 0.79 micrograms for 6 nm and 0.14 micrograms for 15 nm particles. Compared to 15 nm GNPs, the 2 nm and 6 nm GNPs were widely distributed in different organs of the body due to small structures. Histological analysis showed that GNPs had almost no effect on tissues including liver, spleen, kidney, lung and heart, indicating good tissue biocompatibility of the GNPs.

Cell Line Used in Studies with GNPs: Radiation enhancement by GNPs is cell line specific. They enhance the radiation when treated with some cells but not all. Significant radiosensitization occurred in MDA-MB-231 cells at 160 kVp. However, no significant radiosensitization was observed in DU 145 or L132 cells, even though there was uptake of GNPs in both of these cell lines. In an *in vitro* experiment, uptake of GNPs was greater in MDA-MB-231 cells than in DU 145 or L132 cells, and hence radiation enhancement was better in MDA-MB-231 cells. (6).

Intracellular Localization of GNPs: The location of gold nanoparticles inside of the cells affects radiation enhancement; for example, a GNP attached to DNA (Deoxyribonucleic acid) will likely have a greater impact than a GNP in other locations (for example, the local effect model discussed in (25)). Typically, not targeted nanoparticles will enter cell via endocytotic pathway and will be trapped in endosomal/lysosomal compartments and might exit cell via the exocytosis process. The uptake and removal of particles depend on its size, shape and surface properties(26). The use of pH Low Insertion Peptides (pHLIP® peptides) to target gold nanoparticles to cancer cells (*in vitro*) resulted in location of GNPs to the plasma and nuclear membranes (7, 15) . Ultra-small Au@tiopronin nanoparticles (2 and 6 nm) were localized throughout the cytoplasm and nucleus of cancer cells *in vitro* and *in vivo*, whereas 15 nm nanoparticles were found only in the cytoplasm and were aggregated (24).

The targeting ligands: The targeting ligands enable nanoparticles to bind to cell surface receptors and enter the cells by receptor mediated endocytosis (18). Nanoparticles accumulate at the tumor sites due to leaky, immature vasculature due to enhanced permeability and retention effect (8, 13, 16). Chattopadhyay et al. (27) discusses the molecular targeting approach, which enables a larger amount of GNPs to cross the cellular membrane and accumulate in the cancer cell cytoplasm. The experimental result showed that the GNPs modified with trastuzumab for targeting HER-2 on breast cancer cells with 100kVp x-rays were more effective in decreasing the clonogenic cells survival as compared to the non-targeted GNPs (27). Kong et al. (28) found that the local concentration of GNPs in target locations can be increased by

localized delivery in comparison to the naked GNPs. 15nm GNPs with AET(cysteamine) were bound to the cell membrane when treated with MCF-7 cells whereas 15nm GNPs with Glu were distributed in the cytoplasm when treated with MCF-7 cells. More GNPs were taken up or bound to MCF-7 cells in case of Glu-GNPs and AET-GNPs than the naked GNPs. With the combined effect of 200kVp, 10Gy x-rays Glu-GNPs produced decreased cell survival compared to AET- GNPs (28) . Su et al. (16) used cyclic RGD conjugated with GNP, labeled with Iodine-125 as a radiosensitizer, for tumor targeting and enhanced radio-therapeutic efficacy. The results depicted consistent apoptosis and the volume loss, indicating effective suppression of tumor growth due to radiation therapy on the radio-labeled targeting ligand on GNPs compared to non targeted GNPs.

Biocompatibility of GNPs: Coating gold nanoparticles with polyethylene glycol (PEG) or bovine serum albumin (BSA) can increase the likelihood of each nanoparticle reaching the tumor, since chemically modifying the GNPs by organic molecules such as PEG or BSA helps GNPs to avoid reticuloendothelial system uptake and to increase circulation time in blood (3, 8). BSA capped GNPs are easy to synthesize, resulting in uniform size and stability under physiological conditions (8). A non-exhaustive list of similar or related methods includes the following:

- Kim et al.(29) found that PEG-coated GNPs had a much longer blood circulation time (>4 h) than non-PEG-coated GNPs.

- PEG coated GNPs can accumulate in mouse sarcoma flank tumors to concentration 10 times that of muscle and 50 times that of brain (12).

- Puvanakrishnan et al. (23) investigated the effect of PEG-coated gold nanoshells and gold nanorods, and its tumor targeting efficiency on mice with a subcutaneous tumor. Mice received an IV injection of single and multiple doses of gold nanoshells and gold nanorods. The uptake of nanoshells and nanorods in the tumor was seen to increase for the multiple doses compared to the single dose. The particle accumulation in tumors for three consecutive doses was increased by 2 for gold nanoshells and 2.45 for nanorods, compared to the single dose. Similarly for five consecutive doses the particle accumulation in tumors was increased by 3 fold for nanoshell GNPs and by 1.6 fold for nanorod GNPs, in comparison to the single dose. The uptake of smaller PEG-coated gold nanorods was 12 times more compared to the uptake of larger PEG-coated gold nanoshells in the tumor after 24 hours. The results from this study suggest that multiple dosing might be an effective method to increase GNPs accumulation in tumors.

  Method of Administration of GNPs to Animals: Direct injection of GNPs by intra-tumoral administration can aid tumor uptake (15). Intravenous administration of gold nanoparticles still results in relatively large accumulation in tumor tissue, due to the enhanced permeability and retention effect discussed above, which is related to leaky vasculature within tumors (see for example (14)).

Radiation energy (for photon irradiation): Dose enhancement caused by GNPs has been observed in kilovoltage and megavoltage beams (6, 10, 20). However, enhanced cell killing was monitored when cells and GNPs were irradiated with photons in the

kilovoltage range (9, 11, 30-32). Hainfeld et al. 2008(3) found that dose enhancement factor depends on both radiation energy and the amount of GNPs.

The relative success of lower energy photons is likely due in part to the fact that, in general, lower energy photons have a higher absorption probability in gold than higher energy photons (4). However, lower energy photons also come with the complicating factor that they are less penetrating, and may not be able to reach tumors deeper than skin depth. For most clinical purpose MeV photons are used due to the fact that for high energy photons , the energy is distributed over a wide range in soft tissue (9). Chang et al. (31) used 6MeV electrons to irradiate a 1-inch diameter tumor region of the leg of the mouse model. Chitrani et al.(10) used low energy kVp and high energy MVp for irradiating cells. The results showed that greater radiation sensitization was seen for kVp compared to MVp for the cell experiments. Further it was evidently found for the first time that radiation sensitization was enhanced even at the clinically relevant high X-ray energy of 6MVp. Also Jain et al.(6) showed a radiosensitization effect on cells at MV X-ray energies as well as at kV energies. The MDA-MB-231 cells were seen to be radiosensitized at MV X-ray energies. Popovtzer et al.(33) showed a radiosensitization effect when cetuximab coated GNPs were used for tumor targeting in a clinically relevant radiation treatment of 6MV energy. The results showed that there was no increase in tumor diameter at all for CTX-GNP+RT compared to 1.0cm increase in tumor diameter for the control case.

If the mechanism of cancer destruction is primarily Auger electrons after the photoelectric effect, an intriguing photon energy to use would be an energy just above the k-shell energy of gold, 80.7 keV (see for example, the X-Ray Attenuation

Database from the National Institute of Standards and Technology). Most interactions would occur with the k-shell electrons, and a photon energy just above the k-shell energy would take advantage of two factors: (1) the photoelectron released would be of low energy, and thus would be localized like the Auger electrons; (2) the photoelectric effect has a sharp spike in absorption coefficient at each shell energy, including the k-shell energy.

Radiation dose: Increasing the radiation dose from 30 Gy to 35 Gy increases the survival rate of the mice for the same KeV energy of 100 kVp x-rays (34). However, at some point there must be a radiation dose of maximum effectiveness for a given experimental setup, since an extremely high dose of radiation would kill the experimental subjects.

Radiation type: In most of the experiments with gold nanoparticles photon irradiation was used, but experiments have also been done using proton, electron and LET radiation. Kim et al. (35) found an increase in survival in mice treated with protons and either gold nanoparticles or magnetic nanoparticles. Chang et al (31) found an increase in radiation enhancement from gold nanoparticles using electron radiation. Liu et al. (36) found that the survival fraction for HeLa cells when irradiated with high LET carbon ions was significantly less than when irradiated with low LET X-rays.

In vivo radiation enhancement results for non-targeted gold nanoparticles

Although many gold nanoparticle radiation enhancement studies have been done *in vitro*, only a few studies have been performed *in vivo*. No specific tumor targeting was utilized in the studies described in this section.

Hainfeld et al.(20): The pioneer study of use of GNPs as a radiation enhancement was done in BALB/C mice bearing subcutaneous EMT-mammary carcinoma. In one experiment, the treatment group of mice received 1.9 nm GNPs at a concentration of 1.35 grams of gold per kg of mouse, injected intravenously into the tail, with irradiation started 2 minutes later. The animals received 30 Gy of radiation from a 250 kVp x-ray machine. These mice survived with only 1 of 10 mice having a visible tumor after 1 month, compared to no retardation of tumor growth for mice receiving only x-rays or gold.

In a second experiment, 50% of mice survived for one year after being given 1.35 grams of gold per kg of mouse and 26 Gy of radiation. In contrast, 86% of mice survived after being given 2.7 grams of gold per kg of mouse. 20% of mice survived with just radiation, and 0% of mice survived with just gold or with no treatment.

Other results showed that after injection of GNPs, many blood vessels became visible due to the gold absorption. Pharmacokinetics showed an early rapid rise followed by a slower clearance rate. Gold in tumor peaked at 7.0 ± 1.6 min and fell to half of its peak value at 41.2 ± 19.5 min; gold in muscle peaked at 5.3 ± 0.6 min and fell to half at 24.2 ± 2.6 min. The data showed that the GNPs cleared nearly twice as fast from normal muscle as from tumor. The injected gold solution was dark black/brown and at the periphery of some tumors was similarly dark. These tumor periphery results showed almost twice the gold concentration of the main tumor mass. The periphery of one tumor contained 6.5 mg Au/g, with a tumor to normal tissue ratio of 8.6. This leads to the fact that a targeting molecule, such as an antibody or peptide, attached to the gold nanoparticle would further improve the tumor specificity and distribution of

GNPs within a tumor. The GNPs were shown to be non-toxic to the mice, based on preliminary toxicity testing.

Hainfeld et al.(37): In this study, Hainfeld et al. tested the effects of radiation dose, radiation energy and a preheating strategy. C3H/HeJ mice were given subcutaneous highly radiation resistant SCCVII head and neck squamous cell carcinoma. 1.9 nm GNPs were found to be more effective at 42 Gy than at 30 Gy for the same radiation energy (68 keV median energy photons)**.** GNPs were also found to be more effective when used at 68 keV than at 157 keV for the same radiation dose (42 Gy). Further, GNPs were found to be more effective at 50.6 Gy, 157 keV than at 44 Gy, 157 keV.

The effect of preheating the mice was also investigated. Mice were preheated for 12-17 mins by submerging the legs of anesthetized mice containing tumor in 44^{o}C water bath. GNPs were then injected (1.9 g/kg body weight) and the mice were heated again for 3 mins, and then irradiated a minute later with 30 Gy, 68 keV. As a result it was seen that the GNPs enhanced the synergy of hyperthermia and radiation therapy at sufficiently high radiation doses (30 Gy, compared to 15 and 23 Gy). The experimental results showed that there was not any damage in the leg of mice and that the tumor doubling time was 52 days for heat + radiation + gold compared to 45 days for radiation alone. The surviving fraction was 79% for heat + radiation + gold compared to 14% for radiation alone.

Hainfeld et al.(34): In this study, Hainfeld et al. treated brain cancer in mice using gold nanoparticles. 50% long-term survival (>1 year) was found using B6C3f1 mice bearing Tu-2449 brain tumors. Irradiation (100 kVp x-rays, 30 Gy) occurred 15 hours

after injection of 11 nm GNPs at a concentration of 4 grams of gold per kg of mouse. 0% long-term survival was found for mice given no treatment, GNPs only and radiation only.

Similarly, for a slightly higher radiation dose of 35 Gy, 56% long-term survival was found compared to 0% survival of mice with no treatment and 18% long-term survival for radiation only.

Further results showed that IV injected GNPs specifically localized in brain glioma in a 19:1 tumor to normal brain ratio. The micro CT measured by the tumor uptake of 1.5 ± 0.2% (weight by weight) gold, which was considered to be the highest gold concentration ever achieved in tumor by IV injection. Atomic absorption spectroscopy measured the uptake to be 1.5 ± 0.2% (weight by weight) gold. The GNPs were initially distributed throughout the tumor, very different from the subcutaneous tumors where GNPs of 15 nm were largely confined to the tumor periphery. The amount of gold delivered was high enough to multiply a radiotherapy dose of tumor by a calculated factor of approximately 300%. Hainfeld predicts this is an indication of difference in tumor and vasculature growth pattern, perhaps indicating the brain tumor cells are more migratory, thus not severely compressing central blood vessels limiting internal blood flow. No toxicity was seen for the concentration of gold used in this study.

Chang et al.(31): Chang et al. used electron radiation with gold nanoparticles. C57BL/6 mice with B16F10 melanoma were injected (IV) with 13 nm GNP at a concentration of 1 gram gold per kg of mouse. 24 hours later, 25 gray of 6 MeV electron radiation was given using a Varian 2100C linear accelerator.

The results showed a retarded tumor growth and increase in survival of mice receiving GNPs followed by radiation compared to the radiation alone, GNPs alone and control groups of mice. Survival of mice treated with gold nanoparticles and radiation was 60% after 2 months, whereas survival was less than 20% for radiation treatment alone and 0% for gold nanoparticles alone or no treatment.

Biodistribution of GNPs 24 hours post IV injection of GNPs showed the accumulation of GNPs inside the tumor, with a tumor to tumor surrounding muscle gold ratio of 6.4:1. Also, higher concentrations of GNPs were found in the liver and spleen, indicating uptake of gold by the reticuloendothelial system.

The number of apoptotic cells detected in tumor by a TUNEL assay was significantly higher in mice treated with GNPs followed by radiation than in mice receiving only radiation, GNPs alone and control groups.

Compared to Hainfeld et al.(20), fewer GNPs were injected IV into the mice in Chang et al. 2008 (31) (2.7 g Au/kg versus 1 g Au/kg). Additionally, the irradiation was done 24 hours after injection, versus 2 minutes after injection in Hainfeld et al. (2004)(20).

Bobyk et al.(38): Bobyk et al. studied the effect of gold nanoparticles and radiation in rats with brain tumors. Male Fischer rats bearing F 98 glioma cells were intracerebrally injected by 5 microliters of 15 nm GNP (25 mg/mL or 50 mg/mL) 20 minutes before irradiation using 88 keV x-rays with a dose of 15 Gy.

The untreated groups of rats had a mean survival time of 23.8 ± 1.6 days and the rats receiving GNPs alone had a mean survival time of 24.9 ± 0.8 days and 23.3 ± 0.7 days

for 25 mg/mL and 50 mg/mL. This suggests that the GNPs alone did not improve the animal life span.

The group of rats that received radiation alone had a mean survival time of 33 ± 2.7 days, an increase of 38.8%. The group of rats receiving GNPs and x-rays had mean survival times of 34.9 ± 1.7 days (25 mg/mL) and 41.6 ± 3.2 days (50 mg/mL). Thus, the higher concentration of GNPs, combined with radiation, showed a 74% increase in mean survival time. TEM results showed that GNPs are trapped by endosomes before being fused with lysosomes *in vitro*. *In vivo* results also showed the internalization of 15 nm GNPs by the endosomal pathway in cells on brain tissue biopsies but GNPs were not observed in the mitochondria, Golgi complex or nucleus. Additionally, 15 nm GNPs were observed in the healthy and tumor brain tissues by electron microscopy at all time points, up to 6 days after GNP injection. The clinical signs of toxicity was not seen during the observation period on any mice which received the lowest concentrations of GNPs. At the same concentration of GNPs for different sizes the smaller ones are found to be more toxic than the larger ones *in vivo*.

Joh et al.(39) coated 12 nm gold cores by PEG (polyethylene glycol) to make GNPs of hydrodynamic diameter of 23 nm. These GNPs were injected intravenously in female athymic mice bearing the most prevalent and aggressive primary brain tumor U 251. 48 hours post injection of pegylated GNPs (1.25 grams of gold per kg of mouse), the brain of the mice was given a radiation dose of 20 Gy from a 175 kVp small animal radiation research platform. The combined treatment of GNPs and radiation therapy increased the DNA damage to brain blood vessels *in vivo*, resulting in increased survival of mice and delayed tumor growth. Joh et al. interpret these results as

suggesting that radiation-induced blood brain barrier disruption can be leveraged to improve the tumor-tissue targeting of GNPs, which would further optimize the radiation enhancement of brain tumors by GNPs. The GNP toxicity *in vivo* was very small in this study, as shown by the preliminary data.

Zhang et al.(22) studied size-dependent radiation enhancement using PEG-coated GNPs. PEG-coated GNPs of sizes 4.8, 12.1, 27.3 and 46.6 nm (concentration 4 mg of gold per kg of mouse) were injected intraperitoneally to female BALB/C mice bearing U14 tumors. The tumors were then irradiated by 5 Gy of gamma radiation. Mice were sacrificed after 24 days. The results indicated that all sizes of PEG-coated GNPs decreased the tumor volume and weight after 5 Gy of radiation, but 12.1 and 27.3 nm PEG coated GNPs induced appreciable decreases of tumor volume and weight, indicating that these sizes of particles have greater radiation enhancement effects compared to 4.8 and 46.6 nm particles. The toxicity *in vivo* was appreciably less on the basis of immune response and blood biochemistry. However the liver was slightly damaged. Also it was found that the GSH-protected GNPs had efficient clearance through the kidney.

Kim et al.(35): Kim et al. studied the effects of proton radiation combined with gold and iron nanoparticles in mice. Gold nanoparticles (coated with DTPA, diethylenetriamine pentaacetic acid-cysteine conjugate) or iron nanoparticles (coated with alginate) of sizes 14 ± 1.2 nm and 10.6 ± 0.8 nm respectively were injected intravenously to Balb/c mice with CT26 tumors either on their leg or flank. The injected dose of particles was either 100 or 300 mg of metal per kg mouse. 24 hours after injection, proton irradiation was given with radiation doses of 10-41 gray. Two

different strategies of proton radiation were employed: protons that were absorbed in the mouse (with the Bragg peak located on the tumor) and protons that traversed through the mouse.

The results for tumor uptake showed that 15 minutes after injection of particles the tumor concentration was 137.4 ± 50.2 micrograms of gold per gram of tissue or 56.6 ± 18.2 micrograms of iron per gram of tissue, while the corresponding muscle concentration were 7.5 micrograms of gold per gram and 6.5 micrograms of iron per gram tissue. The tumor to normal tissue ratio was 18.3 for gold and 8.7 for iron after 15 minutes; after 24 hours it was 169.7 for gold and 88 for iron, thus enabling enhanced tumor dose deposition. The ratio of tissue uptake to total injected dose was less than 1% after administration of both 100 and 300 mg of metal per kg of mouse.

In the irradiation experiment, mice receiving a gold or iron nanoparticle injection prior to various doses from the proton beam demonstrated 58% (absorbed protons) or 64-100% (traversing protons) long-term survival. All animals that were not given radiation died in 2-4 weeks. All proton radiation alone groups showed slowed tumor growth and resulted in only 13% (absorbed protons) or 11% (traversing protons) long-term remissions.

Complete tumor regression (CTR) in mice showed a direct dependence on proton and nanoparticle doses. Either 45 Gy proton alone or 21 Gy irradiation with 300 mg/kg magnetic nanoparticles injections produced 100% CTR in mice. *In vitro* experiments showed an increase in the generation of reactive oxygen species from the metallic nanoparticle and proton radiation treatment. Gold nanoparticles had greater tumor

uptake and a more rapid clearance for normal tissue compared with iron nanoparticles, due to different surface coatings.

Chen et al.(8): Chen et al. exploits the potential of BSA capped GNPs as an efficient sensitizer for glioblastoma, both *in vitro* and *in vivo*, on radiotherapy. Clonogenic assay was performed on U87 glioblastoma cells with or without BSA - GNPs of 28nm hydrodynamic diameter with a series of doses in between 0-8 Gy at 160kVp X-ray. Also 250uL of, 1.3mg mL^{-1} BSA-GNPs was injected intravenously to the mice model having U87 glioblastoma tumor of diameter 0.8-1cm. The mice were then irradiated by 160kVp X rays with a dose of 3Gy after 2hr and 2Gy after 24 hr of treatment. The tumor volume was calculated every alternate day .All the mice were euthanized after 20 days of the treatment and the tumors were weighted.

The *in vitro* RT showed that the percentage of cell apoptosis was larger for BSA-GNPs + RT followed by RT alone then BSA-GNPs and the minimum percentage of apoptosis was for the control group. The *in vivo* RT showed that the relative tumor volume after 20 days of treatment was maximum for the control group and minimum for BSA-GNP + RT. The data obtained inferred that BSA-GNP + RT showed maximum tumor regression while X ray alone slowed down the tumor growth while BSA-GNP alone didn't affect tumor growth compared to control group of mice.

The weight of tumor for 4 different cases were in accordance with the results obtained for relative tumor volume, meaning that the weight of tumor was minimum for BSA-GNP-RT and maximum for the control group. There was rapid clearance of GNP level

from the mice after the administration of BSA-GNPs and the *in vivo* toxicity of BSA-GNPs was determined by ICP-AES analysis of GNP level after the treatment of BSA-GNPs. This analysis showed no toxicity.

Nanoparticle Targeting:

Successful targeting increases the likelihood that each gold nanoparticle will reach the tumor. Thus, there is the potential for targeted gold nanoparticles to improve the radiation enhancement effect. This is particularly true when the primary benefit from gold nanoparticles comes from Auger electrons, which have a short range, as discussed in the introduction. In addition to locating gold nanoparticles to cells, the resulting intercellular localization is also important, as discussed above. Targeting strategies can be divided into two categories: those that use cancer-targeting molecules, and other methods that do not.

Cancer cell targeting molecules:

More specific tumor targeting can be done by surface conjugation (attachment) of antibodies, peptides and other tumor targeting molecules (12). This can improve the therapeutic index (16, 40). Conjugating gold nanoparticles with targeting molecules enhances the interaction of the GNPs with the cell surface by enabling the GNPs to bind to the cell surface receptors and enter cells by receptor-mediated endocytosis (18). A non-exhaustive list of targeting molecules used with gold nanoparticles (either *in vitro* or *in vivo*) includes the following strategies:

- Glucose capped GNPs are designed to take advantage of an increased cancer cell requirement for glucose in order to target the cell cytoplasm (28).

- pH-Low Insertion Peptide (pHLIP® peptide) conjugated 1.4 nm GNPs target tumor acidity, which is achieved in a result of membrane-associated folding of pHLIP® peptide . Peptides of the pHLIP® family can tether cargo nanoparticles to the surface of cells in diseased tissues, and it can move cell-impermeable cargo molecules across the membrane into the cytoplasm (41-43). pHLIP® peptide has been shown to increase uptake of gold by a factor of approximately 5-10 in mouse tumors (15).

- Antibodies such as trastuzumab have been successfully used to modify GNPs. Trastuzumab conjugated GNPs has been used for targeting MDA-MB-361 tumors in athymic mice, and combined with x-rays the tumors were reduced to half of their volume at 4 months compared with the treatment by x-rays alone (27).

- GNPs functionalized with RGD peptide (Arg-Gly-Asp), NLS (Nuclear Localization signal) peptide (H-Cys-Gly-Gly-Arg-Lys-Lys-Arg-Arg-Gln-Arg-Arg-Arg-Ala-Pro-OH) and pentapeptide (H-Cys-Ala-Leu-Asn-Asn-OH) were shown to enhance tumor uptake of GNPs (26).

- The conjugation of RGD peptides to radiolabeled GNPs produced biocompatible and stable multimeric systems with target-specific molecular recognition. The properties listed below which are demonstrated by ^{177}Lu-

GNP-RGD compared to the other radiopharmaceuticals make it suitable to be used as a molecular targeting radiotherapy agent. ^{177}Lu-GNP-RGD leads to significant reduction in VEGF gene expression, helps to reduce tumor metabolic activity, induces less tumor progression, fewer intratumoral vessel, yields more uptake and retention in tumor (44).

- Choi et al.(45) modified the surface of 50 nm GNPs with PEG and transferrin (a tumor targeting ligand) to make particles of size 80 nm. $4.5x10^{11}$ particles were injected IV to female A/J mice containing subcutaneous Neuro2A tumors, and all organs were collected after 24 hours. The results showed that the GNP localizations within a particular organ are influenced by the transferrin content whereas the nanoparticle accumulations in the tumors and other organs are independent of transferrin.

- Shah et al.(46) found that 30 nm PEG-coated GNPs interact with blood cells *in vivo*, which results in longer blood circulation that correlates strongly with tumor uptake. In tumors, accumulation was increased by 10 times using GNPs conjugated with a bioactive ligand (tumor necrosis factor) compared to untargeted GNPs.

In vivo radiation enhancement results for targeted gold nanoparticles

To the author's knowledge, there are only a few papers currently existing where targeted gold nanoparticles are used to enhance radiation effects on tumor *in vivo*.

Chattopadhyay et al.(27) used 30 nm GNPs conjugated with monoclonal antibody transtuzumab (AuT) to target the human epidermal growth factor receptor-2 (HER-2). Female athymic CD1nu/nu mice bearing MDA-MB-361 cells were intra-tumorally injected with 4.8 mg/g of AuT (0.8 mg of GNPs per gram of mouse) followed by 11 Gy, 100 KVp x-rays after 24 hours. They found a 46% reduction in tumor volume at 4 months as compared to treatment with x-rays alone (16% increase in tumor volume).The analysis of the body weight index curves for different mice groups revealed no normal tissue toxicity by the use of Au-Ts with RT.

Su et al.(16) used 20nm GNPs conjugated with clinically used therapeutic radionuclide Iodine-125 labeled to cRGD as a tumor targeted radiosensitizer. IV injection of 100uL(containing 1mg Au) was given to Balb/c mice bearing NCI-H446 lung tumors. Co-60 source, 5Gy γ rays were used to irradiate the tumor tissues. RT effect was assessed by IV injection of Tc-99m-Annexin V (18.5MBq/mouse) after 2 days of treatment for evaluation of apoptosis induced by radiosensitized RT and SPECT performed.

The degree of apoptosis which is shown in numerical value was measured for 5 different groups and the results showed that there was a significant difference between targeted radiosensitizer based RT (cRGD-GNP-RT) (9.8±2.7) and non-targeted radiosensitizer (GNP+RT) based RT (5.5±1.4) (P=0.011). Also, a significant difference was seen between radiolabeled (I-125) cRGD-GNP-RT (11.2±2.1) and non-targeted radiosensitizer based RT (5.5±1.4) (P<0.01). However, a significant difference was not seen between the treated and untreated cases between I-125-cRGD-GNP-RT (11.2±2.1) and cRGD-GNP-RT(9.8±2.7) (P=0.093). This showed that

the radiosensitivity was enhanced by the targeting effect. The above results show that I-125 showed the therapeutic effect but the improvement compared to cRGD-GNP-RT was not statistically significant. However the proper choice of more effective radionuclide like I-131 can heavily enhance of therapeutic effect.

Also, after 21 days the percentage volume increase in tumor for different groups of mice was also measured and found that it was maximum in control (312.1%±96.9%), then in RT alone (137.1%±35.5%), then in GNP+RT(85.5%±44.2%). However the increase in tumor volume was suppressed to 33.1%±17.1% for cRGD-GNP-RTand was even less increase (15.2%±17.8%) for the I-125- cRGD-GNP-RT.

Also, the functionalized PEG which was used in this research showed good stability and clearance avoiding the uptake by RES. The *in vivo* toxicity of PEG covered GNPs and cRGD-GNPs was found to be low which was verified because there was no obvious loss of weight of mice.

Popovtzer et al.*(33)* used 1 mg of cetuximab(CTX) alone or 200uL; 25mg mL^{-1} Au of 30nm with I_g G or CTX coating, injected IV into the tail vein of mice having a A431 head and neck cancer model of diameter 10mm, then irradiated after 24 hrs with 6MV, 25Gy X-ray. In contrary to the results obtained by Hainfeld et .al where there was the shrinkage of tumor, here the results showed that there was no increase in tumor diameter at all for CTX-GNP+RT compared to 1.0cm increase in tumor diameter for the control case, 0.4cm for CTX+RT, 0.6 for I_g G-GNP+RT, 0.3cm for RT only and 0.9cm for CTX only cases. This shows that the radiation is enhanced by the tumor

targeted GNPs. A set of experiments to study the biological mechanism of radiosensitized GNPs was done. Decreased vasculatization in tumors was seen after 1 and 6 weeks of the treatment in CTX-GNP+RT group than control, RT only and CTX+RT groups. Also Tunnel assay results showed that apoptosis was higher after 1 week and less apoptosis after 6 weeks of treatment in CTX-GNP+RT group compared to RT only group. And other results showed that the level of proliferation and tissue repair was reduced in CTX-GNP+RT group compared to other groups.. Further, no cytotoxic effect was seen on the mice.

Conclusion

The papers reviewed in this article demonstrate the potential effectiveness of gold nanoparticles in the enhancement of radiation of tumors. Major results and methodologies are summarized in Table 1. Future experiments with gold nanoparticles and radiotherapy will likely involve the following areas: trials in humans, experiments using targeted gold nanoparticles and different radiation energies/types.

The eventual goal of gold nanoparticle treatments is to become viable for use in humans. One potential roadblock is that treatment with kilo-voltage x-rays is only capable of penetrating human tissue to a shallow depth. Perhaps trials using this treatment could be done starting with melanoma or other tumors, which could be accessed via catheterization, and future advances in engineering could help to eliminate this roadblock.

The roadblock mentioned in the paragraph above may also inspire more work with different radiation energies and radiation types. For example, the result of Kim et al.

(35) with protons seems particularly promising. Additionally, *in vitro* studies (6, 10) have shown radiation enhancement with gold nanoparticles and higher energy photons, although the enhancement is generally somewhat less than kilo-voltage photon results.

Regardless of the radiation type, it appears that tumor targeting will be of great use in this type of therapy. To conclude, we can say that GNPs modified with tumor targeting agents as pHLIP, cetuximab, cRGD and trastuzumab successfully enhanced the radio sensitization of GNPs which can lead to more effective clinical radiotherapy with less toxicity in near future(7, 16, 27, 33). Additional trials with other targeting methods would be beneficial and important.

In summary, gold nanoparticles are a promising research area with the potential to reduce the amount of radiation necessary in cancer treatments. Successful experimental work has already been done in this area, including work in mammals. More work is needed, and this future work has the potential of pushing the field into clinical relevance.

Acknowledgements

The authors would like to thank Yun Hu Huang for his help with Auger electron energy concepts and numbers. This work was supported by the NIH grant GM073857 to OAA and YKR.

References

1. Liu C-J, *et al.* (2008) Enhanced x-ray irradiation-induced cancer cell damage by gold nanoparticles treated by a new synthesis method of polyethylene glycol modification. *Nanotechnology* 19(29):295104.

2. Babaei M & Ganjalikhani M (2014) A systematic review of gold nanoparticles as novel cancer therapeutics. *Nanomedicine Journal* 1(4):211-219.

3. Hainfeld JF, Dilmanian FA, Slatkin DN, & Smilowitz HM (2008) Radiotherapy enhancement with gold nanoparticles. *Journal of Pharmacy and Pharmacology* 60(8):977-986.

4. Tables of X-ray mass attenuation coefficients and mass energy-absorption coefficients (version 1.4). [databasse on the Internet]. National Institute of Standards and Technology,Gaithersburg, MD, 2004.

5. Yao X, Huang C, Chen X, Zheng Y, & Sanche L (2015) Chemical radiosensitivity of DNA induced by gold nanoparticles. *Journal of biomedical nanotechnology* 11(3):478-485.

6. Jain S, *et al.* (2011) Cell-specific radiosensitization by gold nanoparticles at megavoltage radiation energies. *International Journal of Radiation Oncology Biology Physics* 79(2):531-539.

7. Antosh MP, *et al.* (2015) Enhancement of radiation effect on cancer cells by gold-pHLIP. *Proceedings of the National Academy of Sciences* 112(17):5372-5376.

8. Chen N, *et al.* (2015) BSA capped Au nanoparticle as an efficient sensitizer for glioblastoma tumor radiation therapy. *RSC Advances* 5(51):40514-40520.

9. Butterworth KT, McMahon SJ, Taggart LE, & Prise KM (2013) Radiosensitization by gold nanoparticles: effective at megavoltage energies and potential role of oxidative stress. *Translational Cancer Research* 2(4):269-279.

10. Chithrani DB, *et al.* (2010) Gold nanoparticles as radiation sensitizers in cancer therapy. *Radiation research* 173(6):719-728.

11. Coulter J, Hyland W, Nicol J, & Currell F (2013) Radiosensitising Nanoparticles as Novel Cancer Therapeutics—Pipe Dream or Realistic Prospect? *Clinical Oncology* 25(10):593-603.

12. Dorsey JF, *et al.* (2013) Gold nanoparticles in radiation research: potential applications for imaging and radiosensitization. *Translational cancer research* 2(4):280.

13. Jain S, Hirst D, & O'sullivan J (2012) Gold nanoparticles as novel agents for cancer therapy. *The British journal of radiology* 85(1010):101-113.

14. Liu C-J, *et al.* (2010) Enhancement of cell radiation sensitivity by pegylated gold nanoparticles. *Physics in medicine and biology* 55(4):931-945.

15. Yao L, *et al.* (2013) pHLIP peptide targets nanogold particles to tumors. *Proceedings of the National Academy of Sciences* 110(2):465-470.

16. Su N, Dang Y, Liang G, & Liu G (2015) Iodine-125-labeled cRGD-gold nanoparticles as tumor-targeted radiosensitizer and imaging agent. *Nanoscale research letters* 10(1):1-9.

17. McMahon SJ, *et al.* (2011) Biological consequences of nanoscale energy deposition near irradiated heavy atom nanoparticles. *Scientific reports* 1:18.

18. Davis ME & Shin DM (2008) Nanoparticle therapeutics: an emerging treatment modality for cancer. *Nature reviews Drug discovery* 7(9):771-782.

19. Boisselier E & Astruc D (2009) Gold nanoparticles in nanomedicine: preparations, imaging, diagnostics, therapies and toxicity. *Chemical Society Reviews* 38(6):1759-1782.

20. Hainfeld JF, Slatkin DN, & Smilowitz HM (2004) The use of gold nanoparticles to enhance radiotherapy in mice. *Physics in medicine and biology* 49(18):N309.

21. Chithrani BD, Ghazani AA, & Chan WC (2006) Determining the size and shape dependence of gold nanoparticle uptake into mammalian cells. *Nano letters* 6(4):662-668.

22. Zhang X-D, *et al.* (2012) Size-dependent radiosensitization of PEG-coated gold nanoparticles for cancer radiation therapy. *Biomaterials* 33(27):6408-6419.

23. Puvanakrishnan P, Park J, Chatterjee D, Krishnan S, & Tunnell JW (2012) In vivo tumor targeting of gold nanoparticles: effect of particle type and dosing strategy. *International journal of nanomedicine* 7:1251.

24. Huang K, *et al.* (2012) Size-dependent localization and penetration of ultrasmall gold nanoparticles in cancer cells, multicellular spheroids, and tumors in vivo. *ACS nano* 6(5):4483-4493.

25. Elsässer T & Scholz M (2007) Cluster effects within the local effect model. *Radiat. Res.* 167(3):319-329.

26. Yang C, Uertz J, Yohan D, & Chithrani B (2014) Peptide modified gold nanoparticles for improved cellular uptake, nuclear transport, and intracellular retention. *Nanoscale* 6(20):12026-12033.

27. Chattopadhyay N, *et al.* (2013) Molecularly targeted gold nanoparticles enhance the radiation response of breast cancer cells and tumor xenografts to X-radiation. *Breast cancer research and treatment* 137(1):81-91.

28. Kong T, *et al.* (2008) Enhancement of Radiation Cytotoxicity in Breast-Cancer Cells by Localized Attachment of Gold Nanoparticles. *small* 4(9):1537-1543.

29. Kim D, Park S, Lee JH, Jeong YY, & Jon S (2007) Antibiofouling polymer-coated gold nanoparticles as a contrast agent for in vivo X-ray computed tomography imaging. *Journal of the American Chemical Society* 129(24):7661-7665.

30. Rahman WN, *et al.* (2009) Enhancement of radiation effects by gold nanoparticles for superficial radiation therapy. *Nanomedicine: Nanotechnology, Biology and Medicine* 5(2):136-142.

31. Chang MY, *et al.* (2008) Increased apoptotic potential and dose-enhancing effect of gold nanoparticles in combination with single-dose clinical electron beams on tumorbearing mice. *Cancer science* 99(7):1479-1484.

32. Cooper DR, Bekah D, & Nadeau JL (2014) Gold nanoparticles and their alternatives for radiation therapy enhancement. *Frontiers in chemistry* 2:86.

33. Popovtzer A, *et al.* (2016) Actively targeted gold nanoparticles as novel radiosensitizer agents: an in vivo head and neck cancer model. *Nanoscale* 8:2678-2685.

34. Hainfeld JF, Smilowitz HM, O'Connor MJ, Dilmanian FA, & Slatkin DN (2013) Gold nanoparticle imaging and radiotherapy of brain tumors in mice. *Nanomedicine* 8(10):1601-1609.

35. Kim J-K, *et al.* (2012) Enhanced proton treatment in mouse tumors through proton irradiated nanoradiator effects on metallic nanoparticles. *Physics in medicine and biology* 57(24):8309.

36. Liu Y, *et al.* (2015) The dependence of radiation enhancement effect on the concentration of gold nanoparticles exposed to low-and high-LET radiations. *Physica Medica* 31(3):210-218.

37. Hainfeld JF, *et al.* (2010) Gold nanoparticles enhance the radiation therapy of a murine squamous cell carcinoma. *Physics in medicine and biology* 55(11):3045.

38. Bobyk L, *et al.* (2013) Photoactivation of gold nanoparticles for glioma treatment. *Nanomedicine: Nanotechnology, Biology and Medicine* 9(7):1089-1097.

39. Joh DY, *et al.* (2013) Selective targeting of brain tumors with gold nanoparticle-induced radiosensitization. *PloS one* 8(4):e62425.

40. Wang AZ, *et al.* (2008) Biofunctionalized targeted nanoparticles for therapeutic applications. *Expert opinion on biological therapy* 8(8):1063-1070.

41. Andreev O, Sandugu S, Engelman D, & Reshetnyak Y (2006) Injection of Molecules into cells using a pH-triggered molecular nanosyringe. *Technical Proceedings of the 2006 Nanotech Conference*, pp 57-60.

42. Andreev OA, *et al.* (2007) Mechanism and uses of a membrane peptide that targets tumors and other acidic tissues in vivo. *Proceedings of the National Academy of Sciences* 104(19):7893-7898.

43. Andreev OA, Engelman DM, & Reshetnyak YK (2010) pH-sensitive membrane peptides (pHLIPs) as a novel class of delivery agents. *Molecular membrane biology* 27(7):341-352.

44. Vilchis-Juárez A, *et al.* (2014) Molecular targeting radiotherapy with cyclo-RGDFK (C) peptides conjugated to 177Lu-labeled gold nanoparticles in tumor-bearing mice. *Journal of biomedical nanotechnology* 10(3):393-404.

45. Choi CHJ, Alabi CA, Webster P, & Davis ME (2010) Mechanism of active targeting in solid tumors with transferrin-containing gold nanoparticles. *Proceedings of the National Academy of Sciences* 107(3):1235-1240.

46. Shah NB, *et al.* (2012) Blood–nanoparticle interactions and in vivo biodistribution: impact of surface PEG and ligand properties. *Molecular pharmaceutics* 9(8):2146-2155.

Table 1: Summary of major *in vivo* experimental results

First author	Year	Animal model	Tumor model	Coating of GNPs	Size GNPs, nm	Time to RT	Radiation	Dose, Gy	Group	Route and Dose of Administration
Hainfeld	2004	Balb/C mice	EMT-6: murine mammary carcinoma		1.9	2 m	x-rays 250kVp	30 26	Control Au only RT only Au+RT	IV injection 1.35gAu/kg 2.7g Au/kg
Chang	2008	C57BL/6 mice	B16F10: murine melanoma		13	24 h	electrons 6 MeV	25	Control Au only RT only Au+RT	IV injection 1gAu/kg
Hainfeld	2010	C3H/HeJ mice	SCCVII: head and neck squamous carcinoma		1.9	1 m	x-rays 68 keV 157keV	30 42 44 50.6	RT only Au+RT	IV injection 1.9fAu/kg
Chattopadhyay	2012	CD1 nude mice	MDA-MB-361: human breast adenocarcinoma	Trastu-zumab	30	24 h	x-rays 100 kVp	11	Control Au only RT only Au+RT	Intratumoral (IT) injection 0.8mg Au or 4.8mg/g tumor
Zhang	2012	Female BALB/c mice	U14: murine cervical carcinoma	PEG	4.8 6.6 12.1 27.3	soon after the injectio	Γ-rays	5	Control Au only RT only Au+RT	Intraperitoneal(IP) injection 4mg/kg
Bobyk	2013	Fischer rats	F98: rat glioma		9 15	20 m	x-rays 88keV	15	Control Au only RT only Au+RT	Intracerebral infusion (5 μL)(5μL) 25mg/mL 50mg/mL
Hainfeld	2013	B6C3f1 mice	Tu-2449: murine highly malignant brain tumor		11	15 h	x-rays 100 kVp	30 35	Control Au only RT only Au+RT	IV injection 4gAu/kg
Joh	2013	nude female athymic mice	U251: human glioblastoma	PEG	23	48 h	x-rays 175 kVp	20	Control Au only RT only Au+RT	IV injection 1.25gAu/kg
Kim	2012	Balb/c mice	CT26: murine colon carcinoma	DTPA+ cysteine FeNPs+alginate	14 10.6	24 h	proton 45MeV	10 41	Control Au only RT only Fe only Au+RT Fe+RT	IV injection 100mg/kg 300mg/kg
Chen	2015	Nude athymic mice	U87:glioblastoma	BSA	28	2h 24h	X-rays 160kVp	3 2	Control BSA+Au RT only BSA+Au+RT	IV injection 250μL, 1.3mg/mL
Su	2015	Balb/c mice	NCI-H446:human lung carcinoma	Iodine-125+cRGD	20	4h	Γ-rays	5	Control RT only Au+RT cRGD+Au+RT 125I+cRGD+Au+RT	IV injection 100μL 1mgAu 50mg/kg
Popovtzer	2016	Nude mice	A431: squamous head and neck carcinoma	I_g G CTX	30	24	X-rays 6MV	1.4/min	Control RT only CTX only CTX+RT IgG-Au+RT CTX-Au+RT	IV injection 200μL;25mg/mL

CHAPTER 3

Published in Journal of Computational Biology on 1st of December 2018

Gene Expression as a Dosimeter in Irradiated *Drosophila melanogaster.*

Samana Shrestha[a,*], Adam Vanasse[a,*], Leon N Cooper[b], Michael P. Antosh[a,b]

[a]University of Rhode Island, Physics department, University of Rhode Island, Kingston, RI 02881, USA

[b]Brown University, Department of Physics and Institute for Brain and Neural Systems, Providence, RI, 02912, USA

[*]Authors contributed equally to this work

Corresponding author:

Dr. Michael Antosh, 2 Lippitt Rd, Kingston, RI, 02881, USA, Tel: 401-874-2048; Email: mantosh@uri.edu

Abstract

Biological indicators would be of use in radiation dosimetry in situations where an exposed person is not wearing a dosimeter, or when physical dosimeters are insufficient to estimate the risk caused by the radiation exposure. In this work, we investigate the use of gene expression as a dosimeter. Gene expression analysis was done on 15,222 genes of *Drosophila melanogaster* (fruit flies) at days 2, 10 and 20 post irradiation, with x-ray exposures of 10, 1000, 5000, 10000 and 20000 roentgens. Several genes were identified which could serve as a bio dosimeter in an irradiated drosophila melanogaster model. Many of these genes have human homologues. 6

genes showed a linear response ($R^2 > 0.9$) with dose at all time points. One of these genes, *Irbp*, is a known DNA repair gene and has a human homologue (*XRCC6*). The lowest dose, 10 R, is very low for fruit flies. If the lowest dose is excluded, 13 genes showed a linear response with dose at all time points. This includes 5 of 6 genes that were linear with all radiation doses included. Of these 13 genes, 4 have human homologues and 8 have known functions. The expression of this panel of genes, particularly those with human homologues, could potentially be used as the biological indicator of radiation exposure in dosimetry applications.

Keywords*:* gene expression, radiation biology, radiation dosimetry

Introduction

In the occurrence of a large-scale nuclear event, such as those at Hiroshima, Nagasaki, Chernobyl and Fukushima Daiichi, the measurement of radiation dose in exposed humans can be of crucial importance to survival (1, 2). However, in this situation it is very likely that many people who are exposed will not be wearing dosimeters. Thus, a method of estimating radiation dose to a patient without a dosimeter would be a very useful procedure.

One possible methodology for this procedure is the use of gene expression [polymerase chain reaction (PCR), gene sequencing, microarray analysis, and other methods]. The hypothesis is that the expression of genes will change due to the absorbed radiation, and that this change can aid or even substitute for physical dosimeters and act as a biomarker to estimate the distributed dose or the overall

exposure. It also helps then to predict the long-term risks of both acute and chronic exposure (3-6).

In addition to not requiring equipment, such as a dosimeter, another potential advantage of a gene-expression dosimeter is the time scale over which the measurements can be made. Even after the radiation exposure has taken place, the biological indicators for bio dosimetry can still be determined. This would certainly be an advantage compared to the physical dosimetry (7). Some biodosimetric techniques could be used long times after exposure (from 6mths to more than 50 years) which makes it unique compared to the requirements for methods used for immediate dose estimation (8).

Biological dosimetry not only provides information about the range of radiation dose but also along with this provides information about the individual radio sensitivity, which depends on age, smoking habits or other environmental toxins. Thus, biological indicators are also a measure of the biological, medical radiation damage. Hence, we can predict about the possible radiation damage by the determination of biological indicators (5, 7, 9, 10).

The possibility of using gene expression changes has been an exciting method to measure and predict the damage due to ionizing radiation. The exposure of cells or animals to ionizing radiation may cause DNA damage and trigger the highly complex molecular response, resulting in changes of gene expression. These molecular responses may provide the prospective indicator of exposure(1, 3). Previous work in this area showed that the variation in the response of genes is due to dose, dose rate, radiation quality and time after radiation exposure. This suggests that gene expression

analysis may be an informative marker of radiation exposure and hence can be used as a potential biomarker. It is important to understand the cellular response to ionizing radiation or biological effects of radiation exposure in order to develop the predictive markers for the risk assessment due to radiation exposure on humans(1). The rigorous research going on in genomics and bioinformatics enables the development of gene expression profiling as a useful biological indicator of radiation exposure (10, 11).

Work on this area until now has shown that the fold change in gene expression in response to radiation must be measured directly to develop a gene expression biomonitor. The expression of the genes would then be a suitable biomarker of radiation exposure (6). The biodosimetry platform obtained by the experiment could also be used for personalized monitoring of radiotherapy treatments received by patients (12).

Several studies have been done to identify the potential biomarkers of radiation exposure. Tucker et al 2013 used reverse transcription real time PCR (qPCR) to quantify the expression of selected 106 genes as a function of time up to 7 days post exposure and concluded that the gene expression analysis by qPCR shows a promising method for radiation bio dosimetry. In their experiment the mice were exposed to C0-60 gamma rays source at doses from 0 to 10Gy. The result showed that only 4-7 different genes explained the variance (R^2) $\geq$ 0.69 whereas for the receiver operator characteristics (a measure of sensitivity and specificity) were $\geq$ 0.93 at each time point. At radiation doses up to 6 Gy, the dosimetry was very accurate. Above 6 Gy, the gene expression dosimetry had limitation. Similar analysis in humans could be done to assess exposures in mass casualty situations (5).

Gene expression analysis in response to radiation was done in human lymphocytes and peripheral blood leukocytes using three different techniques: microarray, multiplex quantitiative real time PCR (MQRT-PCR) and nCounter Analysis System. A set of genes was found to be suitable for biological dosimetry using peripheral blood. Four of the genes (*CDKN1A*, *GADD45A*, *PHPT1*, and *CCNG1*) show good agreement between the three methods and the up-regulation of expression in blood and lymphocytes was detected by all the three techniques. These biomarkers could potentially be used for monitoring radiation exposure during radiotherapy and radiological incidents (13).

A novel study was done using blood from patients receiving targeted radiotherapy (^{131}I-mIBG) to characterize biomarkers that may be useful for bio dosimetry. As an alternative biodosimety approach, real time PCR analysis was done for the gene expression and the data showed that transcripts which have already been proven as biomarkers of external exposures in radiotherapy patients are also good early indicators of internal exposure. Three transcripts showed that modulation in gene expression were still significant enough to differentiate between exposed and unexposed samples after 96 hrs of radiopharmaceutical treatment. A bio dosimetry model for gene expression was developed to predict absorbed dose based on modulation of gene transcripts within whole blood. Thus, this biodosimetry for internal radiation dose or the panel of responsive genes obtained from this study could be used for establishing triage in affected areas due to dirty bombs or nuclear reactor accidents at least by rapidly sorting out the ^{131} I-exposed from unexposed individuals.

Thus, these selected genes could be strong biomarkers of both external and internal exposures to humans (14).

A comprehensive analysis of bone marrow endothelial cell (BMEC) gene expression over time in wild type mice after total body irradiation of 5 Gy was done with a particular focus on the secreted gene products. This study is done to characterize the molecular response of BMECs to ionizing radiation to identify the cellular mechanisms and paracrine factors through which BMECs regulate hematopoietic regeneration. The result of a microarray experiment showed that the gene expression of BMECs is altered within 24 hrs after total body irradiation of 5 Gy and by 14 days this molecular response is resolved. And a number of genes that encode secreted proteins are strongly upregulated (Inhbb, Ccl2, Ptn) and are down regulated (Chl1, Galnt10, Ryk, Pon2, Sdha) more than 10 fold in ECs in response to radiation after 6h (15).

Amundson et al (1999) showed the dose/response relationship for the induction of 5 genes (CDKN1A, GADD45, MDM2, ATF3 and BAX) exposed to γ rays between the doses of 2-50 cGy. As a follow up, Amundson et al. (2003) studied the dose response relationships by reducing the dose rate over three orders of magnitude and found some protection against the induction of apoptosis. They studied the response of 10 cGy and less exposure of γ rays in the ML-1 human cell line and showed that the gene expression could be triggered by the low doses. At different dose responses between 2 and 50 cGy, a linear increase in expression of three genes CDKN1A, GADD45A and MDM2 was observed in the cell line ML-1, whereas dose rate effect was observed only for GADD45A and CDKN1A.The data obtained from the microarray analysis on

RNA samples 2 hours post irradiation with low dose y rays indicate that some genes show a dose rate effect while others don't. This indicates the potential usefulness of gene expression as a biomarker for radiation exposure (4).

Stassen et al. (2003) examined 1176 genes expressed by MCF-7 human mammary carcinoma cells exposed to 2 and 6 Gy of X rays and found that six of them were radiation induced gene targets over 1(3 genes), 2(2 genes) and 3(1 gene) days which was confirmed by quantitative reverse transcription PCR (RTQ-PCR). Of those six (GLUT-1, PCKI, WAF-1, ISGF3G, MRP8, PSME3) the last three were novel gene targets showing a correlation with radiation dose and clonogenicity which suggested an individual dose dependency for all selected genes (16).

Omaruddin et al. (2013) examined the gene expression of the genes MADH7, SEC PRO and CC3 using relative quantitative RT – PCR in blood samples of patients before and after undergoing radiation therapy. This gave a wide range of values, stating the complexity of the response. SEC PRO was found to be down-regulated, while the gene MADH7 was found to be up-regulated in most of the patients. So the gene MADH7 could be used as a molecular marker for radiation exposure (6).

Filiano et al. (2011) performed gene expression analysis using real time quantitative PCR in blood samples from cancer patients undergoing total body irradiation. A set of eight biodosimetry genes (ACTA2, BBC3, CCNG1, CDKN1A, GADD45A, MDK, SERPINE1, TNFRSF10B) was identified. In addition, gene expression analysis was done in C57BL/6 mice at doses 0-8 Gy and times 5, 12, 23 and 48 hours after irradiation. The results showed a significant increase in the expression of five of the above genes (BBC3, CCNG1, CDKN1A, SERPINE1 and TNFRSF10B) (10).

This article focuses on gene expression analysis of *Drosophila melanogaster* (fruit flies). Compared to humans, biodosimetry information can be obtained in a more controlled manner in animal models because the dose received in humans are usually not known, the exposures may be non uniform and the dose rates may not be known. Data collection may not be reliable and uniform post irradiation because a lot of variables have to be taken into consideration like age, health, sex, genotype, time since exposure to radiation, personal lifestyle like cigarette smoking, tobacco and alcohol habits (5, 17). *Drosophila melanogaster* is a model organism with a useful lifespan (~2 months) and a long history in radiation experiments. Its genome has been sequenced, and many genes in *Drosophila* are homologous with human genes (18, 19). This article makes use of a previous gene expression analysis done by Antosh et al. (2014). The experiment was performed in order to discover the biological effects at different levels of ionizing radiation in *D. melanogaster*. The results showed a threshold effect in response to the radiation, both in gene expression and in survival. The gene expression results suggest stress, metabolism, reproduction and mitochondrial function as mechanisms involved in the radiation response (20). The data was taken for five radiation doses (plus a control), at 3 time points. The setup of this data allows it to be repurposed for a new analysis that examines the response of genes as a function of radiation dose.

The aim of this study is to secure a set of genes that are responsive to radiation in a predictable way. These genes, particularly if homologous to human genes, have potential uses in radiation dosimetry.

Methodology

The data used in this paper is obtained from data submitted to the gene expression omnibus by Antosh et al (posted under the reference number GSE47999). Normalized data was calculated using the DESeq (21) package in Bioconductor (22).

The data was obtained from an RNA-sequencing gene expression experiment on drosophila melanogaster. at ages 2, 10 and 20 days after irradiating them Flies were irradiated with x-ray exposures of 0, 10, 1000, 5000, 10000 and 20000 roentgen (a 1 roentgen radiation exposure is ≈ 0.01 gray; here we will use the terms "exposure" and "dose" equivalently). The irradiation came inside a chamber containing cesium-137. Samples were taken at 2, 10 and 20 days after irradiation, with 3 samples per experimental condition (except for sample for 0R, Day 20, where one sample failed quality check). Our re-analysis of this data was done to identify the genes that changed in a predictable way from control, as a function of dose. Genes that behave in a predictable way could potentially be used in a future bio dosimeter.

The fold changes in the expression of genes depending on dose and time after exposure were measured in the fruit fly model. To calculate the fold change, average value of the gene expression of the samples at each time point and radiation dose was divided by the average value of gene expression of control at the same time point (control being zero added radiation). Fold changes were ignored (in a present/absent cutoff) if the average expression in both experimental and control samples was less than a bottom quartile cutoff (~18-20 counts).

One analysis performed was based on linear regression. For each time point, the R^2 value for a linear fit to (fold change vs. radiation dose) was calculated for each gene.

Genes with R^2>0.9 were selected as behaving linearly. In a secondary analysis, the data for 10 R flies was removed (since this is a very small dose of radiation for fruit flies). The linear analysis described above was run again. In both of these analyses, genes were only selected as linear if at least four radiation doses passed the present/absent cutoff (described in the paragraph immediately before this).

As an additional analysis, gene expression data was examined for "spikes" in fold change. For each gene, at each time point, a set of fold changes was examined (one fold change for each radiation dose). Genes were marked as having a spike if the largest fold change was at least five times greater than the second largest fold change. Additionally, genes were only counted as having a spike if the fold change of the spike was > 1 (meaning that the average expression at the spike dose was greater than average gene expression in the corresponding control).

For each time point, and for overlaps between time points, genes found to be significant (meaning, linear or spiking) were analyzed as a group using GOStat (23) to see if any biological functions were had a statistically significant amount of genes in the group. Gene ontologies with a corrected p value < 0.05 were selected.

Genes were examined for human homologues using homologene (19) and functional information was found using flybase (18).

Results

Analysis of Linear Behavior with Full Dataset

Figure 1 shows the number of genes with a linear response in fold change as a function of radiation dose, at each of the three time points (2, 10 and 20 days

postirradiation). Seventy-eight genes showed a linear response at day 2 after irradiation; 677 genes showed a linear response at day 10 after irradiation; 432 genes showed linear response at day 20 after irradiation. A set of 6 genes (*FBgn0011774, FBgn0030189, FBgn0031713, FBgn0032393, FBgn0037020,* and *FBgn0051864*) was found to have a linear response in all time points. Table 1 shows the set of those 6 genes, including homology to human genes (19) and functional information (18). 4 out of these 6 genes have homologues in humans. Genes found to behave linearly across a fairly wide range of times are perhaps most promising for a possible radiation dosimeter. The median lifespan of control flies in this experiment was ~50 days; our time range here is 18 days.

A GOStat analysis (23) was run on genes found to be linear at each time point, and also separately on overlaps between time points. Full lists of significant gene ontologies from the analysis can be found in Supplemental Table S1A-1G. Several of the results suggest that the genes that behave linearly are involved in stress responses. At 2 days postirradiation, 78 genes show linear behavior with dose. These 78 genes contain 13 out of the 23 genes related to protein kinase CK2 regulator activity (a p value of $2.2X10^{-24}$). The protein kinase CK2 inhibits apoptosis following ionizing radiation (24). Gene ontologies for spermatogenesis and reproduction are also affected 2 days postirradiation. Genes found to be linear at 10 days postirradiation were statistically over representative of gene ontologies for oxidoreductase activity (a possible response to radiation damage) and growth factor activity. At 20 days postirradiation, overrepresented gene ontologies included stress-related pathways such as response to stress, receptor activity, signal transducer activity, detection of

bacterium and biotic stimulus and response to DNA damage stimulus. In the genes found in the overlap of day 2 and day 10, overrepresented gene ontologies included peroxisomal transport and NADPH activity. In the genes found in the overlap of day 2 and day 20, overrepresented gene ontologies included several pathways related to the peroxisome, DNA helicase activity, response to hypoxia and telomere maintenance. The overlap between genes in days 10 and 20 found the gene ontology for stress response to be overrepresented. Gene ontologies overrepresented in genes found to be linear at all three time points (2, 10 and 20 days) included peroxisome, DNA helicase activity, ATPase activity and telomere maintenance.

Analysis of Linear Behavior with Lowest Dose Not Included

In the lifespan experiment that accompanied this dataset (20), lifespan effects on fruit flies were not seen until a radiation exposure of 10,000 roentgen (an approximate radiation dose of 100 Gy). The smallest dose in this analysis is 10 roentgen, which is 0.1% of that dose. It is possible that the 10 roentgen dose in this experiment may produce some gene expression at the level of noise. To address that possibility, a secondary analysis for linear behavior was run where the data from 10 roentgen were not included. The results are summarized in figure 2. In this analysis, 13 genes are found to be linear at all three time points. This list includes 5 of the 6 genes found to behave linearly at all three data points when the 10 R data was included in the analysis (Table 1). The 6^{th} gene, *FBgn0031713*, was excluded only because $R^2 = 0.88$ at day 20. The 13 genes in the overlap are described in Table 2. Of these 13 genes, 4 have human homologues.

A GOStat analysis (23) was run on genes found to be linear at each time point, and also separately on overlaps between time points. Full lists of significant gene ontologies from the analysis can be found in Supplemental Table 2A-2G. As with the analysis with all radiation doses, several of the results suggest that the genes that behave linearly are involved in stress responses.

At 2 days postirradiation, overrepresented gene ontologies include protein kinase CK2 regulator activity and spermatogenesis. Genes found to be linear at 10 days postirradiation were statistically over representative of gene ontologies for oxidoreductase activity (a possible response to radiation damage), growth factor activity, GTPase activity, hydrolase activity, electron carrier activity and pathways related to peroxisomes. At 20 days postirradiation, overrepresented gene ontologies included detection of biotic stimulus and bacterium and metabolism of toxins, xenobiotics, insecticide and water-soluble vitamins. In the genes found in the overlap of day 2 and day 20, overrepresented gene ontologies included peroxisomal transport, NADPH regeneration, telomere maintenance, DNA helicase activity, transferase activity and ATPase activity. The overlap between genes in days 10 and 20 found several gene ontologies related to peroxisomes to be overrepresented. Gene ontologies overrepresented in genes found to be linear at all three time points (2, 10 and 20 days) included pathways related to peroxisomes, telomere maintenance and Wnt signaling. No gene ontologies were significantly overrepresented in the overlap between genes linear at day 2 and day 10 postirradiation.

Analysis of Genes for Spikes in Expression

In addition to linear behavior, another potential methodology for using gene expression as a dosimeter would involve genes that "spike"; meaning that a given gene sees a large amount of expression (compared to control flies) at a given radiation dose. In order to search for such an effect in this dataset, we looked for genes where the fold change was at least 5 times higher at one radiation dose than at any other radiation dose examined. The results are shown in figure 3A, and in Supplemental Tables 3A-G and 4A-G. Zero genes were found in the overlap between all three time points, which suggests that there may be no good candidate genes for a biological dosimeter.

Similar to the linear analysis, we performed the analysis a second time with the data for 10 roentgen radiation exposure removed. Results are shown in Figure 3B, and Supplemental Table 4H-4N. In this analysis, one gene was found to be changing at all three time points. This gene, *FBgn0085364*, has no human homologue and no listed functions in Flybase (in Flybase, a search for this gene is directed towards *FBgn0267910*).

For the spike analysis, GOStat analyses were run with the genes being separated by the radiation dose where a spike is found. Any spikes at the largest radiation dose were not considered, because it is likely that a highest expression value at the highest radiation dose is indicative of a gene that is merely increasing with dose (not necessarily in a linear fashion). The radiation doses at which each gene spikes are listed in Supplemental Tables 3A-G and 4A-G. Overall, the GOStat results on spiking genes showed an effect on reproduction and some effect on stress responses.

The analysis with all radiation doses included the following:

- For genes with spikes at day 2 postirradiation at radiation dose 5000 roentgen, overrepresented gene ontologies are all due to *FBgn0013745* and are related to reproduction and behavior.
- For genes with spikes at day 2 postirradiation at radiation dose 1000 R, the only two genes are *yolk protein 1* and *yolk protein 2* (note: in this section, all full gene names were found in Flybase). Overrepresented gene ontologies include vitellogenesis, reproductive development and chromatin remodeling.
- For genes with spikes at day 10 postirradiation, only five genes are not from the highest radiation dose. These five genes are all from dose 10 R. Overrepresented gene ontologies include those related to chorion (*from chorion protein 15 and chorion protein 18*) and sensing of chemical stimulus (*from odorant binding protein 19c*).
- For genes with spikes at day 20 postirradiation, only one gene is not from the highest radiation dose. This gene, *FBgn53222*, spiked at dose 5000 roentgen and gave overrepresented gene ontologies related to ribosomes.

The analysis with the lowest radiation dose (10 roentgen) did not include the following:

- For genes with spikes at day 2 postirradiation, only four genes spiked at doses less than the maximum dose. Two genes spiked at dose 5,000 R; all overrepresented pathways in GOstat were due to *FBgn0013745* (similar to the analysis including 10 roentgen). Two genes spiked at dose 10,000 R – yolk protein 1 (as in the analysis including 10 roentgen) and *FBgn0013675*, which resulted in overrepresented gene ontologies related to oxidative response.

- For genes with spikes at day 10 postirradiation, seven genes spiked at dose 10,000 roentgen. Six of these seven genes were related to reproduction, and include *yolk proteins 1, 2* and *3*.
- For genes with spikes at day 20 postirradiation, one gene (*FBgn0053222*) spiked at dose 5000 R (the same gene as the analysis including 10 roentgen).

GOstat results related to the results reported above can be found in Supplemental Tables 5A-H.

Discussion

A radiation dosimeter based on gene expression could result in the better diagnosis of radiation dose in patients, and thus may help in saving lives after a nuclear event or accidental radiation exposure. The results of this paper indicate several candidate genes that have potential to be used for that purpose. In particular, it seems that the best candidates may be the genes listed in Tables 1 and 2 that have human homologues.

One particularly interesting candidate gene is *Irbp* (inverted Repeat Binding Protein), which was found to behave linearly in all three data points, both with the full data set and with the lowest dose removed. *Irbp* is related to DNA repair. It is reasonable to predict that DNA damage is linear with radiation dose; thus, it is logical that some DNA repair genes may respond linearly in expression. *Irbp* has homologues in organisms that are as complex as humans and chimpanzees, and also in organisms such as Japanese rice (19).

Another possibility, based on the application of GOstat results, is to look at particular cellular functions. In particular, the function of protein kinase CK2 may be useful at time points soon after radiation exposure. Protein kinase CK2 was overrepresented in the GOstat analysis for genes found to behave linearly 2 days after irradiation, with a very high statistical significance. Perhaps the functionality of this protein kinase could be measured directly as a function of radiation to produce a different type of radiation dosimeter.

Several genes listed in Tables 1 and 2 had no known functions in Flybase (18). These results suggest that they are related to radiation responses, and possibly to stress responses.

From a dose-response standpoint, one interesting characteristic of the linear analysis results is that some genes with a linear response in fold change have fold changes that are less than 1 (radiation expression less than control expression) at lower doses, but then transition to fold changes greater than 1 (radiation expression greater than control expression) at high doses. For example, in the linear analysis with all radiation doses the genes FBgn0011774, FBgn0030189, FBgn0037020 and FBgn0051864 are linear at all three time points and exhibit this behavior at day 2 postirradiation. Descriptions of these genes can be found in table 1. This could be representative of some biological effects being in one direction at lower doses of radiation, and in the opposite direction at higher doses of radiation. Fold changes and R^2 values are given in Supplemental Tables 3A-3F.

Future questions related to this research could include:

- How well do results in *Drosophila* genes with human homologues translate to results in humans?
- Do the genes in Tables 1 and 2 continue to respond linearly at more times postirradiation, including times < 2 days?
- How are these results affected by the energy and type of irradiation?

Further development of this methodology is needed before it can be applied to patients, but these results suggest the possibility of a successful gene expression radiation dosimeter.

Author Disclosure Statement

No competing financial interests exist.

References

1. Chaudhry MA (2008) Biomarkers for human radiation exposure. *Journal of biomedical science* 15(5):557-563.
2. Hall E & Giaccia J (2012) Molecular mechanisms of DNA and chromosome damage and repair. *Radiobiology for the radiologist. 7th ed. Philadelphia: Lippincott Williams & Wilkins*:12-34.
3. Amundson SA, Bittner M, Meltzer P, Trent J, & Fornance J, Albert J (2001) Biological indicators for the identification of ionizing radiation exposure in humans. *Expert review of molecular diagnostics* 1(2):211-219.
4. Amundson SA, *et al.* (2003) Differential responses of stress genes to low dose-rate γ irradiation. *Molecular Cancer Research* 1(6):445-452.
5. Tucker JD, *et al.* (2013) Gene expression-based dosimetry by dose and time in mice following acute radiation exposure. *PloS one* 8(12):e83390.
6. Omaruddin RA, Roland TA, Wallace III HJ, & Chaudhry MA (2013) Gene expression as a biomarker for human radiation exposure. *Human cell* 26(1):2-7.
7. Streffer C (1996) Biological indicators for radiation exposures. *IRPA9: 1996 international congress on radiation protection. Proceedings. Volume 1*.
8. Simon SL, *et al.* (2007) BiodosEPR-2006 consensus committee report on biodosimetric methods to evaluate radiation doses at long times after exposure. *Radiation Measurements* 42(6):948-971.
9. Müller W-U & Streffer C (1991) Biological indicators for radiation damage. *International journal of radiation biology* 59(4):863-873.

10. Filiano AN, *et al.* (2011) Gene expression analysis in radiotherapy patients and C57BL/6 mice as a measure of exposure to ionizing radiation. *Radiation research* 176(1):49-61.

11. A. Amundson S & J. Fornace Jr A (2001) Gene expression profiles for monitoring radiation exposure. *Radiation protection dosimetry* 97(1):11-16.

12. Brengues M, *et al.* (2010) Biodosimetry on small blood volume using gene expression assay. *Health physics* 98(2):179.

13. Kabacik S, *et al.* (2011) Gene expression following ionising radiation: identification of biomarkers for dose estimation and prediction of individual response. *International journal of radiation biology* 87(2):115-129.

14. Edmondson DA, *et al.* (2016) Transcript Analysis for Internal Biodosimetry Using Peripheral Blood from Neuroblastoma Patients Treated with 131I-mIBG, a Targeted Radionuclide. *Radiation research* 186(3):235-244.

15. Himburg HA, *et al.* (2016) A molecular profile of the endothelial cell response to ionizing radiation. *Radiation research* 186(2):141-152.

16. Stassen T, Port M, Nuyken I, & Abend M (2003) Radiation-induced gene expression in MCF-7 cells. *International journal of radiation biology* 79(5):319-331.

17. Tucker JD (2008) Low-dose ionizing radiation and chromosome translocations: a review of the major considerations for human biological dosimetry. *Mutation Research/Reviews in Mutation Research* 659(3):211-220.

18. Gramates LS, *et al.* (2017) FlyBase at 25: looking to the future. *Nucleic acids research* 45(D1):D663-D671.

19. Anonymous (2016) Database resources of the National Center for Biotechnology Information. *Nucleic Acids Research* 44(D1):D7-D19.

20. Antosh M, *et al.* (2014) Drosophila melanogaster show a threshold effect in response to radiation. *Dose-Response* 12(4):dose-response. 13-047. Antosh.

21. Anders S & Huber W (2010) Differential expression analysis for sequence count data. *Genome biology* 11(10):R106.

22. Gentleman RC, *et al.* (2004) Bioconductor: open software development for computational biology and bioinformatics. *Genome biology* 5(10):R80.

23. Beißbarth T & Speed TP (2004) GOstat: find statistically overrepresented Gene Ontologies within a group of genes. *Bioinformatics* 20(9):1464-1465.

24. Yamane K & Kinsella TJ (2005) CK2 inhibits apoptosis and changes its cellular localization following ionizing radiation. *Cancer research* 65(10):4362-4367.

Tables

Table 1. Name, homology and functional information on 6 genes found to respond linearly to radiation at all time points examined.

Flybase ID	Chromosome(Gramates, Marygold et al. 2017)	Gene Symbol (from flybase)(Gramates, Marygold et al. 2017)	Human Gene Homolog (From Homologene)-2016	Biological Function(Gramates, Marygold et al. 2017)	Molecular Function(Gramates, Marygold et al. 2017)
FBgn0011774	3R	Irbp	XRCC6	Double-strand break repair via nonhomologous end joining, telomere maintenence	Contributes to DNA binding, protein heterodimerization activity, ATP-dependent,ATP-dependent DNA helicase activity,damage DNA binding,Telomeric DNA binding inferred
FBgn0030189	X	CG2909	none	Not known	Not known
FBgn0031713	2L	CG7277	COQ6	Oxidation reduction process,Ubiquinone biosynthetic process	FAD binding,Oxidoreductase activity, acting on paired donors, with incorporation or reduction of molecular oxygen, NAD(P)H as one donor, and incorporation of one atom of oxygen
FBgn0032393	2L	CG12264	NFS1	Alanine biosynthetic process, Iron-sulfur, cluster assembly,[2Fe-2S] cluster assembly	Cystathionine gamma-lyase activity, Cysteine desulfurase activity,Pyridoxal phosphate binding
FBgn0037020	3L	Pex14	PEX14	Peroxisome organization,Protein import into peroxisome matrix,docking,Protein targeting to peroxisome	Receptor binding
FBgn0051864	2L	Qtzl	none	Not known	Not known

Table 2. Genes found to behave linearly at all three time points, if the lowest radiation dose (10 R) is not included. Name, homology and functional information on 13 genes found to respond linearly to radiation at all time points examined.

Flybase ID	Chromosome(Gramates, Marygold et al. 2017)	Gene Symbol(Gramates, Marygold et al. 2017)	Human Gene Homologue (2016)	Biological Function (Gramates, Marygold et al. 2017)	Molecular Function (Gramates, Marygold et al. 2017)
FBgn0011774	3R	Irbp	XRCC6	Double-strand break repair via nonhomologous end joining, telomere maintenance	DNA binding,Protein heterodimerization activity
FBgn0024912	3R	agt	none	DNA dealkylation involved in DNA repair	Methylated-DNA-[protein]-cysteine S-methyltransferase activity
FBgn0027101	4	Dyrk3	DYRK2	Protein phosphorylation	ATP binding, Protein
FBgn0030189	X	CG2909	none	Not known	Not known
FBgn0032393	2L	CG12264	NFS1	Alanine biosynthetic process,Iron-sulfur cluster assembly,[2Fe-2S] cluster assembly	Cystathionine gamma-lyase activity,Cysteine desulfurase activity,Pyridoxal phosphate binding
FBgn0033926	2R	Arc1	none	Behavioral response to starvation,Muscle system process	Not known
FBgn0033927	2R	CR10102	none	Not known	Not known
FBgn0034184	2R	CG9646	none	Not known	Not known
FBgn0036290	3L	CG10638	none	Oxidation – reduction process inferred	Oxidoreductase activity, inferred
FBgn0037020	3L	Pex14	PEX14	Peroxisome organization,	Not known
FBgn0037850	3R	CG14695	none	Not known	Not known
FBgn0046763	3R	CG17278	none	Negative regulation of Wnt signaling pathway inferred from genetic interaction	Not known
FBgn0051864	2L	Qtzl	none	Not known	Not known

Figures

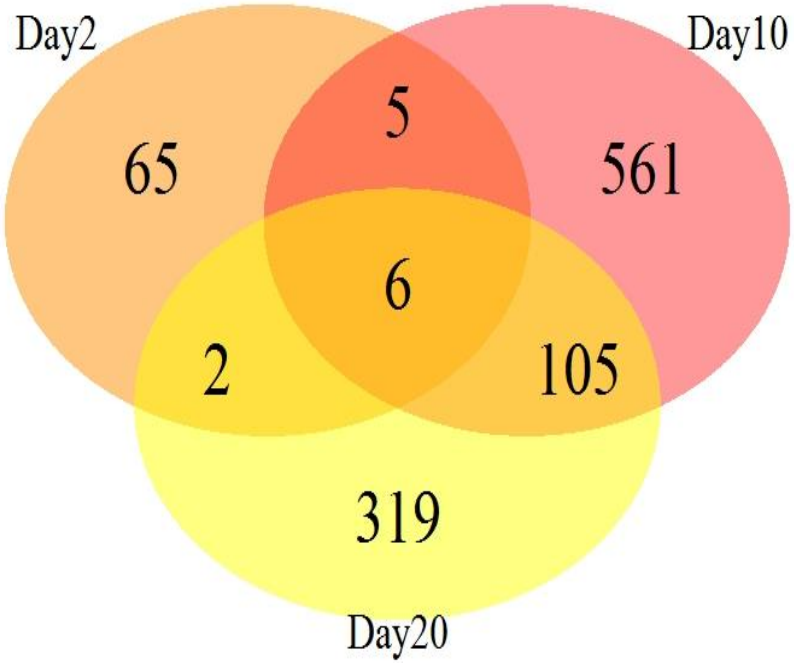

Figure 1. . Number of genes with linear response at each time point, with overlaps

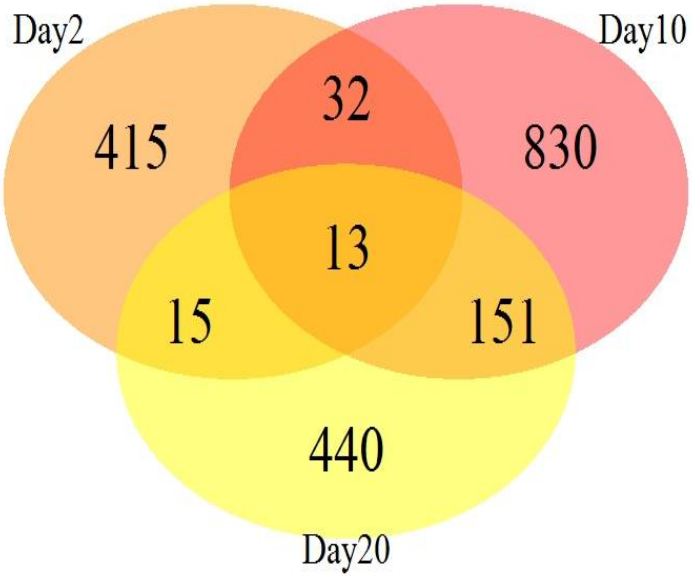

Figure 2. Analysis of linear behavior, not including data from dose 10 Roentgen. Number of genes with linear response ($R^2 > 0.9$) are given for each time point, with overlaps.

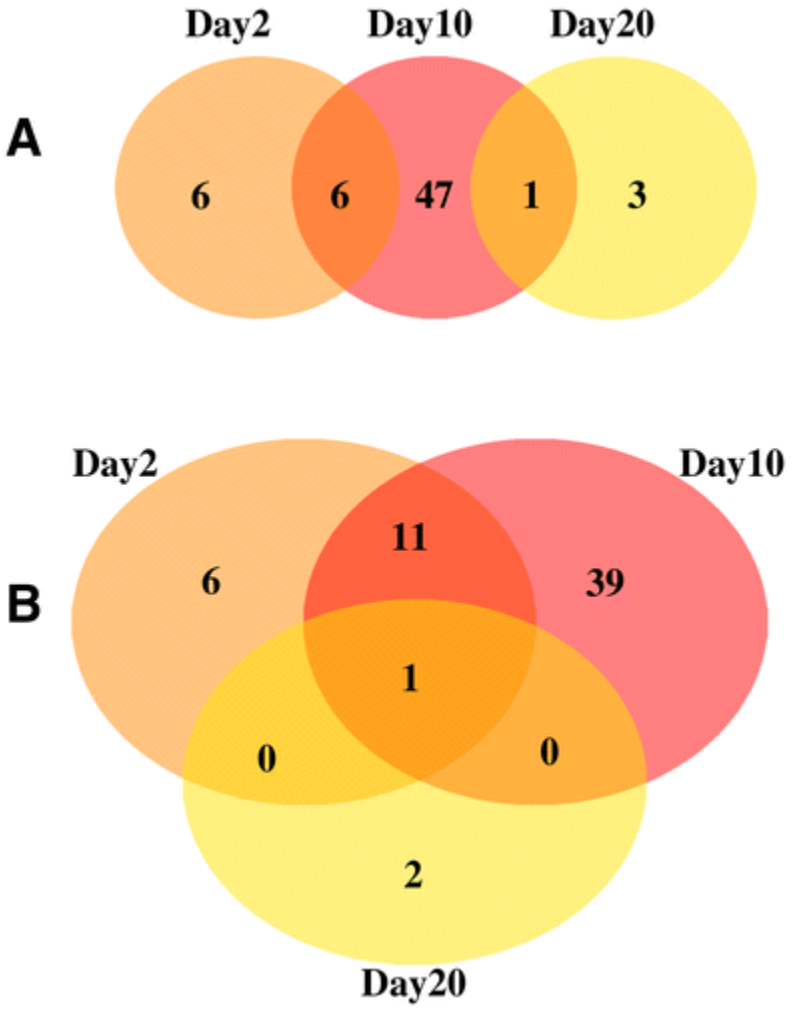

Figure 3. Number of "spike" genes at each time point, with (3A) and without (3B) the lowest radiation dose.

Supplementary Tables

GO	Count	Total	P Value	GO Name
GO:0008605	13	23	2.21E-24	protein kinase CK2 regulator activity
GO:0005956	13	23	2.21E-24	protein kinase CK2 complex
GO:0043549	12	35	2.19E-19	regulation of kinase activity
GO:0051338	12	35	2.19E-19	regulation of transferase activity
GO:0045859	12	35	2.19E-19	regulation of protein kinase activity
GO:0019887	13	53	5.02E-19	protein kinase regulator activity
GO:0019207	13	55	7.39E-19	kinase regulator activity
GO:0050790	12	57	1.10E-16	regulation of catalytic activity
GO:0065009	12	70	1.41E-15	regulation of a molecular function
GO:0007283	10	150	1.13E-08	spermatogenesis
GO:0048232	10	150	1.13E-08	male gamete generation
GO:0043234	19	1371	8.22E-08	protein complex
GO:0032991	20	1652	1.45E-06	macromolecular complex
GO:0007276	11	704	0.00244	gamete generation
GO:0019953	11	730	0.00307	sexual reproduction
GO:0065007	15	1459	0.00307	biological regulation
GO:0044464	30	4358	0.00372	cell#cell part
GO:0005623	30	4358	0.00372	cell
GO:0005737	16	1833	0.0213	cytoplasm
GO:0044459	6	305	0.0303	plasma membrane part
GO:0035147	2	14	0.0311	branch fusion, open tracheal system
GO:0035146	2	14	0.0311	branching morphogenesis of a tube#tube fusion
GO:0005634	13	1420	0.0416	nucleus

Table S1A. Gene Ontologies Overrepresented in Genes Found to Behave Linearly at Day 2 Post-Irradiation. (Analysis with all data included.)

GO	Count	Total	P Value	GO Name
GO:0008083	6	17	0.0333	growth factor activity
GO:0016491	38	541	0.0333	oxidoreductase activity

Table S1B. Gene Ontologies Overrepresented in Genes Found to Behave Linearly at Day 10 Post-Irradiation. (Analysis with all data included.)

GO	Count	Total	P Value	GO Name
GO:0016021	33	608	0.00106	integral to membrane
GO:0031224	33	613	0.00106	intrinsic to membrane
GO:0016020	58	1367	0.0016	membrane
GO:0006950	15	211	0.0069	response to stress
GO:0044459	19	305	0.0069	plasma membrane part
GO:0005887	14	169	0.0115	integral to plasma membrane
GO:0044425	43	1002	0.0115	membrane#membrane part
GO:0031226	14	172	0.0115	intrinsic to plasma membrane
GO:0004872	23	424	0.0115	receptor activity
GO:0004888	20	355	0.0139	transmembrane receptor activity
GO:0004871	26	517	0.0139	signal transducer activity
GO:0060089	26	517	0.0139	molecular transducer activity
GO:0009595	3	5	0.0139	detection of biotic stimulus
GO:0016045	3	5	0.0139	detection of bacterium
GO:0030425	4	12	0.0139	dendrite
GO:0006281	8	67	0.0164	DNA repair
GO:0001871	6	36	0.0164	pattern binding
GO:0042834	4	13	0.0164	peptidoglycan binding
GO:0000270	3	7	0.0353	peptidoglycan metabolic process
GO:0006974	8	79	0.0448	response to DNA damage stimulus

Table S1C. Gene Ontologies Overrepresented in Genes Found to Behave Linearly at Day 20 Post-Irradiation. (Analysis with all data included.)

GO	Count	Total	P Value	GO Name
GO:0004123	1	2	0.0243	cystathionine gamma-lyase activity
GO:0006625	1	2	0.0243	protein targeting to peroxisome
GO:0016226	1	2	0.0243	iron-sulfur cluster assembly
GO:0043574	1	2	0.0243	peroxisomal transport
GO:0031163	1	2	0.0243	metallo-sulfur cluster assembly
GO:0004090	1	3	0.0331	carbonyl reductase (NADPH) activity

Table S1D. Gene Ontologies Overrepresented in Genes Found to Behave Linearly at Days 2 and 10 Post-Irradiation. (Analysis with all data included.)

GO	Count	Total	P Value	GO Name
GO:0006950	9	211	0.00111	response to stress

Table S1E. Gene Ontologies Overrepresented in Genes Found to Behave Linearly at Days 10 and 20 Post-Irradiation. (Analysis with all data included.)

GO	Count	Total	P Value	GO Name
GO:0004123	1	2	0.00745	cystathionine gamma-lyase activity
GO:0006625	1	2	0.00745	protein targeting to peroxisome
GO:0016226	1	2	0.00745	iron-sulfur cluster assembly
GO:0043574	1	2	0.00745	peroxisomal transport
GO:0031163	1	2	0.00745	metallo-sulfur cluster assembly
GO:0016846	1	6	0.0206	carbon-sulfur lyase activity
GO:0001666	1	9	0.0268	response to hypoxia
GO:0032200	1	10	0.0268	telomere organization and biogenesis
GO:0000723	1	10	0.0268	telomere maintenance
GO:0044439	1	12	0.0268	peroxisomal part
GO:0044438	1	12	0.0268	microbody#microbody part
GO:0031903	1	12	0.0268	microbody membrane
GO:0005778	1	12	0.0268	peroxisomal membrane
GO:0007031	1	13	0.0276	peroxisome organization and biogenesis
GO:0008652	1	20	0.0388	amino acid biosynthetic process
GO:0004003	1	20	0.0388	ATP-dependent DNA helicase activity

Table S1F. Gene Ontologies Overrepresented in Genes Found to Behave Linearly at Days 2 and 20 Post-Irradiation. (Analysis with all data included.)

GO	Count	Total	P Value	GO Name
GO:0004123	1	2	0.00517	cystathionine gamma-lyase activity
GO:0006625	1	2	0.00517	protein targeting to peroxisome
GO:0016226	1	2	0.00517	iron-sulfur cluster assembly
GO:0043574	1	2	0.00517	peroxisomal transport
GO:0031163	1	2	0.00517	metallo-sulfur cluster assembly
GO:0016846	1	6	0.0141	carbon-sulfur lyase activity
GO:0032200	1	10	0.0182	telomere organization and biogenesis
GO:0000723	1	10	0.0182	telomere maintenance
GO:0044439	1	12	0.0182	peroxisomal part
GO:0044438	1	12	0.0182	microbody#microbody part
GO:0031903	1	12	0.0182	microbody membrane
GO:0005778	1	12	0.0182	peroxisomal membrane
GO:0007031	1	13	0.0187	peroxisome organization and biogenesis
GO:0008652	1	20	0.0258	amino acid biosynthetic process
GO:0004003	1	20	0.0258	ATP-dependent DNA helicase activity
GO:0008094	1	29	0.0331	DNA-dependent ATPase activity
GO:0042579	1	31	0.0331	microbody
GO:0005777	1	31	0.0331	peroxisome
GO:0009309	1	34	0.0331	amine biosynthetic process
GO:0044271	1	35	0.0331	nitrogen compound biosynthetic process
GO:0043231	3	2283	0.0331	intracellular membrane-bound organelle
GO:0043227	3	2287	0.0331	membrane-bound organelle
GO:0003678	1	36	0.0331	DNA helicase activity

Table S1G: Gene Ontologies Overrepresented in Genes Found to Behave Linearly at Days 2, 10 and 20 Post-Irradiation. (Analysis with all data included.)

GO	Count	Total	P Value	GO Name
GO:0008605	13	23	5.14E-13	xprotein kinase CK2 regulator activity
GO:0005956	13	23	5.14E-13	protein kinase CK2 complex
GO:0043549	12	35	4.92E-09	regulation of kinase activity
GO:0051338	12	35	4.92E-09	regulation of transferase activity
GO:0045859	12	35	4.92E-09	regulation of protein kinase activity
GO:0019887	13	53	6.60E-08	protein kinase regulator activity
GO:0019207	13	55	9.35E-08	kinase regulator activity
GO:0050790	12	57	1.63E-06	regulation of catalytic activity
GO:0065009	13	70	1.72E-06	regulation of a molecular function
GO:0007283	17	150	1.68E-05	xspermatogenesis
GO:0048232	17	150	1.68E-05	male gamete generation
GO:0022411	5	13	0.00115	cellular component disassembly

Table S2A. Gene Ontologies Overrepresented in Genes Found to Behave Linearly at Day 2 Post-Irradiation. (Analysis with lowest dose discluded.)

GO	Count	Total	P Value	GO Name
GO:0003924	17	102	0.0028	GTPase activity
GO:0016798	16	102	0.0118	hydrolase activity, acting on glycosyl bonds
GO:0005102	19	136	0.0129	receptor binding
GO:0004553	15	96	0.0129	hydrolase activity, hydrolyzing O-glycosyl compounds
GO:0009055	21	166	0.0282	electron carrier activity
GO:0005624	14	93	0.0334	membrane fraction
GO:0005515	79	974	0.0334	protein binding
GO:0000267	14	96	0.0411	cell fraction
GO:0016740	70	851	0.0411	transferase activity
GO:0008083	6	17	0.0411	growth factor activity
GO:0005778	5	12	0.0427	peroxisomal membrane
GO:0044438	5	12	0.0427	microbody#microbody part
GO:0031903	5	12	0.0427	microbody membrane
GO:0044439	5	12	0.0427	peroxisomal part
GO:0016491	48	541	0.0499	oxidoreductase activity

Table S2B. Gene Ontologies Overrepresented in Genes Found to Behave Linearly at Day 10 Post-Irradiation. (Analysis with lowest dose discluded.)

GO	Count	Total	P Value	GO Name
GO:0005887	16	169	0.0205	integral to plasma membrane
GO:0031226	16	172	0.0205	intrinsic to plasma membrane
GO:0000270	4	7	0.0205	peptidoglycan metabolic process
GO:0042834	5	13	0.0205	peptidoglycan binding
GO:0017143	4	9	0.0328	insecticide metabolic process
GO:0006805	4	9	0.0328	xenobiotic metabolic process
GO:0009404	4	9	0.0328	toxin metabolic process
GO:0009410	4	9	0.0328	response to xenobiotic stimulus
GO:0016020	70	1367	0.0355	membrane
GO:0046903	15	172	0.0361	secretion
GO:0019752	14	156	0.0361	carboxylic acid metabolic process
GO:0006082	14	156	0.0361	organic acid metabolic process
GO:0009056	15	174	0.037	catabolic process
GO:0044459	22	305	0.0377	plasma membrane part
GO:0016192	26	386	0.0377	vesicle-mediated transport
GO:0006767	4	11	0.0377	water-soluble vitamin metabolic process
GO:0009595	3	5	0.0377	detection of biotic stimulus
GO:0016045	3	5	0.0377	detection of bacterium
GO:0030425	4	12	0.0486	dendrite
GO:0016021	36	608	0.0486	integral to membrane

Table S2C. Gene Ontologies Overrepresented in Genes Found to Behave Linearly at Day 20 Post-Irradiation. (Analysis with lowest dose discluded.)

(none)					

Table S2D. Gene Ontologies Overrepresented in Genes Found to Behave Linearly at Days 2 and 10 Post-Irradiation. (Analysis with lowest dose discluded.)

GO	Count	Total	P Value	GO Name
GO:0005778	3	12	0.0165	peroxisomal membrane
GO:0044438	3	12	0.0165	microbody#microbody part
GO:0044439	3	12	0.0165	xperoxisomal part
GO:0031903	3	12	0.0165	microbody membrane
GO:0007031	3	13	0.0171	peroxisome organization and biogenesis

Table S2E. Gene Ontologies Overrepresented in Genes Found to Behave Linearly at Days 10 and 20 Post-Irradiation. (Analysis with lowest dose discluded.)

GO	Count	Total	P Value	GO Name
GO:0000723	2	10	0.0169	telomere maintenance
GO:0032200	2	10	0.0169	telomere organization and biogenesis
GO:0004003	2	20	0.0217	ATP-dependent DNA helicase activity
GO:0016772	5	446	0.0217	transferase activity, transferring phosphorus-containing groups
GO:0008094	2	29	0.0217	DNA-dependent ATPase activity
GO:0043296	2	36	0.0217	apicolateral plasma membrane#apical junction complex
GO:0003678	2	36	0.0217	DNA helicase activity
GO:0016740	6	851	0.0217	transferase activity
GO:0016327	2	40	0.0237	apicolateral plasma membrane
GO:0005911	2	50	0.0302	intercellular junction
GO:0006081	1	2	0.0302	aldehyde metabolic process
GO:0004105	1	2	0.0302	choline-phosphate cytidylyltransferase activity
GO:0031163	1	2	0.0302	metallo-sulfur cluster assembly
GO:0004345	1	2	0.0302	glucose-6-phosphate dehydrogenase activity
GO:0004123	1	2	0.0302	cystathionine gamma-lyase activity
GO:0006625	1	2	0.0302	protein targeting to peroxisome
GO:0016226	1	2	0.0302	iron-sulfur cluster assembly
GO:0043574	1	2	0.0302	peroxisomal transport
GO:0016337	2	59	0.0361	cell-cell adhesion
GO:0017116	1	3	0.0415	single-stranded DNA-dependent ATP-dependent DNA helicase activity
GO:0043142	1	3	0.0415	single-stranded DNA-dependent ATPase activity
GO:0016779	2	68	0.0438	nucleotidyltransferase activity
GO:0008026	2	70	0.0443	ATP-dependent helicase activity
GO:0051186	2	75	0.0443	cofactor metabolic process
GO:0030054	2	75	0.0443	cell junction
GO:0006740	1	4	0.0443	NADPH regeneration
GO:0009225	1	4	0.0443	nucleotide-sugar metabolic process
GO:0006098	1	4	0.0443	pentose-phosphate shunt
GO:0006739	1	4	0.0443	NADP metabolic process
GO:0005923	1	4	0.0443	apicolateral plasma membrane#apical junction complex#tight junction
GO:0016616	2	79	0.0471	oxidoreductase activity, acting on the CH-OH group of donors, NAD or NADP as acceptor

Table S2F. Gene Ontologies Overrepresented in Genes Found to Behave Linearly at Days 2 and 20 Post-Irradiation. (Analysis with lowest dose discluded.)

GO	Count	Total	P Value	GO Name
GO:0004123	1	2	0.0123	cystathionine gamma-lyase activity
GO:0006625	1	2	0.0123	protein targeting to peroxisome
GO:0006081	1	2	0.0123	aldehyde metabolic process
GO:0016226	1	2	0.0123	iron-sulfur cluster assembly
GO:0043574	1	2	0.0123	xperoxisomal transport
GO:0031163	1	2	0.0123	metallo-sulfur cluster assembly
GO:0004032	1	6	0.0323	aldehyde reductase activity
GO:0016846	1	6	0.0323	carbon-sulfur lyase activity
GO:0004033	1	8	0.0405	aldo-keto reductase activity
GO:0004674	2	190	0.0412	protein serine/threonine kinase activity
GO:0032200	1	10	0.0412	telomere organization and biogenesis
GO:0000723	1	10	0.0412	xtelomere maintenance
GO:0030178	1	11	0.0412	xnegative regulation of Wnt receptor signaling pathway
GO:0044439	1	12	0.0412	peroxisomal part
GO:0044438	1	12	0.0412	microbody#microbody part
GO:0031903	1	12	0.0412	microbody membrane
GO:0005778	1	12	0.0412	peroxisomal membrane
GO:0007031	1	13	0.0429	peroxisome organization and biogenesis

Table S2G. Gene Ontologies Overrepresented in Genes Found to Behave Linearly at Days 2, 10 and 20 Post-Irradiation. (Analysis with lowest dose discluded.)

Flybase ID	Spike Ratio	Dose Causing Spike	Day 2 Fold Change 10R	Day 2 Fold Change 1000R	Day 2 Fold Change 50000R	Day 2 Fold Change 10000R	Day 2 Fold Change 20000R
FBgn0005391	6.018	10000R	2.573	0.888	0.545	15.486	1.268
FBgn0004045	15.787	10000R	0.936	0.447	0.849	16.168	1.024
FBgn0038191	5.379	1000R	0.248	1.332	0.141	0.183	0.154
FBgn0013672	7.952	20000R	1.114	0.656	0.783	0.651	8.855
FBgn0013678	7.046	20000R	1.028	0.774	0.681	0.729	7.242
FBgn0034152	6.826	20000R	0.780	6.282	2.196	6.885	46.999
FBgn0013676	6.461	20000R	1.278	0.876	1.026	0.772	8.256
FBgn0013674	6.025	20000R	1.271	1.155	0.874	0.985	7.656
FBgn0259968	5.361	20000R	0.945	1.163	0.673	0.789	6.237
FBgn0013675	13.108	20000R	1.336	0.673	0.855	0.522	17.518
FBgn0013745	7.176	5000R	0.371	0.966	11.772	1.155	1.640
FBgn0262099	6.609	5000R	0.591	5.446	44.237	6.693	5.023

Table S3A. Values of Spike Ratio and Fold Changes for Genes Found to Spike at Day 2 Post-Irradiation. (Analysis with all data included.) Spike ratio = (largest fold change)/(second largest fold change)

Flybase ID	SpikeRatio	Dose Causing Spike	Day10 Fold Change 10R	Day10 Fold Change 1000R	Day10 Fold Change 5000R	Day10 Fold Change 10000R	Day10 Fold Change 20000R
FBgn0013679	9.785	20000R	2.051	1.087	1.137	1.197	20.065
FBgn0025740	9.617	20000R	0.429	0.708	0.469	0.462	6.805
FBgn0013672	9.472	20000R	0.758	0.864	1.744	0.981	16.520
FBgn0085364	9.183	20000R	1.107	1.655	1.378	1.306	15.201
FBgn0013676	8.690	20000R	0.921	0.799	1.255	1.007	10.907
FBgn0031111	8.280	10R	13.211	1.114	1.485	1.011	1.596
FBgn0013681	7.360	20000R	1.370	0.709	1.617	0.388	11.902
FBgn0000427	68.582	20000R	164.035	1.051	1.101	1.066	2.392
FBgn0259968	6.846	20000R	1.012	1.200	1.482	1.239	10.143
FBgn0041709	6.434	10R	24.479	0.793	0.771	1.388	3.805
FBgn0013686	6.416	20000R	0.563	0.882	0.650	0.863	5.657
FBgn0021738	6.346	20000R	0.478	0.673	0.860	0.708	5.455
FBgn0262972	6.089	20000R	0.770	0.886	0.821	0.256	5.397
FBgn0000357	52.726	10R	76.612	0.932	1.159	1.218	1.453
FBgn0039916	5.769	20000R	0.351	0.749	1.016	0.939	5.862
FBgn0037836	5.715	20000R	0.869	1.050	1.071	0.741	6.122
FBgn0036790	5.703	20000R	0.355	0.705	0.575	0.469	4.018
FBgn0036985	5.546	20000R	0.568	1.104	0.578	0.905	6.126
FBgn0032946	5.427	20000R	1.689	1.590	1.541	1.264	9.167
FBgn0086782	5.393	20000R	0.684	0.802	0.592	0.965	5.205
FBgn0052350	5.357	20000R	0.610	0.803	0.900	1.126	6.034
FBgn0013675	5.229	20000R	0.857	0.937	2.220	0.813	11.611
FBgn0039925	35.389	20000R	0.305	0.413	0.446	0.518	18.324
FBgn0013680	28.243	20000R	1.126	1.065	1.218	0.802	34.413
FBgn0053855	21.401	20000R	2.643	0.651	0.897	2.320	56.555
FBgn0053858	21.234	20000R	2.791	0.722	0.928	2.390	59.260
FBgn0053810	20.386	20000R	2.449	0.632	0.869	1.988	49.934
FBgn0053831	19.800	20000R	2.574	0.582	0.855	1.974	50.972
FBgn0053837	19.797	20000R	2.442	0.651	0.838	1.921	48.348
FBgn0053822	19.649	20000R	2.621	0.607	0.794	2.017	51.495
FBgn0053816	19.527	20000R	2.529	0.583	0.874	1.958	49.377
FBgn0053861	19.524	20000R	3.118	0.737	0.932	2.407	60.868

FBgn0053819	19.465	20000R	2.609	0.640	0.853	2.004	50.776
FBgn0053807	19.436	20000R	2.337	0.593	0.804	1.836	45.416
FBgn0053828	19.260	20000R	2.519	0.617	0.848	1.931	48.524
FBgn0053825	19.255	20000R	2.568	0.628	0.829	1.966	49.449
FBgn0053843	19.255	20000R	2.712	0.715	0.846	1.989	52.223
FBgn0053864	19.048	20000R	2.565	0.597	0.861	1.925	48.861
FBgn0053852	19.034	20000R	2.534	0.624	0.825	1.921	48.235
FBgn0053813	18.977	20000R	2.776	0.680	0.875	2.202	52.672
FBgn0053846	18.904	20000R	2.613	0.603	0.845	1.988	49.390
FBgn0051617	18.804	20000R	2.440	0.540	0.811	1.893	45.879
FBgn0053801	18.653	20000R	2.549	0.612	0.815	1.928	47.551
FBgn0053849	18.323	20000R	2.771	0.623	0.858	1.975	50.782
FBgn0053840	17.922	20000R	2.677	0.660	0.830	1.901	47.978
FBgn0053804	17.761	20000R	2.622	0.601	0.851	1.913	46.573
FBgn0013678	15.720	20000R	0.806	0.784	1.009	0.988	15.862
FBgn0000355	141.389	10R	130.305	0.922	0.687	0.127	0.165
FBgn0013685	14.707	20000R	1.367	0.670	0.853	0.396	20.105
FBgn0052602	13.143	10R	20.045	0.874	0.626	0.624	1.525
FBgn0052580	124.695	20000R	0.208	0.620	0.240	0.751	93.597
FBgn0013674	12.216	20000R	0.910	0.963	0.947	1.071	13.085
FBgn0262952	12.152	20000R	1.639	1.050	0.703	1.111	19.912
FBgn0013684	11.816	20000R	1.266	0.696	0.642	0.729	14.954

Table S3B. Values of Spike Ratio and Fold Changes for Genes Found to Spike at Day 10 Post-Irradiation. (Analysis with all data included.) Spike ratio = (largest fold change)/(second largest fold change)

Flybase ID	Spike Ratio	Dose Causing Spike	Day 20 Fold Change 10R	Day 20 Fold Change 1000R	Day 20 Fold Change 5000R	Day 20 Fold Change 10000R	Day 20 Fold Change 20000R
FBgn0053222	9.209	5000R	1.164	1.180	10.869	0.146	0.026
FBgn0085364	8.050	20000R	1.094	1.610	0.895	1.364	12.963
FBgn0039480	6.902	20000R	0.158	0.105	0.090	0.173	1.193
FBgn0040637	6.835	20000R	1.457	1.511	2.097	NA	14.334

Table S3C. Values of Spike Ratio and Fold Changes for Genes Found to Spike at Day 20 Post-Irradiation. (Analysis with all data included.) Spike ratio = (largest fold change)/(second largest fold change)

FlyBase ID	Spike Ratio Day 2	Dose Causing Spike Day2	SpikeRatio Day10	Dose Causing Spike Day10	Day 2 Fold Change 10R	Day 2 Fold Change 1000R	Day 2 Fold Change 5000R	Day 2 Fold Change 10000R	Day 2 Fold Change 20000R	Day10 Fold Change 10R	Day10 Fold Change 1000R	Day10 Fold Change 5000R	Day10 Fold Change 10000R	Day10 Fold Change 20000R
FBgn0013672	7.952	20000R	9.472	20000R	1.114	0.656	0.783	0.651	8.855	0.758	0.864	1.744	0.981	16.520
FBgn0013678	7.046	20000R	8.690	20000R	1.028	0.774	0.681	0.729	7.242	0.921	0.799	1.255	1.007	10.907
FBgn0013676	6.461	20000R	6.846	20000R	1.278	0.876	1.026	0.772	8.256	1.012	1.200	1.482	1.239	10.143
FBgn0013674	6.025	20000R	5.229	20000R	1.271	1.155	0.874	0.985	7.656	0.857	0.937	2.220	0.813	11.611
FBgn0259968	5.361	20000R	15.72	20000R	0.945	1.163	0.673	0.789	6.237	0.806	0.784	1.009	0.988	15.862
FBgn0013675	13.108	20000R	12.216	20000R	1.336	0.673	0.855	0.522	17.518	0.910	0.963	0.947	1.071	13.085

Table S3D. Values of Spike Ratio and Fold Changes for Genes Found to Spike at Days 2 and 10 Post-Irradiation. (Analysis with all data included.) Spike ratio = (largest fold change)/(second largest fold change)

Flybase ID	SpikeRatio Day 10	Dose Causing Spike Day10	SpikeRatio Day 20	Dose Causing Spike Day20	Day 10 Fold Change 10R	Day10 Fold Change 1000R	Day10 Fold Change 5000R	Day10 Fold Change 10000R	Day10 Fold Change 20000R	Day 20 Fold Change 10R	Day 20 Fold Change 1000R	Day 20 Fold Change 5000R	Day 20 Fold Change 10000R	Day 20 Fold Change 20000R
FBgn0085364	9.183	20000R	8.050	20000R	1.107	1.655	1.378	1.306	15.201	1.094	1.610	0.895	1.364	12.963

Table S3E. Values of Spike Ratio and Fold Changes for Genes Found to Spike at Days 10 and 20 Post-Irradiation. (Analysis with all data included.) Spike ratio = (largest fold change)/(second largest fold change)

(none)						

Table S3F. Values of Spike Ratio and Fold Changes for Genes Found to Spike at Days 2 and 20 Post-Irradiation. (Analysis with all data included.) Spike ratio = (largest fold change)/(second largest fold change)

(none)				

Table S3G. Values of Spike Ratio and Fold Changes for Genes Found to Spike at Days 2, 10 and 20 Post-Irradiation. (Analysis with all data included.) Spike ratio = (largest fold change)/(second largest fold change)

Flybase ID	SpikeRatio	Dose Causing Spike	Day 2 Fold Change 1000R	Day 2 Fold Change 5000R	Day 2 Fold Change 10000R	Day 2 Fold Change 20000R
FBgn0013678	9.356	20000R	0.774	0.681	0.729	7.242
FBgn0013680	9.132	20000R	0.563	0.683	0.420	6.233
FBgn0013676	8.044	20000R	0.876	1.026	0.772	8.256
FBgn0013673	7.347	20000R	0.466	0.685	0.372	5.031
FBgn0013683	7.239	20000R	0.944	0.695	0.318	6.832
FBgn0013745	7.176	5000R	0.966	11.772	1.155	1.640
FBgn0034152	6.826	20000R	6.282	2.196	6.885	46.999
FBgn0013674	6.631	20000R	1.155	0.874	0.985	7.656
FBgn0262099	6.609	5000R	5.446	44.237	6.693	5.023
FBgn0013681	6.558	20000R	0.798	0.916	0.515	6.005
FBgn0013684	6.476	20000R	0.788	0.633	0.788	5.102
FBgn0013679	5.956	20000R	1.004	0.879	0.867	5.981
FBgn0085364	5.415	20000R	1.298	0.718	0.916	7.026
FBgn0259968	5.361	20000R	1.163	0.673	0.789	6.237
FBgn0013685	24.186	20000R	0.338	0.246	0.237	8.163
FBgn0013675	20.490	10000R	0.673	0.855	0.522	17.518
FBgn0004045	15.787	10000R	0.447	0.849	16.168	1.024
FBgn0013672	11.306	20000R	0.656	0.783	0.651	8.855

Table S4A. Values of Spike Ratio and Fold Changes for Genes Found to Spike at Day 2 Post-Irradiation. (Analysis with lowest dose discluded.) Spike ratio = (largest fold change)/(second largest fold change)

Flybase ID	Spike Ratio	Dose Causing Spike	Day 10 Fold Change 1000R	Day 10 Fold Change 5000R	Day 10 Fold Change 10000R	Day 10 Fold Change 20000R
FBgn0004045	87.528	10000R	1.684	2.465	515.653	5.891
FBgn0260780	7.925	10000R	1.245	1.084	19.861	2.506
FBgn0002962	7.160	10000R	1.413	2.257	16.159	1.356
FBgn0003023	5.911	10000R	0.741	0.755	8.156	1.380
FBgn0004047	34.886	10000R	0.937	1.088	37.960	1.078
FBgn0004649	19.854	10000R	1.338	0.734	26.571	0.523
FBgn0005391	158.647	10000R	1.399	1.805	391.716	2.469
FBgn0025740	9.617	20000R	0.708	0.469	0.462	6.805
FBgn0013672	9.472	20000R	0.864	1.744	0.981	16.520
FBgn0085364	9.183	20000R	1.655	1.378	1.306	15.201
FBgn0013676	8.690	20000R	0.799	1.255	1.007	10.907
FBgn0013681	7.360	20000R	0.709	1.617	0.388	11.902
FBgn0259968	6.846	20000R	1.200	1.482	1.239	10.143
FBgn0013686	6.416	20000R	0.882	0.650	0.863	5.657
FBgn0262972	6.089	20000R	0.886	0.821	0.256	5.397
FBgn0032946	5.765	20000R	1.590	1.541	1.264	9.167
FBgn0037836	5.715	20000R	1.050	1.071	0.741	6.122
FBgn0036790	5.703	20000R	0.705	0.575	0.469	4.018
FBgn0086782	5.393	20000R	0.802	0.592	0.965	5.205
FBgn0052350	5.357	20000R	0.803	0.900	1.126	6.034
FBgn0013675	5.229	20000R	0.937	2.220	0.813	11.611
FBgn0039925	35.389	20000R	0.413	0.446	0.518	18.324
FBgn0013680	28.243	20000R	1.065	1.218	0.802	34.413
FBgn0053843	26.253	20000R	0.715	0.846	1.989	52.223
FBgn0053831	25.818	20000R	0.582	0.855	1.974	50.972
FBgn0053849	25.717	20000R	0.623	0.858	1.975	50.782
FBgn0053822	25.530	20000R	0.607	0.794	2.017	51.495
FBgn0053864	25.387	20000R	0.597	0.861	1.925	48.861
FBgn0053819	25.332	20000R	0.640	0.853	2.004	50.776
FBgn0053861	25.293	20000R	0.737	0.932	2.407	60.868
FBgn0053840	25.241	20000R	0.660	0.830	1.901	47.978
FBgn0053816	25.222	20000R	0.583	0.874	1.958	49.377
FBgn0053837	25.174	20000R	0.651	0.838	1.921	48.348
FBgn0053825	25.150	20000R	0.628	0.829	1.966	49.449
FBgn0053828	25.132	20000R	0.617	0.848	1.931	48.524
FBgn0053810	25.121	20000R	0.632	0.869	1.988	49.934
FBgn0053852	25.107	20000R	0.624	0.825	1.921	48.235

FBgn0053846	24.838	20000R	0.603	0.845	1.988	49.390
FBgn0053858	24.791	20000R	0.722	0.928	2.390	59.260
FBgn0053807	24.743	20000R	0.593	0.804	1.836	45.416
FBgn0053801	24.666	20000R	0.612	0.815	1.928	47.551
FBgn0053855	24.373	20000R	0.651	0.897	2.320	56.555
FBgn0053804	24.341	20000R	0.601	0.851	1.913	46.573
FBgn0051617	24.233	20000R	0.540	0.811	1.893	45.879
FBgn0053813	23.919	20000R	0.680	0.875	2.202	52.672
FBgn0013684	20.510	20000R	0.696	0.642	0.729	14.954
FBgn0262952	17.927	20000R	1.050	0.703	1.111	19.912
FBgn0013679	16.768	20000R	1.087	1.137	1.197	20.065
FBgn0013678	15.720	20000R	0.784	1.009	0.988	15.862
FBgn0052580	124.695	20000R	0.620	0.240	0.751	93.597
FBgn0013674	12.216	20000R	0.963	0.947	1.071	13.085

Table S4B. Values of Spike Ratio and Fold Changes for Genes Found to Spike at Day 10 Post-Irradiation. (Analysis with lowest dose discluded.) Spike ratio = (largest fold change)/(second largest fold change)

Flybase ID	**Spike Ratio**	**Dose Causing Spike**	**Day 20 Fold Change 1000R**	**Day 20 Fold Change 5000R**	**Day 20 Fold Change 10000R**	**Day 20 Fold Change 20000R**
FBgn0053222	9.209	5000R	1.180	10.869	0.146	0.026
FBgn0085364	8.050	20000R	1.610	0.895	1.364	12.963
FBgn0039480	6.902	20000R	0.105	0.090	0.173	1.193

Table S4C. Values of Spike Ratio and Fold Changes for Genes Found to Spike at Day 20 Post-Irradiation. (Analysis with lowest dose discluded.) Spike ratio = (largest fold change)/(second largest fold change)

Flybase ID	Spike Ratio Day2	Dose Causing Spike Day2	Spike Ratio Day10	Dose Causing Spike Day10	Day 2 Fold Change 1000R	Day 2 Fold Change 5000R	Day 2 Fold Change 10000R	Day 2 Fold Change 20000R	Day 10 Fold Change 1000R	Day 10 Fold Change 5000R	Day 10 Fold Change 10000R	Day 10 Fold Change 20000R
FBgn0004045	15.787	10000R	87.528	10000R	0.447	0.849	16.168	1.024	1.684	2.465	515.653	5.891
FBgn0013672	11.306	20000R	9.472	20000R	0.656	0.783	0.651	8.855	0.864	1.744	0.981	16.520
FBgn0013674	6.631	20000R	12.216	20000R	1.155	0.874	0.985	7.656	0.963	0.947	1.071	13.085
FBgn0013675	20.490	20000R	5.229	20000R	0.673	0.855	0.522	17.518	0.937	2.220	0.813	11.611
FBgn0013676	8.044	20000R	8.690	20000R	0.876	1.026	0.772	8.256	0.799	1.255	1.007	10.907
FBgn0013678	9.356	20000R	15.720	20000R	0.774	0.681	0.729	7.242	0.784	1.009	0.988	15.862
FBgn0013679	5.956	20000R	16.768	20000R	1.004	0.879	0.867	5.981	1.087	1.137	1.197	20.065
FBgn0013680	9.132	20000R	28.243	20000R	0.563	0.683	0.420	6.233	1.065	1.218	0.802	34.413
FBgn0013681	6.558	20000R	7.360	20000R	0.798	0.916	0.515	6.005	0.709	1.617	0.388	11.902
FBgn0013684	6.476	20000R	20.510	20000R	0.788	0.633	0.788	5.102	0.696	0.642	0.729	14.954
FBgn0085364	5.415	20000R	9.183	20000R	1.298	0.718	0.916	7.026	1.655	1.378	1.306	15.201
FBgn0259968	5.361	20000R	6.846	20000R	1.163	0.673	0.789	6.237	1.200	1.482	1.239	10.143

Table S4D. Values of Spike Ratio and Fold Changes for Genes Found to Spike at Days 2 and 10 Post-Irradiation. (Analysis with lowest dose discluded.) Spike ratio = (largest fold change)/(second largest fold change)

Flybase ID	Spike Ratio Day 10	Dose Causing Spike Day 10	Spike Ratio Day 20	Dose Causing Spike Day 20	Day 10 Fold Change 1000R	Day 10 Fold Change 5000R	Day 10 Fold Change 10000R	Day 10 Fold Change 20000R	Day 20 Fold Change 1000R	Day 20 Fold Change 5000R	Day 20 Fold Change 10000R	Day 20 Fold Change 20000R
FBgn0085364	9.183	20000R	8.050	20000R	1.655	1.378	1.306	15.201	1.610	0.895	1.364	12.963

Table S4E. Values of Spike Ratio and Fold Changes for Genes Found to Spike at Days 10 and 20 Post-Irradiation. (Analysis with lowest dose discluded.) Spike ratio = (largest fold change)/(second largest fold change)

Flybase ID	Spike Ratio Day 2	Dose Causing Spike Day 2	Spike Ratio Day 20	Dose Causing Spike Day20	Day 2 Fold Change 1000R	Day 2 Fold Change 5000R	Day 2 Fold Change 10000R	Day 2 Fold Change 20000R	Day 20 Fold Change 1000R	Day 20 Fold Change 5000R	Day 20 Fold Change 10000R	Day 20 Fold Change 20000R
FBgn0085364	5.415	20000R	8.050	20000R	1.298	0.718	0.916	7.026	1.610	0.895	1.364	12.963

Table S4F. Values of Spike Ratio and Fold Changes for Genes Found to Spike at Days 2 and 20 Post-Irradiation. (Analysis with lowest dose discluded.) Spike ratio = (largest fold change)/(second largest fold change)

Flybase ID	Spike Ratio Day 2	Dose Causing Spike Day 2	SpikeRatio Day 10	Dose Causing Spike Day 10	Spike Ratio Day 20	Dose Causing Spike Day 20	Day 2 Fold Change 1000R	Day 2 FC 5000R	Day 2 FC 10000R	Day 2 FC 20000R	Day 10 FC 10000R	Day 10 FC 5000R	Day 10 FC 10000R	Day 10 FC 20000R	Day 20 FC 10000R	Day 20 FC 5000R	Day 20 FC 10000R	Day 20 FC 20000R
FBgn0085364	5.415	20000R	9.183	20000R	8.050	20000R	1.298	0.718	0.916	7.026	1.655	1.378	1.306	15.201	1.610	0.895	1.364	12.963

Table S4G. Values of Spike Ratio and Fold Changes (FC) for Genes Found to Spike at Days 2, 10 and 20 Post-Irradiation. (Analysis with lowest dose discluded.) Spike ratio = (largest fold change)/(second largest fold change)

GO	Count	Total	P Value	GO Name
GO:0045434	1	7	0.00511	negative regulation of female receptivity, post-mating
GO:0007621	1	8	0.00511	negative regulation of female receptivity
GO:0048521	1	8	0.00511	negative regulation of behavior
GO:0046008	1	10	0.00511	regulation of female receptivity, post-mating
GO:0045924	1	16	0.00511	regulation of female receptivity
GO:0060180	1	16	0.00511	mating behavior#female mating behavior
GO:0060181	1	16	0.00511	female receptivity
GO:0045297	1	18	0.00511	post-mating behavior
GO:0050795	1	18	0.00511	regulation of behavior
GO:0005179	1	47	0.012	hormone activity
GO:0033057	1	69	0.0139	reproductive behavior in a multicellular organism
GO:0032504	1	81	0.0139	multicellular organism reproduction
GO:0048609	1	81	0.0139	multicellular organism reproduction#reproductive process in a multicellular organism
GO:0007617	1	82	0.0139	mating behavior
GO:0051705	1	82	0.0139	behavioral interaction between organisms
GO:0019098	1	87	0.0139	reproductive behavior
GO:0007618	1	94	0.0141	mating
GO:0005102	1	136	0.0193	receptor binding
GO:0022414	1	203	0.0271	reproduction#reproductive process
GO:0051704	1	212	0.0271	multi-organism process

Table S5A. Overrepresented Gene Ontologies in Genes Found to Spike at Day 2 Post-Irradiation at Dose 5000 R. (Analysis with all data included.)

GO	Count	Total	P Value	GO Name
GO:0007296	2	8	1.81E-05	vitellogenesis
GO:0007548	2	57	0.000515	sex differentiation
GO:0003006	2	77	0.00063	reproductive developmental process
GO:0007028	2	109	0.000951	cytoplasm organization and biogenesis
GO:0005811	2	129	0.00107	lipid particle
GO:0022414	2	203	0.00221	reproduction#reproductive process
GO:0016590	1	6	0.00584	ACF complex
GO:0005678	1	9	0.00767	chromatin assembly complex
GO:0007292	2	528	0.00999	female gamete generation
GO:0007276	2	704	0.0156	gamete generation
GO:0019953	2	730	0.0156	sexual reproduction
GO:0016585	1	33	0.0187	chromatin remodeling complex

Table S5B. Overrepresented Gene Ontologies in Genes Found to Spike at Day 2 Post-Irradiation at Dose 10,000 R. (Analysis with all data included.)

GO	Count	Total	P Value	GO Name
GO:0005213	2	9	8.52E-05	structural constituent of chorion
GO:0007306	2	64	0.00229	ovarian follicle cell development#chorion-containing eggshell formation#eggshell chorion formation
GO:0007304	2	88	0.00229	ovarian follicle cell development#chorion-containing eggshell formation
GO:0030703	2	89	0.00229	eggshell formation
GO:0030707	2	184	0.00779	ovarian follicle cell development
GO:0048646	2	235	0.0105	anatomical structure development#anatomical structure morphogenesis#anatomical structure formation
GO:0048477	2	519	0.0385	oogenesis
GO:0007292	2	528	0.0385	female gamete generation
GO:0005549	1	54	0.0496	odorant binding

Table S5C. Overrepresented Gene Ontologies in Genes Found to Spike at Day 10 Post-Irradiation at Dose 10,000 R. (Analysis with all data included.)

(none)				

Table S5D. Overrepresented Gene Ontologies in Genes Found to Spike at Day 2 Post-Irradiation at Dose 5000 R. (Analysis with all data included.)

GO	Count	Total	P Value	GO Name
GO:0045434	1	7	0.00511	negative regulation of female receptivity, post-mating
GO:0007621	1	8	0.00511	negative regulation of female receptivity
GO:0048521	1	8	0.00511	negative regulation of behavior
GO:0046008	1	10	0.00511	regulation of female receptivity, post-mating
GO:0045924	1	16	0.00511	regulation of female receptivity
GO:0060180	1	16	0.00511	mating behavior#female mating behavior
GO:0060181	1	16	0.00511	female receptivity
GO:0045297	1	18	0.00511	post-mating behavior
GO:0050795	1	18	0.00511	regulation of behavior
GO:0005179	1	47	0.012	hormone activity
GO:0033057	1	69	0.0139	reproductive behavior in a multicellular organism
GO:0032504	1	81	0.0139	multicellular organism reproduction
GO:0048609	1	81	0.0139	multicellular organism reproduction#reproductive process in a multicellular organism
GO:0007617	1	82	0.0139	mating behavior
GO:0051705	1	82	0.0139	behavioral interaction between organisms
GO:0019098	1	87	0.0139	reproductive behavior
GO:0007618	1	94	0.0141	mating
GO:0005102	1	136	0.0193	receptor binding
GO:0022414	1	203	0.0271	reproduction#reproductive process
GO:0051704	1	212	0.0271	multi-organism process

Table S5E. Overrepresented Gene Ontologies in Genes Found to Spike at Day 2 Post-Irradiation at Dose 5000 R. (Analysis with lowest dose discluded.)

GO	Count	Total	P Value	GO Name
GO:0007296	1	8	0.0268	vitellogenesis
GO:0006123	1	14	0.0268	organelle ATP synthesis coupled electron transport#mitochondrial electron transport, cytochrome c to oxygen
GO:0005751	1	17	0.0268	mitochondrial inner membrane#mitochondrial respiratory chain#mitochondrial respiratory chain complex IV
GO:0045277	1	17	0.0268	respiratory chain complex IV
GO:0004129	1	18	0.0268	cytochrome-c oxidase activity
GO:0016675	1	18	0.0268	oxidoreductase activity, acting on heme group of donors
GO:0016676	1	18	0.0268	oxidoreductase activity, acting on heme group of donors, oxygen as acceptor
GO:0015002	1	18	0.0268	heme-copper terminal oxidase activity

Table S5F. Overrepresented Gene Ontologies in Genes Found to Spike at Day 2 Post-Irradiation at Dose 10,000 R. (Analysis with lowest dose discluded.)

GO	Count	Total	P Value	GO Name
GO:0007296	4	8	4.14E-10	vitellogenesis
GO:0007292	6	528	1.55E-06	female gamete generation
GO:0003006	4	77	2.64E-06	reproductive developmental process
GO:0007276	6	704	4.37E-06	gamete generation
GO:0019953	6	730	4.37E-06	sexual reproduction
GO:0007028	4	109	5.40E-06	cytoplasm organization and biogenesis
GO:0022414	4	203	5.63E-05	reproduction#reproductive process
GO:0007548	3	57	7.52E-05	sex differentiation
GO:0005737	6	1833	0.000616	cytoplasm
GO:0005811	3	129	0.000708	lipid particle
GO:0048134	2	20	0.000944	germ cell development#germ-line cyst formation
GO:0048477	4	519	0.00136	oogenesis
GO:0016043	5	1962	0.0134	cellular component organization and biogenesis
GO:0044424	6	3454	0.0134	intracellular#intracellular part
GO:0005622	6	3465	0.0134	intracellular
GO:0032502	5	2243	0.0217	developmental process
GO:0008283	2	133	0.0222	cell proliferation
GO:0007542	1	5	0.0252	multicellular organismal development#germ-line sex determination#primary sex determination, germ-line
GO:0019099	1	5	0.0252	female germ-line sex determination
GO:0016590	1	6	0.0278	ACF complex
GO:0018992	1	6	0.0278	multicellular organismal development#germ-line sex determination
GO:0007281	2	170	0.0291	germ cell development
GO:0016709	1	7	0.0297	oxidoreductase activity, acting on paired donors, with incorporation or reduction of molecular oxygen, NADH or NADPH as one donor, and incorporation of one atom of oxygen
GO:0008156	1	8	0.0297	negative regulation of DNA replication
GO:0020037	1	8	0.0297	heme binding
GO:0046906	1	8	0.0297	tetrapyrrole binding
GO:0044464	6	4358	0.0297	cell#cell part
GO:0005623	6	4358	0.0297	cell
GO:0051053	1	9	0.0297	negative regulation of DNA metabolic process
GO:0005678	1	9	0.0297	chromatin assembly complex
GO:0006275	1	9	0.0297	regulation of DNA replication
GO:0044444	4	1537	0.0297	cytoplasm#cytoplasmic part
GO:0030237	1	11	0.0344	multicellular organismal development#female sex

				determination
GO:0006378	1	12	0.0356	mRNA polyadenylation
GO:0043631	1	12	0.0356	RNA polyadenylation
GO:0045495	1	14	0.0405	pole plasm
GO:0031124	1	16	0.0451	mRNA 3'-end processing
GO:0007280	1	17	0.0457	pole cell migration
GO:0031123	1	17	0.0457	RNA 3'-end processing
GO:0007538	1	18	0.0472	multicellular organismal development#primary sex determination

Table S5G. Overrepresented Gene Ontologies in Genes Found to Spike at Day 10 Post-Irradiation at Dose 10,000 R. (Analysis with lowest dose discluded.)

(none)				

Table S5H. Overrepresented Gene Ontologies in Genes Found to Spike at Day 20 Post-Irradiation at Dose 5000 R. (Analysis with lowest dose discluded.)

CHAPTER 4

In Preparation for Publication

X-ray Induced Photodynamic Therapy with Targeted Copper-Cysteamine Nanoparticles in Mice

Samana Shrestha[a], Bindeshwar Sah[a], Adam Vanasse[a] , Leon N Cooper[b,c] , Lun Ma[d], Wei Chen[d] and Michael P. Antosh[a,b]

[a]Physics Department , University of Rhode Island, 2 Lippitt Rd,Kingston, RI, 02881

[b]Institute for Brain and Neural Systems, Brown University, 184 Hope St, Providence, RI, 02906

[c]Department of Physics, Brown University, 184 Hope St, Providence, RI, 02906

[d]Department of Physics and the SAVANT Center, The University of Texas at Arlington, Texas 76019-0059,USA

Keywords: radiation, photosensitization, nanoparticles, tumor, treatment type

Abstract

Photodynamic therapy is a promising cancer treatment method. However, one possible limitation is its dependence on light that is not highly penetrating. Copper-Cysteamine

nanoparticles are a new type of photosensitizer, which generates cytotoxic singlet oxygen molecules upon activation by x-rays. In this paper, we report the use of copper cysteamine nanoparticles, targeted to tumors using pH-Low Insertion Peptide. In an *in vivo* study, results show significant tumor destruction under x-ray activation. An analysis of variance shows that mice treated with targeted particles had a significantly different tumor sizes than mice treated with no particles, as well as mice treated with non-targeted particles. An additional analysis of variance shows that the use of targeted copper-cysteamine nanoparticles affected the survival time after irradiation, compared to irradiation using no particles on mice. This work confirms the effectiveness of Copper-Cysteamine nanoparticles, targeted to tumors, as a photosensitizer when activated by radiation therapy. Combined with radiation therapy, targeted and non-targeted Cu-Cy nanoparticles are good candidates for photodynamic therapy in deeply seated tumors.

Introduction

Photodynamic therapy (PDT) involves the use of light, a photosensitizer (PS) and molecular oxygen to kill cells (1-16). Photosensitizers induce the production of reactive oxygen species (ROS) at the tumor site after the absorption of light energy, killing the tumor cells. (5, 8, 9, 14, 15, 17, 18). Singlet oxygen has a short lifetime in biologic systems, less than 0.04 μs, and therefore has a short radius of action of less than 0.02 μm (17, 19). Photodynamic therapy is safe (2, 10, 12), minimally invasive and can be used with methods to selectively target cancerous cells, avoiding side effects to the healthy tissues (1-3, 10-12, 17, 20). Ma et al. successfully used copper

cysteamine nanoparticles (NPs) activated by microwaves for production of singlet oxygen to treat cancer using microwave induced photodynamic therapy (21). Copper sulfide (CuS) nanoparticles excited by 808 nm lasers produced reactive oxygen species and strong anticancer effects *in vitro* and *in vivo* (22). Organically modified silica (ORMOSIL) nanoparticles (approximately 20 nm) generated cytotoxic singlet molecules upon photo irradiation after uptake by tumor cells (23). Zinc Oxide (ZnO) nanoparticles conjugated to porphyrin derivatives showed high phototoxicity in human ovarian carcinoma cell line when activated with 365 nm UV light, showing a potential use in photodynamic therapy for deeper cancer treatment (24).

Some advantages of PDT are the available options for photosensitizer and therapeutic dose, time of irradiation post treatment and light fluence rate (which can be adjusted to target biological tissues (8)). Although many photosensitizers have been developed, only a few have shown successful results *in vitro* and *in vivo* and made it to clinical trials(14). One of the drawbacks of PDT is tissue penetration ability because of the fact that the wavelengths of light for most of the clinically approved photosensitizers are in the UV/visible range. This limits the use of conventional PDT methods to skin (surface) tumors only and are not effective for deep tumors (11, 12, 25-28). Another disadvantage is that the quantum yield of ROS production is lowered under physiological conditions because photosensitizing drugs have poor solubility in water and are easily aggregated due to a hydrophobic nature (3, 11, 28). Recently, nanomaterials combined with photosensitization drugs have been an important method in photodynamic therapy to overcome the limitation of conventional

photosensitization drugs by increasing the cellular uptake and solubility of drugs in water (3).

As stated above, one important issue with photodynamic therapy is the tissue depth at which it can be used as a treatment. One way to address this issue is to use particles that can interact with more energetic photons. Depending on the source of excitation energy, nanoparticles can be designed to be excited by near infrared light (NIR), internal light and X-rays (12). Near infrared light (NIR) can be used to excite upconversion nanoparticles deep in tissue, with higher penetrating capacity compared to visible light and low phototoxicity to normal cells and tissues (26, 29). The upconversion nanoparticles showed a strong photodynamic effect on MB49 cells upon irradiation with 980 nm near infrared light (30). However, its penetration ability is still limited compared to X-rays, and it requires high laser light intensity. Further, it is difficult to design and synthesize because the energy gap of near infrared-absorbing photosensitizers is narrow, and the quantum yield of singlet oxygen is usually low (12). Another method for photodynamic therapy is to attach a nanoscintillator to a photosensitizer. When this is done *in vivo* and exposed to radiation, the nanoparticles emit scintillation. This light is absorbed by the photosensitizers, resulting in the release of singlet oxygen at the tumor site for effective cancer killing. Another alternative strategy is to use luminescent nanoparticles instead of light sources *in vivo* to support photodynamic therapy with more localized therapy and less potential damage to healthy cells (18, 27). X-rays (0.05 – 6 MeV) have more tissue penetrating ability than UV/visible/infrared light, which makes it a potential candidate to initiate photodynamic therapy for deeply seated tumors (12). At present, the use of high

energy X-rays has been the most common radiation therapy treatment (31). However, radiation therapy often impacts healthy tissue as well as tumors. If the effect of radiation on the tumor can be enhanced, less radiation could be used to get the same effect thus reducing the side effects and damage to the healthy tissues (32). A combination of conventional radiation therapy with photodynamic therapy has been an exciting technique for deep tumor penetration (33) and has the potential to result in lower doses of radiation when scintillation nanoparticles are attached to photosensitizers (12, 18). The nanoparticles emit light when induced by ionizing radiation; the scintillation activates the photosensitizers and results in the release of singlet oxygen. In this case, photodynamic therapy takes place even without the aid of an external light source, and the effectiveness of the radiation is increased (18). Since the site of damage from photodynamic therapy depends on the location of the photosensitizer at the time of irradiation, (20) conjugating the particles with tumor specific targeting molecules can enhance the uptake of particles with efficient cancer treatment reducing the damage to the healthy tissues and important organs near the tumor with the reduced radiation dose (32). X-rays can initiate the photodynamic agent (LaF_3 : Tb^{3+}- meso-tetra (4-carbosyphenyl) porphine (MTCP)) scintillating nanoparticle, even at low dose, for deep cancer treatment (34). The core of a nanoscintillator coated with a mesoporous silica forms an integrated nanosystem which when irradiated by X-rays (25). Liu et al. (2008) showed enhanced X-ray damage by gold nanoparticles treated with a new synthesis method of polyethylene glycol modification. Trifluorocerium-verteporfin (CeF_3 –VP) conjugates, lanthanide complexes, Copper and cobalt co-doped zinc sulfide (ZnS:Cu,Co) afterglow NPs, and

nanoscintillator coupled porphyrins have been shown to produce singlet oxygen when activated by X-ray and are effective for cancer cell destruction (4, 5, 35, 36). Zhang et al. used a conjugated semiconductor scintillator particle as a photosensitizer with ionizing radiation, and found diminished oxygen dependence (37). The combined effect of radiation therapy and photodynamic therapy with indocyanine green as a sensitizer resulted in killing of MCF7 human breast cancer cells with a reduction in percentage cell viability, down to 3.42%. A one way ANOVA was used to analyze data for statistical differences ($p < 0.05$) (38). When activated by X-rays at 90 kV, energy was transferred from Ce^{3+}-doped lanthanum(iii) fluoride ($LaF_3:Ce^{3+}$)/DMSO nanoparticles to protoporphyrin IX (PPIX) with the production of singlet oxygen to kill cancer cells (39). Porphyrin conjugated with SiC/SiO_x nanowires has been an efficient source of singlet oxygen at low doses of 6MV X-rays (0.4 – 2 Gy), showing the enhancement of radiation therapy for cancer treatment (40).

In addition to improving upon the depth that photodynamic therapy can reach, another opportunity for improvement is the use of active targeting agents like peptides, antibodies and proteins. These agents could reduce the side effects to the surrounding healthy tissues (3, 41) and problems associated with multidrug resistance (11). There is a need for more precise photosensitization drug delivery into target cells and tissues (3), and efforts have been made to search for alternative photodynamic therapy methods for deep tissue penetration (26, 27). Targeted photodynamic therapy has been a new promising therapeutic strategy that enhances specificity and efficiency of photodynamic therapy by improving the delivery of photosensitizers to cancer tissue (15). Yoon et al. successfully inhibited tumor growth using the hydrophobic

photosensitizer chlorin e6 (Ce6), conjugated with tumor targeting hyaluronic acid nanoparticles (HANPs), to generate singlet oxygen in tumor cells when irradiated by laser. They analyzed the differences between experimental and control groups using a one-way analysis of variance (ANOVA) and found their results to be considered statistically significant if $p<0.05$ (42).

Copper cysteamine nanoparticles (Cu-Cy, $Cu_3cl(SR)_2$) are a new option for photosensitization and radiation therapy. They were used to kill SW620 colorectal cancer cells by inducing apoptosis as well as autophagy. The difference between the control and experimental groups was determined using Student's t test and a one one-way analysis of variance (ANOVA) (43). Copper cysteamine particles under X-ray activation generated singlet oxygen ($^1O_2$) and were successful at killing MCF-7 cells both *in vitro* and *in vivo* and can be used in the treatment of both shallow and deep cancers (44, 45). Copper cysteamine has been demonstrated as an X-ray activated nanoparticle in photodynamic therapy for cancer treatment, which when conjugated by tumor specific targeting molecules can enhance the uptake (44).

In this paper, we demonstrate the use of copper cysteamine nanoparticles to enhance radiation therapy, using photodynamic therapy. We targeted copper cysteamine nanoparticles to tumors using the targeting peptide pH-Low Insertion Peptide (pHLIP), which targets molecules to tumors using the property that tumors have low pH. Among many uses, pHLIP has been used to effectively target gold nanoparticles to tumors and to treat cancer using gold nanoparticles (46-49).

Materials and methods

Preparation of pHLIP conjugated copper cysteamine nanoparticles

2 mg of Var3 pHLIP (Ala-28-Gly), from CS Bio Company, was added in 5 mL of deionized water followed by the addition of 3.19 mg of 1 Ethyl-3-(3-dimethylaminopropyl) carbodiimide (EDC) under mild stirring for 10 minutes at room temperature. After adjusting the pH to 7.5 using NaoH, 5 mL of 1 mM copper cysteamine water solution was added under constant stirring overnight at room temperature in a dark environment. The copper cysteamine-pHLIP conjugates were centrifuged at 4400 rpm for 25 minutes and washed with deionized water 3-4 times.

Cell Culture

JC Breast murine cancer cells of BALB/cRos strain were purchased from American Type Culture Collection (ATCC) and were grown in Roswell Park Memorial Institute (RPMI) medium with L-glutamine and sodium bicarbonate, 10% Fetal Bovine Serum (Sigma-Aldrich) and 0.1% Ciprofloxacin. The cells were maintained in a humidified atmosphere at 5% carbon dioxide at 37 degrees centigrade in an incubator.

Animal Models and Cell Injection

All animal work followed the guidelines of URI IACUC protocol AN1516-003. Males and Females, 18-25g Balb/c AnNHsd, 3-4 weeks mice were ordered from Envigo. This strain of mice came to Harlan Sprague Dawley (Hsd-now Envigo) from National Institutes of Health, Bethesda. The NIH received this strain from Andevont (An). 1.5 million cells suspended in 100uL RPMI were injected subcutaneously on the right flank of the mice using 1 mL 27 $G^{1/2}$ latex free BD syringes.

Radiation Therapy on Mice

Mice were divided into 6 treatment groups: i) targeted copper cysteamine + radiation ii) untargeted copper cysteamine + radiation iii) PBS (control) + radiation iv) targeted copper cysteamine v) untargeted copper cysteamine vi) PBS (control). In total, 51 mice (24 males and 27 females) were used for the experiment.

Treatment was undertaken when the tumor size reached approximately 4-8mm. Mice were anesthetized using isoflurane gas. For groups of mice given nanoparticles, the particles were injected intratumorally in 20 μL PBS at a particle concentration of 0.8 μg/μL. For the groups given radiation therapy, the mice were irradiated 30 minutes post injection of particles at an irradiation dose of 5 Gy. No external X-ray filter was used, and the source to surface distance was set to 30.5 cm with a field size of 18.3 by 20.1 cm. The current and voltage settings of the X-ray machine (a Faxitron MultiRad 350) were 90 kVp and 30 mA. The non-irradiated mice were placed in the x-ray chamber in the same settings but with no irradiation. The tumor size was measured daily using digital Vernier calipers (VCD001, from United Scientific Supply) to get the tumor volume. The tumor volume was calculated using the formula: tumor volume = ½ length * width^2 (50). Mice were euthanized if they reached the endpoint size of 20 mm, or if they showed signs of distress.

Particle characterization

The copper – cysteamine nanoparticles were synthesized in The University of Texas at Arlington in Wei Chen's lab along with the singlet oxygen measurement and photoluminescence and X- ray luminescence measurements (44).

Statistics and Analysis of Data

In total, 51 mice were used - 24 males and 27 females. Each of the radiation therapy groups had 3 males and 4 females, whereas the non-RT groups had 5 males and 5 females.

The effect of experimental variables on tumor size in our experiment was quantified by running an analysis of variance (ANOVA), using the command “anova” in the statistical computer language R (51). The input given was a linear model (lm command in R). The independent variable in the linear model was tumor volume, and the dependent variables were treatment type, time of measurement after irradiation, age at irradiation, radiation dose (0 or 5 Gy), sex (M or F) and original tumor volume. Treatment types were run two at a time to generate a comparison between the following pairs of treatments: i) targeted copper cysteamine particles and untargeted copper cysteamine particles; ii) targeted copper cysteamine particles and no particles; iii) untargeted copper cysteamine particles and no particles. p values for individual variables, as well as interactions of variables were determined using the F test (part of the anova command in R). p values were ruled significant if the Bonferroni correction criteria was met. Including interactions, 59 p values were found for each pairwise comparison of treatment types. We used 0.05/59 = 0.000847 as the cutoff P value for statistical significance.

Results

Tumor Size Data and Analysis of Variance

Figures 1A and 1B show tumor volume versus time, for male mice (fig. 1) and female mice (fig. 2) after the intra-tumoral injection of targeted (CuCyP), untargeted (CuCy)

or no particles (PBS) followed by irradiation with 5 Gray after 30 minutes. In these figures, each individual curve represents one mouse. Figures 2A (males) and 2B (females) show tumor volume as a function of time for mice given targeted particles and either 0 or 5 Gray of radiation. Figures 3A (males) and 3B (females) show tumor volume growth as a function of time post different treatments either at 0 or 5 Gray radiation. Supplemental figures 1A, 1B, 2A and 2B show tumor volume as a function of time for mice given non-targeted particles and no particles.

An analysis of variance (ANOVA) was performed to compare the effects of (targeted copper cysteamine particles + radiation) with the effects of (non-targeted copper cysteamine particles + radiation). As described in detail in the methods section, the dependent variable of the analysis was tumor size and the independent variables were time after irradiation, sex (male or female), radiation dose (0 or 5 Gy), treatment type (targeted particles or non-targeted particles), age of mouse at irradiation, and volume of tumor at time of irradiation. Mice with a treatment of no particles were excluded from this analysis, so that the variable for treatment type would be a 2-factor comparison of targeted and non-targeted particles.

Table 1 shows the ANOVA results for an analysis where only two treatment types were included: targeted and non-targeted particles. In this analysis, the p value for treatment type is significant (less than 0.000847, the Bonferroni cutoff). This indicates that mice treated with targeted particles had a significantly different tumor size than mice treated with non-targeted particles, even when other relevant experimental variables were also considered.

In addition to treatment type, the p values for the following variables were also significant: time after irradiation, radiation dose, treatment type, age of mouse at irradiation, volume of tumor at time of irradiation. The p value for sex of the mice shows that sex does not play an important role in the experimental outcome. Several interaction terms were also significant in the analysis of variance. Of particular note are: the interactions between time after irradiation and radiation dose (p value < $2.2*10^{-16}$), radiation dose and treatment type ($p < 5.02*10^{-9}$), time after irradiation and age at irradiation ($p<2.2*10^{-16}$), treatment type and age at irradiation ($p< 3.576*10^{-11}$), time after irradiation and tumor volume at irradiation ($p< 6.739*10^{-10}$), age at irradiation and tumor volume at irradiation (p<0.000219). See supplemental table 1 for full information on interaction terms for this analysis.

Table 2 shows the ANOVA results when the following treatment types were included: non-targeted particles and no particles. In this analysis, all experimental variables tested had a significant effect on tumor size, including sex. Notable significant interaction terms included: time after irradiation and radiation dose ($p<2.2*10^{-16}$), time after irradiation and age at irradiation ($p<2.2*10^{-16}$), radiation dose and age at irradiation ($p<2.308*10^{-13}$), time after irradiation and tumor volume at irradiation ($p< 2.2*10^{-16}$), radiation dose and tumor volume at irradiation ($p< 6.238*10^{-6}$), treatment type and tumor volume at irradiation ($p<1.001*10^{-6}$), age at irradiation and tumor volume at irradiation (p<0.0029175). See supplemental table 2 for full information on interaction terms for this analysis.

Table 3 shows the analysis of variance when the following treatment types were included: targeted particles and no particles. Similar to table 1, all experimental variables included were significant except sex. Notable significant interaction terms included: time after irradiation and sex ($p<5.753*10^{-5}$), time after irradiation and radiation dose ($p<2.2*10^{-16}$), radiation dose and treatment type ($p<1.15*10^{-8}$), time after irradiation and age at irradiation ($p<2.2*10^{-16}$), treatment type and age at irradiation ($p<1.243*10^{-10}$), time after irradiation and tumor volume at irradiation ($p<2.2*10^{-16}$), radiation dose and tumor volume at irradiation ($p<0.002$), age at irradiation and tumor volume at irradiation ($p<0.003374$). See supplemental table 3 for full information on interaction terms for this analysis.

ANOVA Analysis of Survival

The number of mice used in this experiment was insufficient to run an effective log rank test for differences between survival curves. As a substitute analysis, an analysis of variance was run with time between irradiation and death as the dependent variable. (Here, death is defined as either actual death or as reaching a humane endpoint following our institution's IACUC policies.) The independent variables were sex (M or F), radiation dose (0 or 5 Gy), treatment type (targeted particles, non-targeted particles, no particles), age of mouse at time of irradiation, and size of the mouse's tumor at time of irradiation. Including interaction terms, there were 29 variable combinations assessed for significance; we used a Bonferroni cutoff p value of 0.05/29 = 0.00172 to claim significance.

A comparison using mice treated with targeted particles or no particles found a statistically significant effect from treatment (targeted particles versus no particles), sex and radiation dose. Thus, the anova analysis indicates that targeted particles increase survival time, compared to irradiation using no particles. Notable interaction terms that were significant included radiation dose with treatment type, and radiation dose with tumor size at time of irradiation. The input and output of this analysis is supplemental tables 4 and 5. Analyses run with the other combinations of treatments (targeted particles versus non-targeted particles, non-targeted particles versus no particles) found no significant effects from the treatment differences.

Discussion

In this paper, we demonstrated that copper cysteamine nanoparticles, targeted with pH-Low Insertion Peptide, can be used to reduce tumor size and to increase survival in mammals. Copper cysteamine can be used in the treatment of both shallow and deep tumors because it can be activated by X-rays as well as light (44). In this result, we particularly emphasize the effect on tumor size.

The targeted Copper cysteamine particles showed the enhanced radiation effect with better tumor killing in both the male and female mice. The sex of the mice might not be an important variable in this kind of experiment as this parameter was not statistically significant in targeted vs non tartgeted and targeted versus no particles. However for nontargeted versus no particles it played an important role. The original volume of tumor and age factor of mice at irradiation time are also very important to be considered while performing the experiment. The dose of the radiation given to the

mice could be altered to see the affect in the tumor size as the radiation dose is statistically significant.

One particularly important variable that was not tested in this paper is radiation energy. Few, if any, photoluminescent particles have been shown to work at energies as high as 90 kVp, as shown in this paper. However, most clinically relevant energies are higher still.

Overall, this paper represents a firm demonstration of the effectiveness of copper-cysteamine nanoparticles in the treatment of mammalian cancer.

References

1. AlSalhi M, Atif M, Alobiadi A, & Aldwayyan A (2012) A study of the photodynamic effect on cancerous cells. *Laser Physics Letters* 9(8):611.
2. Brown SB, Brown EA, & Walker I (2004) The present and future role of photodynamic therapy in cancer treatment. *The lancet oncology* 5(8):497-508.
3. Hong EJ, Choi DG, & Shim MS (2016) Targeted and effective photodynamic therapy for cancer using functionalized nanomaterials. *Acta Pharmaceutica Sinica B* 6(4):297-307.
4. Kaščáková S*, et al.* (2015) X-ray-induced radiophotodynamic therapy (RPDT) using lanthanide micelles: Beyond depth limitations. *Nano Research* 8(7):2373-2379.
5. Ma L*, et al.* (2014) X-ray excited ZnS: Cu, Co afterglow nanoparticles for photodynamic activation. *Applied Physics Letters* 105(1):013702.
6. Kinsella TJ, Colussi VC, Oleinick NL, & Sibata CH (2001) Photodynamic therapy in oncology. *Expert opinion on pharmacotherapy* 2(6):917-927.

7. Peng Q, Moan J, & Nesland JM (1996) Correlation of subcellular and intratumoral photosensitizer localization with ultrastructural features after photodynamic therapy. *Ultrastructural pathology* 20(2):109-129.

8. Wilson BC & Patterson MS (2008) The physics, biophysics and technology of photodynamic therapy. *Physics in Medicine & Biology* 53(9):R61.

9. Sharman WM, Allen CM, & Van Lier JE (1999) Photodynamic therapeutics: basic principles and clinical applications. *Drug discovery today* 4(11):507-517.

10. Master A, Livingston M, & Gupta AS (2013) Photodynamic nanomedicine in the treatment of solid tumors: perspectives and challenges. *Journal of controlled release* 168(1):88-102.

11. Lim C-K*, et al.* (2013) Nanophotosensitizers toward advanced photodynamic therapy of cancer. *Cancer letters* 334(2):176-187.

12. Hu J*, et al.* (2015) Nanocomposite-based photodynamic therapy strategies for deep tumor treatment. *Small* 11(44):5860-5887.

13. Moan J & Peng Q (2003) An outline of the hundred-year history of PDT. *Anticancer research* 23(5A):3591-3600.

14. Palumbo G (2007) Photodynamic therapy and cancer: a brief sightseeing tour. *Expert opinion on drug delivery* 4(2):131-148.

15. Bugaj AM (2011) Targeted photodynamic therapy–a promising strategy of tumor treatment. *Photochemical & Photobiological Sciences* 10(7):1097-1109.

16. Castano AP, Mroz P, & Hamblin MR (2006) Photodynamic therapy and anti-tumour immunity. *Nature Reviews Cancer* 6(7):535.

17. Dougherty TJ*, et al.* (1998) Photodynamic therapy. *JNCI: Journal of the National Cancer Institute* 90(12):889-905.

18. Chen W & Zhang J (2006) Using nanoparticles to enable simultaneous radiation and photodynamic therapies for cancer treatment. *Journal of nanoscience and nanotechnology* 6(4):1159-1166.

19. Chatterjee DK, Fong LS, & Zhang Y (2008) Nanoparticles in photodynamic therapy: an emerging paradigm. *Advanced drug delivery reviews* 60(15):1627-1637.

20. Oleinick NL & Evans HH (1998) The photobiology of photodynamic therapy: cellular targets and mechanisms. *Radiation research* 150(5s):S146-S156.

21. Yao M*, et al.* (2016) A new modality for cancer treatment—nanoparticle mediated microwave induced photodynamic therapy. *Journal of Biomedical Nanotechnology* 12(10):1835-1851.

22. Li L*, et al.* (2017) CuS nanoagents for photodynamic and photothermal therapies: Phenomena and possible mechanisms. *Photodiagnosis and photodynamic therapy* 19:5-14.

23. Ohulchanskyy TY*, et al.* (2007) Organically modified silica nanoparticles with covalently incorporated photosensitizer for photodynamic therapy of cancer. *Nano letters* 7(9):2835-2842.

24. Liu Y, Zhang Y, Wang S, Pope C, & Chen W (2008) Optical behaviors of ZnO-porphyrin conjugates and their potential applications for cancer treatment. *Applied Physics Letters* 92(14):143901.

25. Chen H*, et al.* (2015) Nanoscintillator-mediated X-ray inducible photodynamic therapy for in vivo cancer treatment. *Nano letters* 15(4):2249-2256.

26. Wang C, Cheng L, & Liu Z (2013) Upconversion nanoparticles for photodynamic therapy and other cancer therapeutics. *Theranostics* 3(5):317.

27. Chen W (2008) Nanoparticle self-lighting photodynamic therapy for cancer treatment. *Journal of Biomedical Nanotechnology* 4(4):369-376.

28. Bechet D*, et al.* (2008) Nanoparticles as vehicles for delivery of photodynamic therapy agents. *Trends in biotechnology* 26(11):612-621.

29. Wang C, Tao H, Cheng L, & Liu Z (2011) Near-infrared light induced in vivo photodynamic therapy of cancer based on upconversion nanoparticles. *Biomaterials* 32(26):6145-6154.

30. Guo H, Qian H, Idris NM, & Zhang Y (2010) Singlet oxygen-induced apoptosis of cancer cells using upconversion fluorescent nanoparticles as a carrier of photosensitizer. *Nanomedicine: Nanotechnology, Biology and Medicine* 6(3):486-495.

31. Boyer AL, Goitein M, Lomax AJ, & Pedroni ES (2002) Radiation in the treatment of cancer. *Physics Today* 55(9):34-37.

32. Shrestha S, Cooper LN, Andreev OA, Reshetnyak YK, & Antosh MP (2016) Gold nanoparticles for radiation enhancement in vivo. *Jacobs journal of radiation oncology* 3(1).

33. Morgan NY, Kramer-Marek G, Smith PD, Camphausen K, & Capala J (2009) Nanoscintillator conjugates as photodynamic therapy-based radiosensitizers: calculation of required physical parameters. *Radiation research* 171(2):236-244.

34. Liu Y, Chen W, Wang S, & Joly AG (2008) Investigation of water-soluble x-ray luminescence nanoparticles for photodynamic activation. *Applied Physics Letters* 92(4):043901.

35. Clement S, Deng W, Camilleri E, Wilson BC, & Goldys EM (2016) X-ray induced singlet oxygen generation by nanoparticle-photosensitizer conjugates for photodynamic therapy: determination of singlet oxygen quantum yield. *Scientific reports* 6:19954.

36. Bulin A-L*, et al.* (2013) X-ray-induced singlet oxygen activation with nanoscintillator-coupled porphyrins. *The Journal of Physical Chemistry C* 117(41):21583-21589.

37. Zhang C*, et al.* (2015) Marriage of scintillator and semiconductor for synchronous radiotherapy and deep photodynamic therapy with diminished oxygen dependence. *Angewandte Chemie International Edition* 54(6):1770-1774.

38. Montazerabadi AR, Sazgarnia A, Bahreyni-Toosi MH, Ahmadi A, & Aledavood A (2012) The effects of combined treatment with ionizing radiation and indocyanine green-mediated photodynamic therapy on breast cancer cells. *Journal of Photochemistry and Photobiology B: Biology* 109:42-49.

39. Zou X*, et al.* (2014) X-ray-induced nanoparticle-based photodynamic therapy of cancer. *Nanomedicine* 9(15):2339-2351.

40. Rossi F*, et al.* (2015) Porphyrin conjugated SiC/SiO x nanowires for X-ray-excited photodynamic therapy. *Scientific reports* 5:7606.

41. Byrne JD, Betancourt T, & Brannon-Peppas L (2008) Active targeting schemes for nanoparticle systems in cancer therapeutics. *Advanced drug delivery reviews* 60(15):1615-1626.

42. Yoon HY*, et al.* (2012) Tumor-targeting hyaluronic acid nanoparticles for photodynamic imaging and therapy. *Biomaterials* 33(15):3980-3989.

43. Liu Z*, et al.* (2017) Investigation of copper cysteamine nanoparticles as a new type of radiosensitiers for colorectal carcinoma treatment. *Scientific reports* 7(1):9290.

44. Ma L, Zou X, & Chen W (2014) A new X-ray activated nanoparticle photosensitizer for cancer treatment. *Journal of biomedical nanotechnology* 10(8):1501-1508.

45. Ma L*, et al.* (2014) A new Cu–cysteamine complex: structure and optical properties. *Journal of Materials Chemistry C* 2(21):4239-4246.

46. Antosh MP*, et al.* (2015) Enhancement of radiation effect on cancer cells by gold-pHLIP. *Proceedings of the National Academy of Sciences* 112(17):5372-5376.

47. Andreev OA*, et al.* (2007) Mechanism and uses of a membrane peptide that targets tumors and other acidic tissues in vivo. *Proceedings of the National Academy of Sciences* 104(19):7893-7898.

48. Andreev OA, Engelman DM, & Reshetnyak YK (2010) pH-sensitive membrane peptides (pHLIPs) as a novel class of delivery agents. *Molecular membrane biology* 27(7):341-352.

49. Andreev OA, Engelman DM, & Reshetnyak YK (2014) Targeting diseased tissues by pHLIP insertion at low cell surface pH. *Frontiers in physiology* 5:97.

50. Rofstad EK & Brustad T (1985) Tumour growth delay following single dose irradiation of human melanoma xenografts. Correlations with tumour growth parameters, vascular structure and cellular radiosensitivity. *British Journal Of Cancer* 51:201.

51. CoreTeam R (2015) R: A Language and Environment for Statistical Computing. Vienna, Austria: R Foundation for Statistical Computing; 2015.

Tables:

Table 1. Analysis of variance results, comparing treatment with targeted copper cysteamine particles to treatment with non-targeted particles.

pHLIP Targeted Copper Cysteamine Particles Vs Non-targeted Copper Cysteamine Particles	
Variable	p Value
Time After Irradiation (Days)	$< 2.2*10^{-16}$
Sex	< 0.9968
Radiation Dose (Gray)	$< 2.2*10^{-16}$
Treatment Type	< 0.0006079
Age of Mouse at Irradiation (Days)	$< 2.2*10^{-12}$
Volume of Tumor at Irradiation (mm^3)	$< 2.2*10^{-10}$

Table 2. Analysis of variance results, comparing treatment with non-targeted copper cysteamine particles to treatment with no particles.

Non-targeted Copper Cysteamine Particles Vs No Particles	
Variable	pValues
Day after irradiation(days)	$< 2.2*10^{-16}$
Sex	< 0.0001556
Radiation Dose (Gray)	$< 2.2*10^{-16}$
Treatment Type	$< 2.467*10^{-7}$
Age at irradiation (Days)	$< 2.2*10^{-16}$
Original Tumor Volume(mm^3)	$< 2.2*10^{-16}$

Table 3. Analysis of variance results, comparing treatment with targeted copper cysteamine particles to treatment with no particles.

pHLIP Targeted Copper Cysteamine Vs No Particles	
Variable	pValues
Day after irradiation(days)	$< 2.2*10^{-16}$
Sex	< 0.282
Radiation Dose (Gray)	$< 2.2*10^{-16}$
Treatment Type	$< 2.49*10^{-19}$
Age at irradiation (Days)	$< 4.11*10^{-13}$
Original Tumor Volume(mm^3)	$< 2.2*10^{-16}$

Figures:

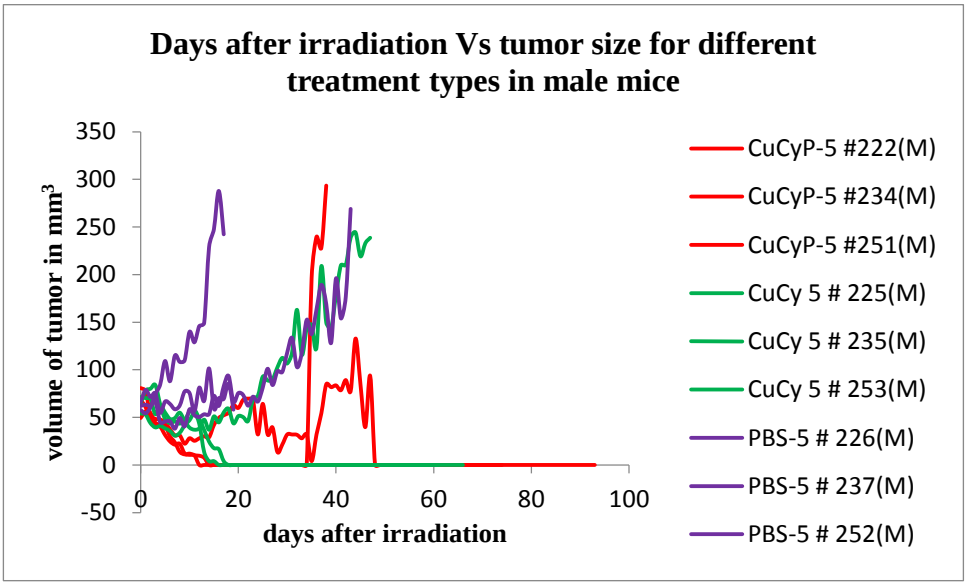

Figure 1A

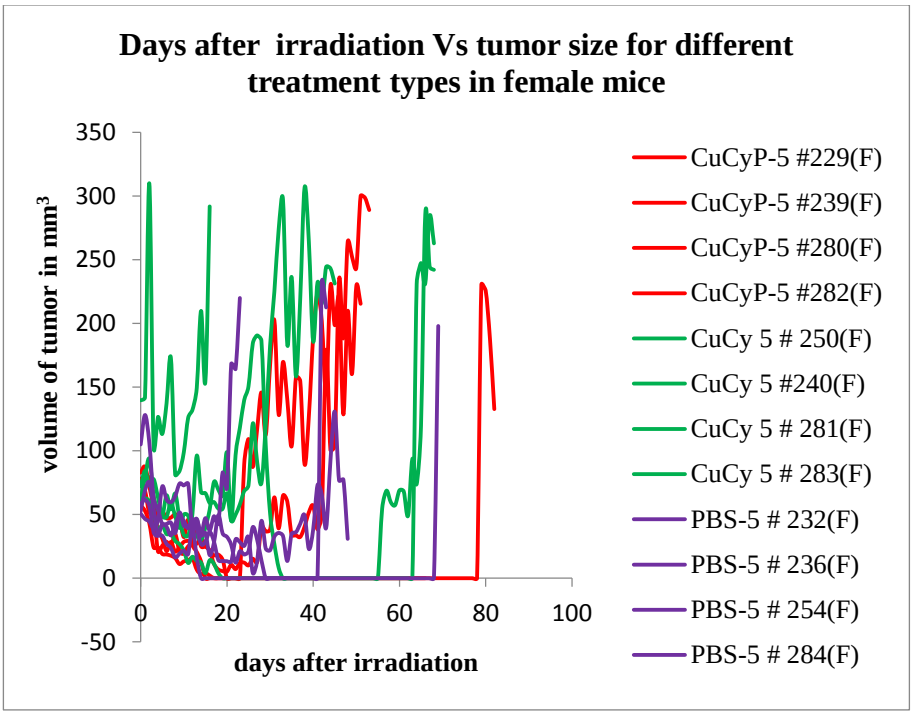

Figure 1B

Figure 1. Tumor size as a function of time, for mice given 5 Gray of radiation. Each individual curve represents one mouse. CuCyP mice were given a targeted copper-cysteamine treatment; CuCy mice were given a non-targeted copper-cysteamine treatment; PBS mice were injected with a control solution containing no particles. Figure A is male mice; figure B is female mice.

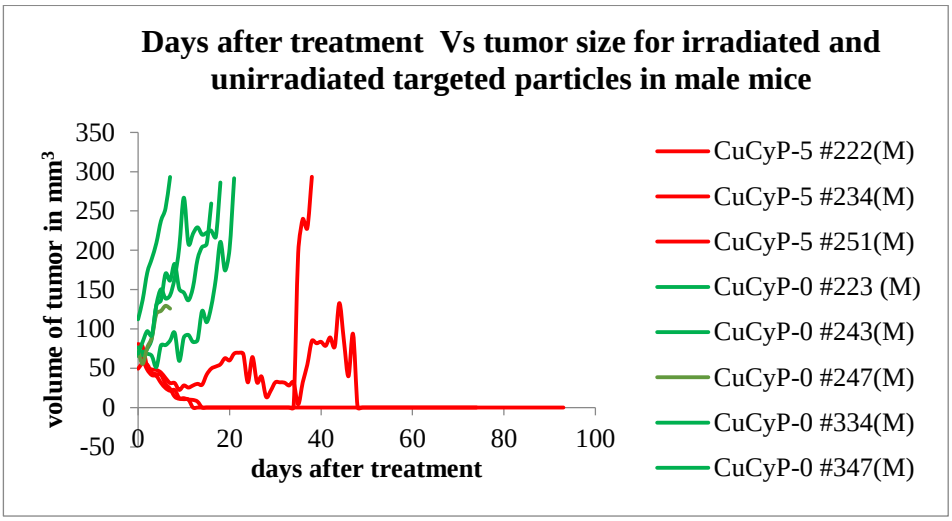
Days after treatment Vs tumor size for irradiated and unirradiated targeted particles in male mice
volume of tumor in mm3
350
300
250
200
150
100
50
0
-50
0
20
40
60
80
100
days after treatment
CuCyP-5 #222(M)
CuCyP-5 #234(M)
CuCyP-5 #251(M)
CuCyP-0 #223 (M)
CuCyP-0 #243(M)
CuCyP-0 #247(M)
CuCyP-0 #334(M)
CuCyP-0 #347(M)

Figure 2A

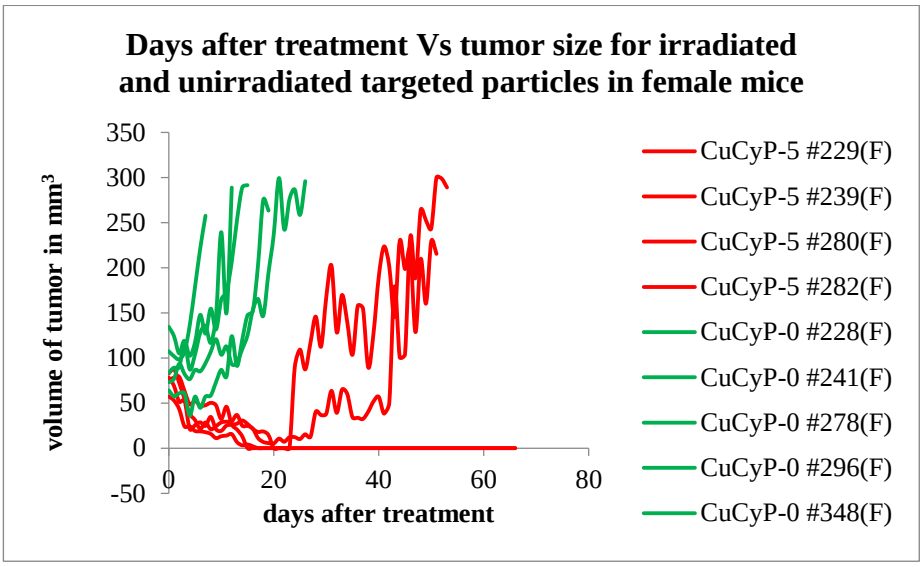

Figure 2B

Figure 2. Tumor size as a function of time, for mice given a targeted copper cysteamine treatment. Each individual curve represents one mouse. Red curves are mice given 5 Gy of radiation; green curves are mice given 0 Gy of radiation. Figure A is male mice; figure B is female mice.

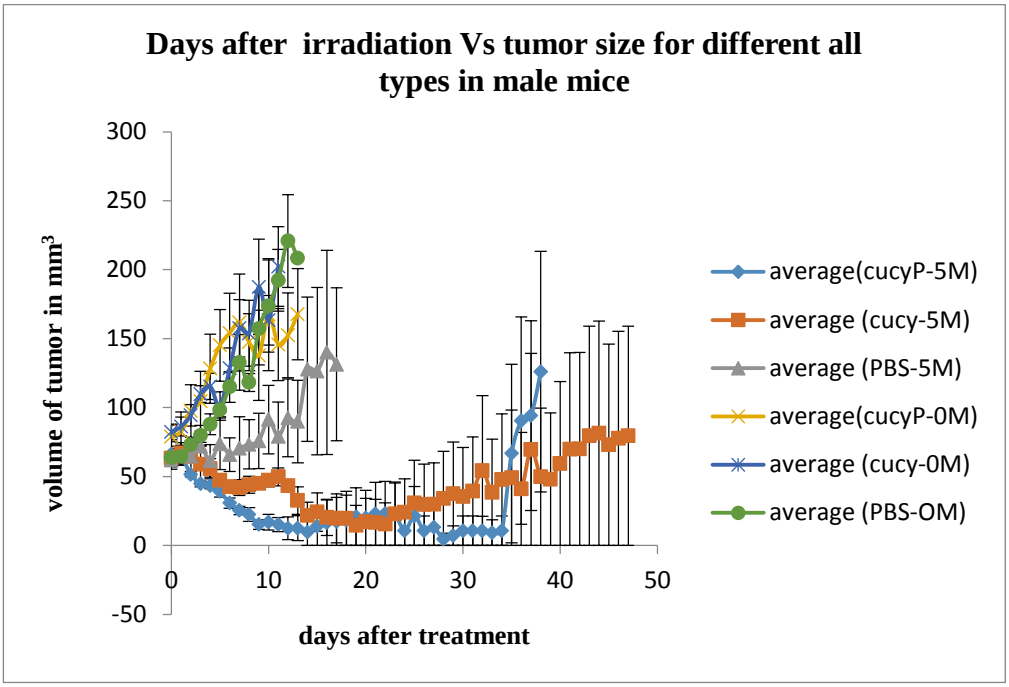
Days after irradiation Vs tumor size for different all types in male mice
volume of tumor in mm3
300
250
200
150
100
50
0
-50
0
10
20
30
40
50
days after treatment
average(cucyP-5M)
average (cucy-5M)
average (PBS-5M)
average(cucyP-0M)
average (cucy-0M)
average (PBS-OM)

Figure 3A

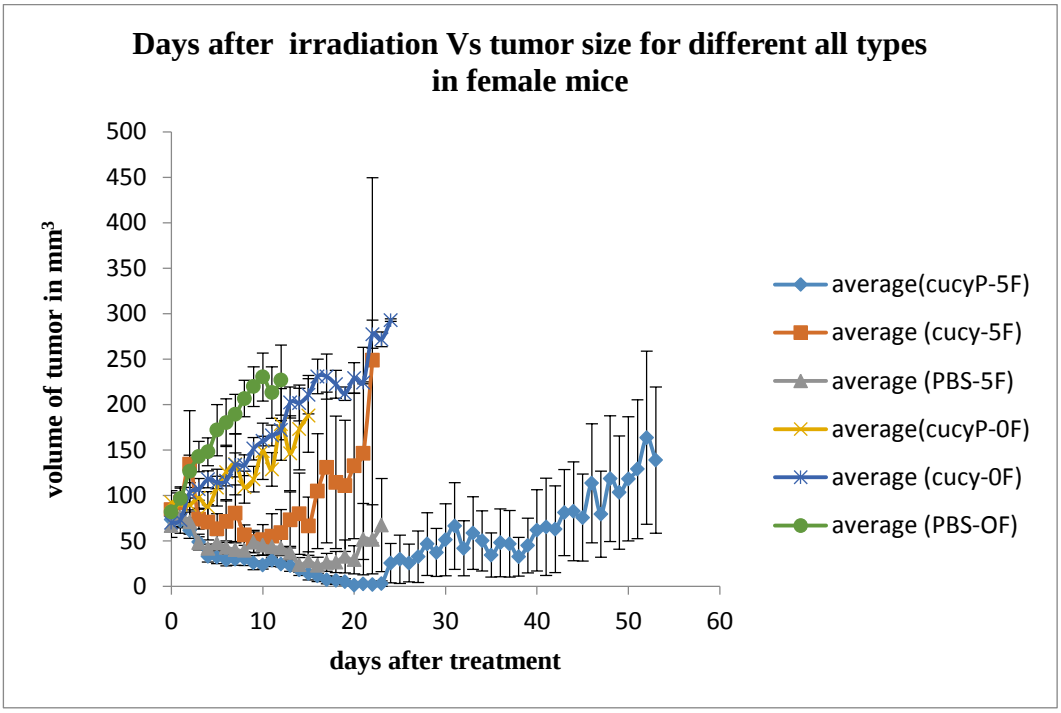

Figure 3B

Figure 3. Tumor size as a function of time, for mice given different treatments. Each individual curve represents a single treatment either at 5 Gy or at 0 Gy of radiation. Figure A is male mice; figure B is female mice.

SUPPLEMENTARY DATA

Supplemental Figures 1A – 2 B

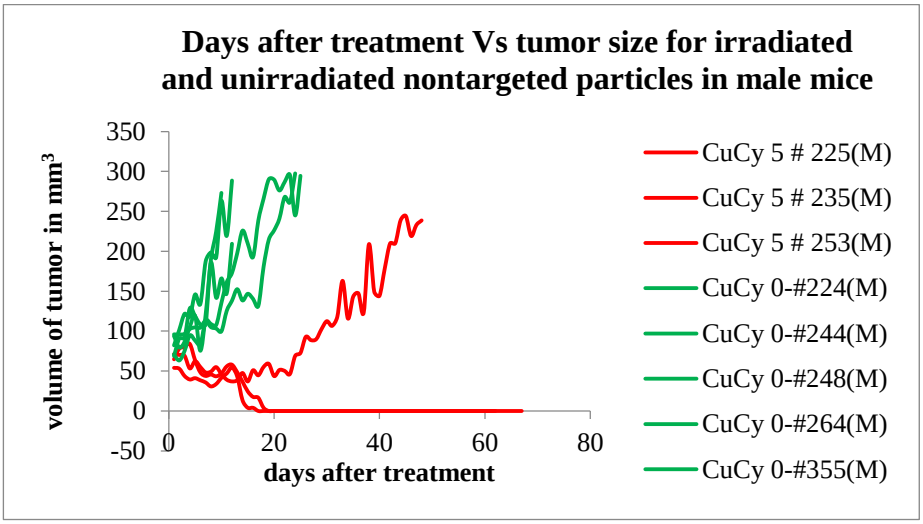

Figure S1A

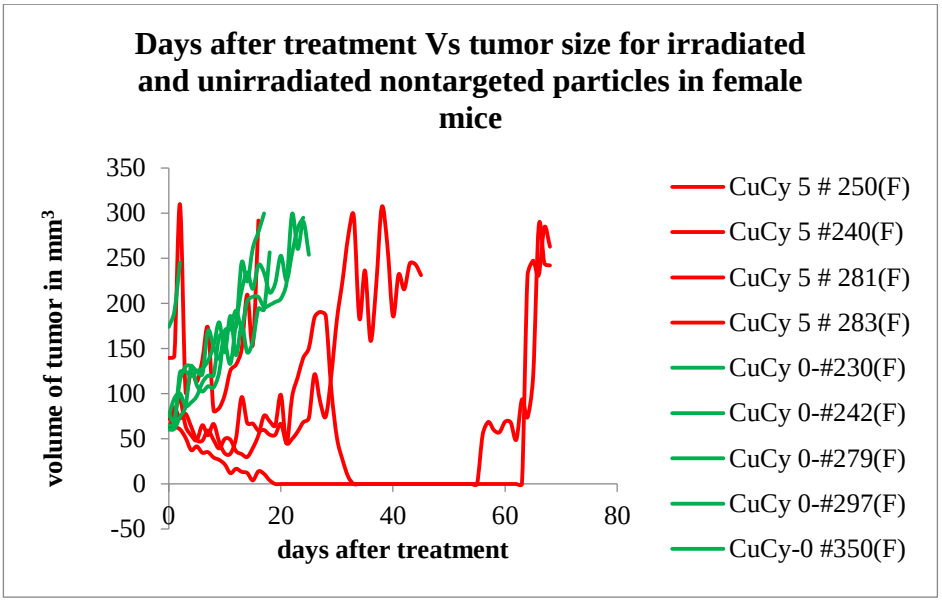

Figure S1B

Figure S1. Tumor size as a function of time, for mice given a non-targeted copper cysteamine treatment. Each individual curve represents one mouse. Red curves are mice given 5 Gy of radiation; green curves are mice given 0 Gy of radiation. Figure A is male mice; figure B is female mice.

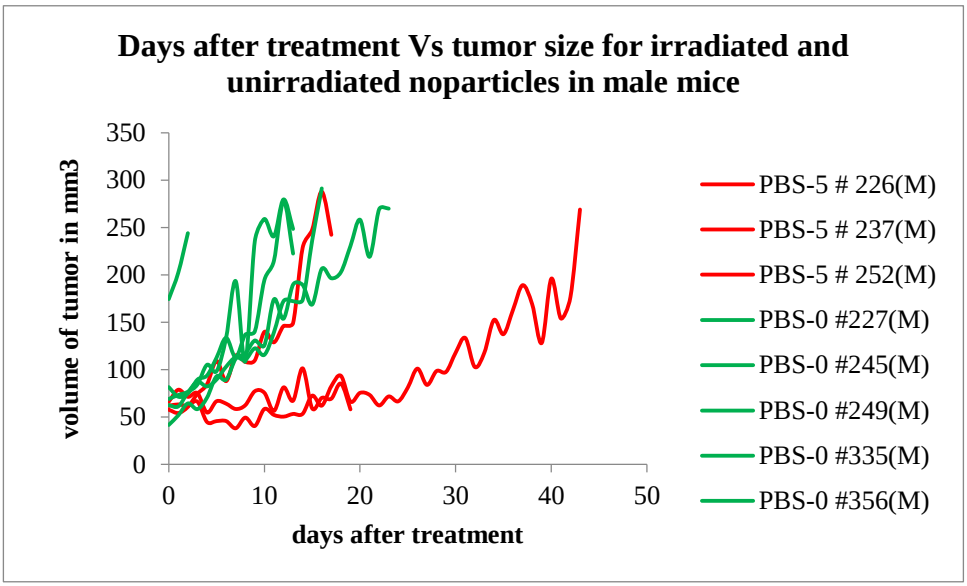
Days after treatment Vs tumor size for irradiated and unirradiated noparticles in male mice
volume of tumor in mm3
350
300
250
200
150
100
50
0
0
10
20
30
40
50
days after treatment
PBS-5 # 226(M)
PBS-5 # 237(M)
PBS-5 # 252(M)
PBS-0 #227(M)
PBS-0 #245(M)
PBS-0 #249(M)
PBS-0 #335(M)
PBS-0 #356(M)

Figure S2A

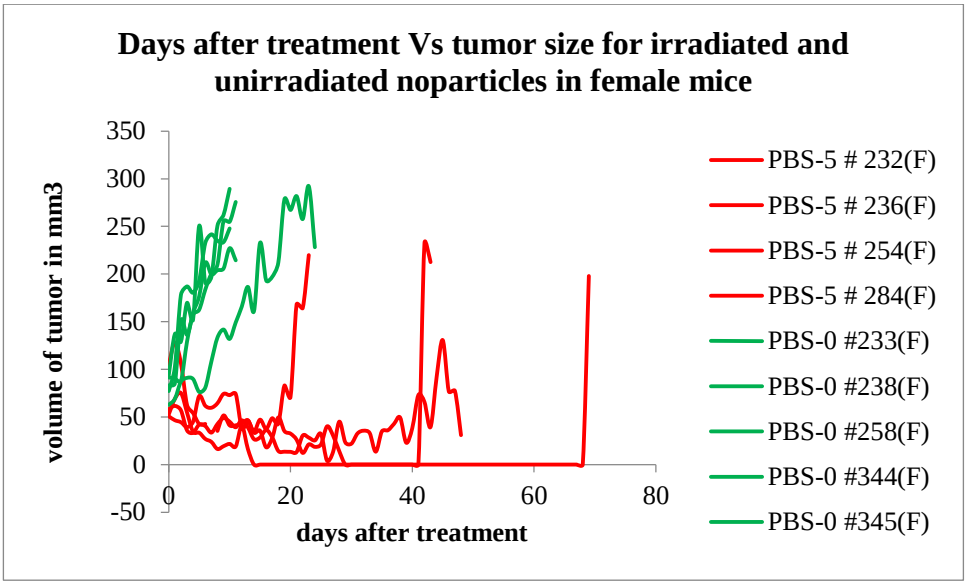

Figure S2B

Figure S2. Tumor size as a function of time, for mice given a control (no particles) treatment. Each individual curve represents one mouse. Red curves are mice given 5 Gy of radiation; green curves are mice given 0 Gy of radiation. Figure A is male mice; figure B is female mice.

Table S1: Information on interaction terms for targeted and non-targeted copper-cysteamine

day.after.irradiation	< 2.2e-16
sex	0.9968423
radiation.dose.Gy.	< 2.2e-16
treatment.type	0.0006079
age.at.irradiation.days.	1.07E-12
Original.tumor.volume	< 2.2e-16
day.after.irradiation:sex	0.0052499
day.after.irradiation:radiation.dose.Gy.	< 2.2e-16
sex:radiation.dose.Gy.	0.2877592
day.after.irradiation:treatment.type	0.2422588
sex:treatment.type	0.925823
radiation.dose.Gy.:treatment.type	5.02E-09
day.after.irradiation:age.at.irradiation.days.	< 2.2e-16
sex:age.at.irradiation.days.	0.0581423
radiation.dose.Gy.:age.at.irradiation.days.	0.0741023
treatment.type:age.at.irradiation.days.	3.58E-11
day.after.irradiation:Original.tumor.volume	6.74E-16
sex:Original.tumor.volume	0.0893735
radiation.dose.Gy.:Original.tumor.volume	0.3569157
treatment.type:Original.tumor.volume	0.3732059
age.at.irradiation.days.:Original.tumor.volume	0.000219
day.after.irradiation:sex:radiation.dose.Gy.	0.0002324

day.after.irradiation:sex:treatment.type	0.0642263
day.after.irradiation:radiation.dose.Gy.:treatment.type	2.48E-09
sex:radiation.dose.Gy.:treatment.type	0.4166221
day.after.irradiation:sex:age.at.irradiation.days.	0.002378
day.after.irradiation:radiation.dose.Gy.:age.at.irradiation.days.	0.709861
sex:radiation.dose.Gy.:age.at.irradiation.days.	0.0825586
day.after.irradiation:treatment.type:age.at.irradiation.days.	0.690005
sex:treatment.type:age.at.irradiation.days.	1.10E-06
radiation.dose.Gy.:treatment.type:age.at.irradiation.days.	1.54E-10
day.after.irradiation:sex:Original.tumor.volume	0.0023348
day.after.irradiation:radiation.dose.Gy.:Original.tumor.volume	0.0098703
sex:radiation.dose.Gy.:Original.tumor.volume	0.9326714
day.after.irradiation:treatment.type:Original.tumor.volume	0.0147587
sex:treatment.type:Original.tumor.volume	0.1858568
radiation.dose.Gy.:treatment.type:Original.tumor.volume	0.0021191
day.after.irradiation:age.at.irradiation.days.:Original.tumor.volume	4.63E-06
sex:age.at.irradiation.days.:Original.tumor.volume	0.0001083
radiation.dose.Gy.:age.at.irradiation.days.:Original.tumor.volume	0.914267
treatment.type:age.at.irradiation.days.:Original.tumor.volume	2.10E-15
day.after.irradiation:sex:radiation.dose.Gy.:treatment.type	0.1826445
day.after.irradiation:sex:radiation.dose.Gy.:age.at.irradiation.days.	0.0002631
day.after.irradiation:sex:treatment.type:age.at.irradiation.days.	0.0017918
day.after.irradiation:radiation.dose.Gy.:treatment.type:age.at.irradiation.days.	1.41E-10
sex:radiation.dose.Gy.:treatment.type:age.at.irradiation.days.	0.0015014
day.after.irradiation:sex:radiation.dose.Gy.:Original.tumor.volume	0.0008715
day.after.irradiation:sex:treatment.type:Original.tumor.volume	1.16E-11
day.after.irradiation:radiation.dose.Gy.:treatment.type:Original.tumor.volume	0.7065459

sex:radiation.dose.Gy.:treatment.type:Original.tumor.volume	< 2.2e-16
day.after.irradiation:sex:age.at.irradiation.days.:Original.tumor.volume	0.8580931
day.after.irradiation:radiation.dose.Gy.:age.at.irradiation.days.:Original.tumor.volume	5.60E-06
day.after.irradiation:treatment.type:age.at.irradiation.days.:Original.tumor.volume	0.0001225
sex:treatment.type:age.at.irradiation.days.:Original.tumor.volume	0.8950907
radiation.dose.Gy.:treatment.type:age.at.irradiation.days.:Original.tumor.volume	1.82E-09
day.after.irradiation:sex:radiation.dose.Gy.:treatment.type:age.at.irradiation.days.	1.67E-05
day.after.irradiation:sex:radiation.dose.Gy.:treatment.type:Original.tumor.volume	< 2.2e-16
day.after.irradiation:sex:treatment.type:age.at.irradiation.days.:Original.tumor.volume	0.0282005
day.after.irradiation:radiation.dose.Gy.:treatment.type:age.at.irradiation.days.:Original.tumor.volume	0.1153768

Table S2: Information on interaction terms for non-targeted copper-cysteamine and no particles

day.after.irradiation	< 2.2e-16
sex	0.0001556
radiation.dose.Gy.	< 2.2e-16
treatment.type	2.47E-07
age.at.irradiation.days.	< 2.2e-16
Original.tumor.volume	< 2.2e-16
day.after.irradiation:sex	0.0137652
day.after.irradiation:radiation.dose.Gy.	< 2.2e-16
sex:radiation.dose.Gy.	0.8973791
day.after.irradiation:treatment.type	0.0412466
sex:treatment.type	0.4474246
radiation.dose.Gy.:treatment.type	0.2525226
day.after.irradiation:age.at.irradiation.days.	< 2.2e-16
sex:age.at.irradiation.days.	0.5539768
radiation.dose.Gy.:age.at.irradiation.days.	2.31E-13
treatment.type:age.at.irradiation.days.	0.0036885
day.after.irradiation:Original.tumor.volume	< 2.2e-16
sex:Original.tumor.volume	0.0793622
radiation.dose.Gy.:Original.tumor.volume	6.24E-06
treatment.type:Original.tumor.volume	1.00E-06
age.at.irradiation.days.:Original.tumor.volume	0.0029175
day.after.irradiation:sex:radiation.dose.Gy.	0.6529036
day.after.irradiation:sex:treatment.type	0.4082707
day.after.irradiation:radiation.dose.Gy.:treatment.type	0.0155393
sex:radiation.dose.Gy.:treatment.type	0.0153287
day.after.irradiation:sex:age.at.irradiation.days.	0.3772449
day.after.irradiation:radiation.dose.Gy.:age.at.irradiation.days.	1.73E-06
sex:radiation.dose.Gy.:age.at.irradiation.days.	5.69E-06
day.after.irradiation:treatment.type:age.at.irradiation.days.	0.4607212
sex:treatment.type:age.at.irradiation.days.	0.1209064
radiation.dose.Gy.:treatment.type:age.at.irradiation.days.	< 2.2e-16
day.after.irradiation:sex:Original.tumor.volume	0.9639791
day.after.irradiation:radiation.dose.Gy.:Original.tumor.volume	0.0003828
sex:radiation.dose.Gy.:Original.tumor.volume	0.2379018

day.after.irradiation:treatment.type:Original.tumor.volume	0.0007917
sex:treatment.type:Original.tumor.volume	9.74E-10
radiation.dose.Gy.:treatment.type:Original.tumor.volume	0.710651
day.after.irradiation:age.at.irradiation.days.:Original.tumor.volume	0.2090692
sex:age.at.irradiation.days.:Original.tumor.volume	1.78E-12
radiation.dose.Gy.:age.at.irradiation.days.:Original.tumor.volume	1.06E-05
treatment.type:age.at.irradiation.days.:Original.tumor.volume	0.2889579
day.after.irradiation:sex:radiation.dose.Gy.:treatment.type	0.1049055
day.after.irradiation:sex:radiation.dose.Gy.:age.at.irradiation.days.	0.0222449
day.after.irradiation:sex:treatment.type:age.at.irradiation.days.	0.0038017
day.after.irradiation:radiation.dose.Gy.:treatment.type:age.at.irradiation.days.	< 2.2e-16
sex:radiation.dose.Gy.:treatment.type:age.at.irradiation.days.	0.0013554
day.after.irradiation:sex:radiation.dose.Gy.:Original.tumor.volume	4.04E-11
day.after.irradiation:sex:treatment.type:Original.tumor.volume	2.50E-14
day.after.irradiation:radiation.dose.Gy.:treatment.type:Original.tumor.volume	3.51E-06
sex:radiation.dose.Gy.:treatment.type:Original.tumor.volume	0.0003807
day.after.irradiation:sex:age.at.irradiation.days.:Original.tumor.volume	6.10E-13
day.after.irradiation:radiation.dose.Gy.:age.at.irradiation.days.:Original.tumor.volume	1.42E-09
day.after.irradiation:treatment.type:age.at.irradiation.days.:Original.tumor.volume	1.40E-07
sex:treatment.type:age.at.irradiation.days.:Original.tumor.volume	0.0119215
radiation.dose.Gy.:treatment.type:age.at.irradiation.days.:Original.tumor.volume	< 2.2e-16
day.after.irradiation:sex:radiation.dose.Gy.:treatment.type:age.at.irradiation.days.	0.0005915
day.after.irradiation:sex:radiation.dose.Gy.:treatment.type:Original.tumor.volume	0.2044633
day.after.irradiation:sex:treatment.type:age.at.irradiation.days.:Original.tumor.volume	3.34E-08
day.after.irradiation:radiation.dose.Gy.:treatment.type:age.at.irradiation.days.:Original.tumor.volume	2.23E-09

Table S3: Information on interaction terms for targeted copper-cysteamine particles and no particles

day.after.irradiation	< 2.2e-16
sex	0.282695
radiation.dose.Gy.	< 2.2e-16
treatment.type	2.49E-14
age.at.irradiation.days.	4.11E-13
Original.tumor.volume	< 2.2e-16
day.after.irradiation:sex	5.75E-05
day.after.irradiation:radiation.dose.Gy.	< 2.2e-16
sex:radiation.dose.Gy.	0.554205
day.after.irradiation:treatment.type	0.002546
sex:treatment.type	0.422989
radiation.dose.Gy.:treatment.type	1.15E-08
day.after.irradiation:age.at.irradiation.days.	< 2.2e-16
sex:age.at.irradiation.days.	0.303295
radiation.dose.Gy.:age.at.irradiation.days.	0.66228
treatment.type:age.at.irradiation.days.	1.24E-10
day.after.irradiation:Original.tumor.volume	< 2.2e-16
sex:Original.tumor.volume	0.0287
radiation.dose.Gy.:Original.tumor.volume	0.002048
treatment.type:Original.tumor.volume	0.880755
age.at.irradiation.days.:Original.tumor.volume	0.003374
day.after.irradiation:sex:radiation.dose.Gy.	0.103475
day.after.irradiation:sex:treatment.type	0.82539
day.after.irradiation:radiation.dose.Gy.:treatment.type	1.84E-10
sex:radiation.dose.Gy.:treatment.type	0.652948
day.after.irradiation:sex:age.at.irradiation.days.	4.55E-05
day.after.irradiation:radiation.dose.Gy.:age.at.irradiation.days.	0.069363
sex:radiation.dose.Gy.:age.at.irradiation.days.	0.399175
day.after.irradiation:treatment.type:age.at.irradiation.days.	0.025123
sex:treatment.type:age.at.irradiation.days.	0.003863
radiation.dose.Gy.:treatment.type:age.at.irradiation.days.	< 2.2e-16
day.after.irradiation:sex:Original.tumor.volume	0.012177
day.after.irradiation:radiation.dose.Gy.:Original.tumor.volume	0.538656
sex:radiation.dose.Gy.:Original.tumor.volume	< 2.2e-16

day.after.irradiation:treatment.type:Original.tumor.volume	2.31E-06
sex:treatment.type:Original.tumor.volume	0.302969
radiation.dose.Gy.:treatment.type:Original.tumor.volume	< 2.2e-16
day.after.irradiation:age.at.irradiation.days.:Original.tumor.volume	0.337459
sex:age.at.irradiation.days.:Original.tumor.volume	0.265691
radiation.dose.Gy.:age.at.irradiation.days.:Original.tumor.volume	1.31E-05
treatment.type:age.at.irradiation.days.:Original.tumor.volume	0.653384
day.after.irradiation:sex:radiation.dose.Gy.:treatment.type	2.43E-05
day.after.irradiation:sex:radiation.dose.Gy.:age.at.irradiation.days.	3.60E-11
day.after.irradiation:sex:treatment.type:age.at.irradiation.days.	6.86E-05
day.after.irradiation:radiation.dose.Gy.:treatment.type:age.at.irradiation.days.	< 2.2e-16
sex:radiation.dose.Gy.:treatment.type:age.at.irradiation.days.	7.71E-07
day.after.irradiation:sex:radiation.dose.Gy.:Original.tumor.volume	< 2.2e-16
day.after.irradiation:sex:treatment.type:Original.tumor.volume	0.061314
day.after.irradiation:radiation.dose.Gy.:treatment.type:Original.tumor.volume	4.88E-10
sex:radiation.dose.Gy.:treatment.type:Original.tumor.volume	5.73E-06
day.after.irradiation:sex:age.at.irradiation.days.:Original.tumor.volume	0.612714
day.after.irradiation:radiation.dose.Gy.:age.at.irradiation.days.:Original.tumor.volume	1.64E-09
day.after.irradiation:treatment.type:age.at.irradiation.days.:Original.tumor.volume	8.51E-07
sex:treatment.type:age.at.irradiation.days.:Original.tumor.volume	0.15134
radiation.dose.Gy.:treatment.type:age.at.irradiation.days.:Original.tumor.volume	0.008293
day.after.irradiation:sex:radiation.dose.Gy.:treatment.type:age.at.irradiation.days.	0.024138
day.after.irradiation:sex:radiation.dose.Gy.:treatment.type:Original.tumor.volume	0.00421
day.after.irradiation:sex:treatment.type:age.at.irradiation.days.:Original.tumor.volume	0.35164
day.after.irradiation:radiation.dose.Gy.:treatment.type:age.at.irradiation.days.:Original.tumor.volume	5.02E-07

Table S4: Survival Experiment Data

Mouse Number	Days between Irradiation and death	Sex	Irradiation Dose (Gy)	Treatment Type	Age at Irradiation (days)	Size of tumor on day of irradiation
222	93	M	5	CuCyP	59	49.36
234	64	M	5	CuCyP	66	68.26
251	74	M	5	CuCyP	66	80.76
229	66	F	5	CuCyP	48	75.16
239	65	F	5	CuCyP	94	78.14
280	79	F	5	CuCyP	90	82.86
282	103	F	5	CuCyP	96	57.24
225	70	M	5	CuCy	59	64.71
235	66	M	5	CuCy	66	54.05
253	68	M	5	CuCy	66	71.35
250	68	F	5	CuCy	83	61.58
240	73	F	5	CuCy	59	63.01
281	29	F	5	CuCy	90	139.66
283	82	F	5	CuCy	96	72.15
226	19	M	5	No Particles	59	66.13
237	17	M	5	No Particles	66	57.74
252	73	M	5	No Particles	66	61.9
232	91	F	5	No Particles	83	52.65
236	64	F	5	No Particles	52	50.66
254	48	F	5	No Particles	66	58.16
284	49	F	5	No Particles	117	104.97
223	39	M	0	CuCyP	59	76.46
243	57	M	0	CuCyP	73	65.59
247	26	M	0	CuCyP	76	72.04
347	24	M	0	CuCyP	67	68.36
228	40	F	0	CuCyP	83	64.09
241	51	F	0	CuCyP	59	73

278	25	F	0	CuCyP	100	83.48
296	38	F	0	CuCyP	125	134.57
348	34	F	0	CuCyP	67	107.4
224	65	M	0	CuCy	59	96
244	44	M	0	CuCy	59	96
248	39	M	0	CuCy	76	70.63
264	44	M	0	CuCy	80	68.88
355	35	M	0	CuCy	90	93.88
230	62	F	0	CuCy	48	75.57
242	57	F	0	CuCy	59	60.15
279	29	F	0	CuCy	100	78.42
297	25	F	0	CuCy	125	173.94
350	41	F	0	CuCy	75	64.85
227	39	M	0	No Particles	59	41.65
245	40	M	0	No Particles	59	174.44
249	28	M	0	No Particles	76	81.57
335	39	M	0	No Particles	49	62.53
356	28	M	0	No Particles	48	62.72
238	49	F	0	No Particles	52	91.39
258	45	F	0	No Particles	52	93.95
344	37	F	0	No Particles	59	83.15
345	28	F	0	No Particles	59	77.13

Table S5 Analysis of Variance Results on Survival Data

data$sex	0.0013965
data$radiation_dose.Gy.	8.55E-05
data$treatment_type	0.0016282
data$age_at_irradiation.days.	0.0066644
data$size_of_tumor_on_day_of_irradiation	0.0400424
data$sex:data$radiation_dose.Gy.	0.0072156
data$sex:data$treatment_type	0.0095929
data$radiation_dose.Gy.:data$treatment_type	0.0005156
data$sex:data$age_at_irradiation.days.	0.018785
data$radiation_dose.Gy.:data$age_at_irradiation.days.	0.0426896
data$treatment_type:data$age_at_irradiation.days.	0.123847
data$sex:data$size_of_tumor_on_day_of_irradiation	0.0038603
data$radiation_dose.Gy.:data$size_of_tumor_on_day_of_irradiation	0.0008749
data$treatment_type:data$size_of_tumor_on_day_of_irradiation	0.0410717
data$age_at_irradiation.days.:data$size_of_tumor_on_day_of_irradiation	0.0049635
data$sex:data$radiation_dose.Gy.:data$treatment_type	0.0599268
data$sex:data$radiation_dose.Gy.:data$age_at_irradiation.days.	0.0598588
data$sex:data$treatment_type:data$age_at_irradiation.days.	0.1531105
data$radiation_dose.Gy.:data$treatment_type:data$age_at_irradiation.days.	0.0024378
data$sex:data$radiation_dose.Gy.:data$size_of_tumor_on_day_of_irradiation	0.0047904
data$sex:data$treatment_type:data$size_of_tumor_on_day_of_irradiation	0.0026771
data$radiation_dose.Gy.:data$treatment_type :data$size_of_tumor_on_day_of_irradiation	0.0397707
data$sex:data$age_at_irradiation.days .:data$size_of_tumor_on_day_of_irradiation	0.1807822
data$radiation_dose.Gy.:data$age_at_irradiation.days .:data$size_of_tumor_on_day_of_irradiation	0.0224007

data$treatment_type:data$age_at_irradiation.days .:data$size_of_tumor_on_day_of_irradiation	0.0023849
data$sex:data$radiation_dose.Gy.:data$treatment_type :data$age_at_irradiation.days.	0.0060847
data$sex:data$radiation_dose.Gy.:data$treatment_type :data$size_of_tumor_on_day_of_irradiation	0.0006902
data$sex:data$treatment_type:data$age_at_irradiation.days .:data$size_of_tumor_on_day_of_irradiation	0.0283519
data$radiation_dose.Gy.:data$treatment_type:data$age_at_irradiation.days .:data$size_of_tumor_on_day_of_irradiation	0.0291779